

Effects of CuO/ZnO/Al₂O₃ catalyst modification using Zr, Mn and Si for methanol
synthesis via CO₂ hydrogenation



A Thesis Submitted in Partial Fulfillment of the Requirements
for the Degree of Master of Engineering in Chemical Engineering

Department of Chemical Engineering

FACULTY OF ENGINEERING

Chulalongkorn University

Academic Year 2019

Copyright of Chulalongkorn University

ผลของการปรับปรุงตัวเร่งปฏิกิริยา CuO/ZnO/Al₂O₃ ด้วย Zr Mn และ Si สำหรับการสังเคราะห์เม
ทานอลโดยไฮโดรจิเนชันของคาร์บอนไดออกไซด์



วิทยานิพนธ์นี้เป็นส่วนหนึ่งของการศึกษาตามหลักสูตรปริญญาวิศวกรรมศาสตรมหาบัณฑิต
สาขาวิชาวิศวกรรมเคมี ภาควิชาวิศวกรรมเคมี
คณะวิศวกรรมศาสตร์ จุฬาลงกรณ์มหาวิทยาลัย
ปีการศึกษา 2562
ลิขสิทธิ์ของจุฬาลงกรณ์มหาวิทยาลัย

กมลลักษณ์ พงศ์ภาณุมาพร : ผลของการปรับปรุงตัวเร่งปฏิกิริยา CuO/ZnO/Al₂O₃ ด้วย Zr Mn และ Si สำหรับการสังเคราะห์เมทานอลโดยไฮโดรเจนชั้นของคาร์บอนไดออกไซด์. (Effects of CuO/ZnO/Al₂O₃ catalyst modification using Zr, Mn and Si for methanol synthesis via CO₂ hydrogenation) อ.ที่ปรึกษาหลัก : ศ. ดร.บรรเจิด จงสมจิตร

ในปัจจุบันการกำจัดแก๊สคาร์บอนไดออกไซด์มีแนวโน้มที่จะเพิ่มความน่าสนใจของมนุษยชาติ หนึ่งในวิธีที่มีประสิทธิภาพที่สุดในการนำแก๊สคาร์บอนไดออกไซด์ไปใช้ประโยชน์คือการเปลี่ยนแก๊สคาร์บอนไดออกไซด์ให้เป็นสารเคมีที่มีมูลค่าเพิ่ม ดังนั้นเมทานอลจึงถูกคัดสรรผ่านทางกระบวนการไฮโดรเจนชั้นของคาร์บอนไดออกไซด์โดยใช้ตัวเร่งปฏิกิริยา CuO/ZnO/Al₂O₃ ในลำดับแรกตัวเร่งปฏิกิริยา CZA ถูกเตรียมด้วยวิธีเอ็บซุบภายใต้สภาวะความแตกต่างของค่าความเป็นกรดเบส (7,8 และ 9) ระหว่างการตกตะกอนร่วมพบว่าค่าความเป็นกรดเบสที่เหมาะสมคือ 8 (CZA-PH8) นำไปสู่พื้นที่ผิว ค่าเป็นเบส และค่าการรีดักชันที่สูง ค่าการเปลี่ยนแก๊สคาร์บอนไดออกไซด์และค่าการเลือกเกิดเมทานอลคือ 2.6% และ 10% ตามลำดับที่สภาวะ 250 °C ภายใต้ความดันบรรยากาศ อย่างไรก็ตามคาร์บอนมอนอกไซด์เป็นผลิตภัณฑ์หลักสำหรับสภาวะนี้ ในส่วนที่สองความแตกต่างของตัวปรับปรุงเช่น Zr, Mn และ Si ถูกใช้เพื่อที่จะปรับปรุงความว่องไวของตัวเร่งปฏิกิริยา CZA-PH8 เห็นได้ชัดว่าตัวปรับปรุง Mn เพิ่มค่าการเปลี่ยนของคาร์บอนไดออกไซด์สูงถึง 4.7% โดยให้ค่าสูงสุดของผลได้เมทานอลที่สภาวะเดียวกัน อย่างไรก็ตามค่าการเลือกเกิดเมทานอลมีค่า 9.86% ถูกค้นพบโดยการปรับปรุงด้วย Mn ในตัวเร่งปฏิกิริยา CZA-PH8 นอกจากนี้ตัวปรับปรุง Mn สามารถส่งเสริมค่าการเปลี่ยนคาร์บอนไดออกไซด์มากกว่าสองเท่าโดยปราศจากการเปลี่ยนค่าการเลือกเกิดเมทานอล จึงสามารถสรุปได้ว่าตัวปรับปรุง Mn เป็นสารเคมีที่อำนวยความสะดวกในการกระจายตัวของ CuO และค่าความเป็นเบสของตัวเร่งปฏิกิริยา CZA ในส่วนสุดท้ายค่าความคงตัวของตัวเร่งปฏิกิริยา CZA-PH8 และ CZA-PH8-Mn จะถูกตรวจสอบความแตกต่างระหว่างตัวเร่งปฏิกิริยาที่ไม่ถูกใช้งานและถูกใช้งานหลักจากใช้ไป 5 ชั่วโมงและพบว่าตัวปรับปรุง Mn สามารถลดการเกาะกลุ่มตัวของ CuO นำไปสู่ความว่องไวที่เพิ่มขึ้นของ CZA-PH8 ที่ปรับปรุงด้วย Mn

สาขาวิชา วิศวกรรมเคมี
ปีการศึกษา 2562

ลายมือชื่อนิสิต
ลายมือชื่อ อ.ที่ปรึกษาหลัก

6170105521 : MAJOR CHEMICAL ENGINEERING

KEYWORD: methanol synthesis; CO₂ hydrogenation; CuO/ZnO/Al₂O₃; CO₂ utilization;
Zr; Mn; Si

Kamonlak Pongpanumaporn : Effects of CuO/ZnO/Al₂O₃ catalyst modification using Zr, Mn and Si for methanol synthesis via CO₂ hydrogenation. Advisor: Prof. BUNJERD JONGSOMJIT, Ph.D.

Currently, the estimated CO₂ amount has tended to increase interesting of population. One of the most effective utilization ways of CO₂ is to convert CO₂ to higher valued chemicals. Thus, methanol was chosen to produce via CO₂ hydrogenation by using CuO/ZnO/Al₂O₃ (CZA) catalyst. In the first part, CZA was prepared by co-impregnation method under different pH (7, 8 and 9) during co-precipitation. It was found that the suitable pH was 8 (CZA-PH8) due to high surface area, high basicity, and reducibility. The CO₂ conversion and methanol selectivity were 2.6% and 10%, respectively at 250°C under atmospheric pressure. However, it should be noted that CO was the main product of this study. In the second part, different promoters such as Zr, Mn and Si were employed to improve the catalytic activity of CZA-PH8. It was found that Mn promoter apparently increased the CO₂ conversion up to 4.7% (giving the highest methanol yield of ca. 0.46% under the same condition. However, the methanol selectivity of ca. 10% was found over Mn-promoted CZA-PH8 catalyst. On the other hand, the Mn promoter can enhance the CO₂ conversion without a change in methanol selectivity. It can be concluded that Mn promoter is chemical promoters since it facilitates the dispersion of CuO and basicity of CZA catalyst. In the final part, the stability of CZA-PH8 and CZA-PH8-Mn catalysts was investigated. It was found that the differences between the fresh and spent catalysts were a decrease of agglomeration of CuO leading to higher activity of the CZA-PH8 with Mn promotion.

Field of Study: Chemical Engineering

Student's Signature

Academic Year: 2019

Advisor's Signature

ACKNOWLEDGEMENTS

This work was supported by the Malaysia Thailand Joint Authority (MTJA) project for facility of methanol reaction construction and experimental lab scale, the author would like to appreciate my advisor, Professor Bunjerd Jongsomjit for supporting of knowledge such as contents of experimental, how to study in master degree and life planning.

Additionally, the author thank to committee: chairman Pimporn Ponpesh (Ph.D), examine Supareak Praserthdam (Ph.D) and external examine Sasiradee Jantasee for new knowledge of this project.

Finally, the author thanks to my family which support my life and motivation, my friend that create a cheerfulness for studying.

Kamonlak Pongpanumaporn



TABLE OF CONTENTS

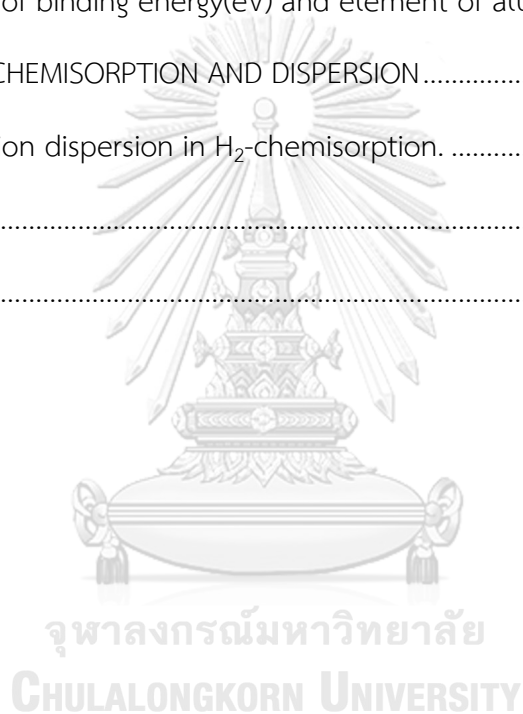
	Page
.....	iii
ABSTRACT (THAI).....	iii
.....	iv
ABSTRACT (ENGLISH).....	iv
ACKNOWLEDGEMENTS.....	v
TABLE OF CONTENTS.....	vi
LIST OF TABLES.....	xi
LIST OF FIGURES.....	xiii
INTRODUCTION.....	1
1.1 Statement of problem.....	1
1.2. Objective of research.....	2
1.3. Scope of research.....	3
1.4 Research methodology.....	4
1.5 Research plan.....	6
BACKGROUND AND LITERATURE REVIEW.....	7
2.1 The reaction of methanol synthesis via CO ₂ hydrogenation.....	7
2.2 Coke formation.....	8
2.3 Methanol.....	9
2.4 Cu, Zn, Al oxide.....	12
2.5 Zirconium.....	12
2.6 Manganese.....	13

2.7 Silica	14
2.8 Literature reviews.....	14
EXPERIMENT	35
3.1 Catalysts preparation.....	35
3.1.1 Preparation of different pH affected of CZA.....	35
3.1.2 Preparation of modifier CZA-Zr, CZA-Mn, CZA-Si.....	36
3.2 Catalysts characterizations	36
3.2.1. X-ray diffraction (XRD).....	36
3.2.2. Scanning Electron Microscope (SEM).....	37
3.2.3. Energy-dispersive X-ray spectroscopy (EDX).....	37
3.2.4. N ₂ physisorption	37
3.2.5. Temperature-programmed reduction (TPR).....	37
3.2.6. Temperature-programmed desorption of carbon dioxide (CO ₂ -TPD).....	37
3.2.8. X-ray Photoelectron spectroscopy (XPS).....	38
3.2.9. H ₂ -Chemisorption (H ₂ -Chem).....	38
3.3 Activity test.....	39
RESULTS AND DISCUSSION.....	41
4.1. Effect of pH value in CZA catalyst preparation.	41
4.1.1 Characterization	41
4.1.1.1 X – ray diffraction (XRD).....	41
4.1.1.2. Scanning electron microscope (SEM) and energy-dispersive X-ray spectroscopy (EDX).....	42
4.1.1.3. N ₂ physisorption (BET)	44
4.1.1.4 Temperature-programmed reduction (TPR).....	46

4.1.1.5 Temperature-programmed desorption of carbon dioxide (CO ₂ -TPD)	47
4.1.1.6 Temperature-programmed desorption of ammonia (NH ₃ -TPD).....	49
4.1.1.7 X-ray photoelectron spectroscopy (XPS)	51
4.1.2 Reaction performance	54
4.2 The effect of Zr, Mn, and Si promoters.....	57
4.2.1 Characterization	57
4.2.1.1 X – ray Diffraction (XRD).....	57
4.2.1.2 N ₂ physisorption (BET)	58
4.2.1.3 Temperature-programmed reduction (TPR).....	60
4.2.1.4 Temperature-programmed desorption of carbon dioxide (CO ₂ -TPD)	61
4.2.1.5 Temperature-programmed desorption of ammonia (NH ₃ -TPD).....	63
4.2.1.6 X-ray photoelectron spectroscopy (XPS)	65
4.2.1.7 H ₂ -Chemisorption (H ₂ -Chem).....	67
4.2.2 Reaction performance	67
4.3 The stability of CZA catalyst.....	70
4.3.1 Characterization	70
4.3.1.1 X – ray diffraction (XRD).....	70
4.3.1.2 Scanning Electron Microscope (SEM) and energy-dispersive X-ray spectroscopy (EDX).....	72
4.3.1.3 X-ray photoelectron spectroscopy (XPS)	75
CONCLUSIONS AND RECOMMENDATIONS.....	78
Part 1: The effect of increasing pH value in CZA catalyst preparation.....	78
Part 2: The effect of Mn, Zr, and Si promoters on CZA-PH8 catalyst.....	78

Part 3: The stability of CZA catalyst.....	79
APPENDIX.....	81
APPENDIX.A CALCULATION OF CATALYSTS PERFORMANCE	81
A.1 CO ₂ Conversion by C balance	81
A.2 Methanol selectivity.....	81
A.3 Methanol Yield.....	81
A.4 CO ₂ reaction rate	81
A.5 CH ₃ OH production rate.....	81
A.6 CO ₂ reaction rate and CH ₃ OH production rate at time on stream.....	81
A.7 Activity of CZA catalyst.....	87
APPENDIX.B CALCULATION OF CRYSTALLINE SIZE	91
B.1 The Scherrer's equation.....	91
APPENDIX.C CALBRATION	92
C.1 CO ₂ calibration.....	92
C.2 CH ₃ OH calibration.....	92
C.3 NH ₃ -TPD calibration.....	93
C.4 CO ₂ -TPD calibration.....	93
APPENDIX.D SCANNING ELECTRON MICROSCOPE (SEM) AND ENERGY-DISPERSIVE X- RAY SPECTROSCOPY (EDX).....	94
D.1 SEM-EDX of effect of metals promoters.....	94
D.2 SEM-EDX of effect of metals promoters in stability test.....	97
APPENDIX.E X-RAY PHOTOELECTRON SPECTROSCOPY	101
E.1 Chemical species of CZA-PH7 catalyst.....	101
E.2 Chemical species of CZA-PH8 catalyst.....	104

E.3 Chemical species of CZA-PH9 catalyst.....	107
E.4 Chemical species of CZA-PH8-Zr catalyst.....	110
E.5 Chemical species of CZA-PH8-Mn catalyst.....	113
E.6 Chemical species of CZA-PH8-Si catalyst.....	117
E.7 Chemical species of sCZA-PH8 catalyst.....	120
E.8 Chemical species of sCZA-PH8-Mn catalyst.....	123
E.9 Position of binding energy(eV) and element of all species.....	127
APPENDIX.F H ₂ -CHEMISORPTION AND DISPERSION.....	129
F.1 Calculation dispersion in H ₂ -chemisorption.....	129
REFERENCES.....	131
VITA.....	136



LIST OF TABLES

	Page
Table 1 Properties of methanol.....	11
Table 2 The review Cu-based in Manufacturer.....	12
Table 3 Properties of Zirconium	13
Table 4 Properties of Manganese	13
Table 5 Properties of Silica	14
Table 6 The conditions and significant review.....	14
Table 7 List of chemical prepared catalyst.....	35
Table 8 The characterization data equipment of this study	38
Table 9 Condition of TCD detector.....	40
Table 10 Condition of FID detector.....	40
Table 11 Crystalline size of CZA catalysts.....	42
Table 12 EDX elemental analysis without O element on surface of different CZA catalysts (wt%).....	44
Table 13 surface properties of catalysts	44
Table 14 The amounts of basic sites of all CZA catalysts.	48
Table 15 the amounts of basic sites of all CZA catalysts.	50
Table 16 Property of XPS spectra and mass of Cu,Zn,Al,O species.....	52
Table 17 Catalyst activity of CZA catalysts (0 h = initial after proceeding of mixing reactant 30 min).....	56
Table 18 Crystalline size of CuO in CZA catalysts.....	57
Table 19 surface properties of catalysts	58
Table 20 The amounts of basic sites of metals loading of CZA catalysts.....	62

Table 21 the amounts of basic sites of metals loading of CZA catalysts.....	64
Table 22 The property of XPS spectra and mass of Cu, Zn, and Al ₂ O ₃ species of the effect of Zr, Mn, and Si promoters in CZA catalysts by X=Si, Mn, and Zr.....	66
Table 23 H ₂ -adsorption and Cu ⁰ dispersion of CZA catalyst.....	67
Table 23 reaction test of CZA-PH8-X (X=Si, Mn, Zr) catalysts. (0 h = initial after proceeding of mixing reactant 30 min)	69
Table 24 Crystalline size of CZA catalysts.....	71
Table 25 EDX elemental analysis Cu, Zn, Al, O, and C element on surface of fresh CZA catalysts (CZA-PH8) and spent catalyst (sCZA-PH8)	74
Table 26 The property of XPS spectra and mass of Cu,Zn,Al ₂ O ₃ species of the effect of activity test, before activity test; CZA-PH8 and after activity test; sCZA-PH8.....	77
Table 27 The property of XPS spectra and mass of Cu,Zn,Al ₂ O ₃ species of the effect of Zr,Mn promoter of the effect of activity test, before activity test; CZA-PH8-Mn and after activity test; sCZA-PH8-Mn.....	77

LIST OF FIGURES

	Page
Figure 1 The coke formation and coke removing reactions [6].	8
Figure 2 The coke formation from hydrocarbon [7].	9
Figure 3 The application of methanol feed stock [8].	9
Figure 4 The Thai customer review of methanol importation and exportation.	11
Figure 5 The reduced surface of the catalysts via hydrotalcite-like precursors and the functionality of the various surface sites for CO ₂ hydrogenation to methanol.	33
Figure 6 XRD patterns of Cu/ZnO/Al ₂ O ₃ catalyst (a) before calcination, (b) after calcination.	34
Figure 7 The Schematic of methanol synthesis via CO ₂ hydrogenation.	39
Figure 8 XRD patterns of different Cu/Zn/Al catalysts (●) CuO ; (Δ) ZnO ; (○) Zincian malachite, (Cu,Zn) ₂ (OH) ₂ CO ₃ .	41
Figure 9 SEM and EDX images of different pH of CZA catalysts, A; CZA-PH7, B; CZA-PH8. C; CZA-PH9.	43
Figure 10 N ₂ physisorption of different pH of Cu/Zn/Al catalysts at -196 °C liquid N ₂ .	45
Figure 11 pore size distribution (BJH technique) of different pH of CZA catalysts.	46
Figure 12 TPR profile of different pH of CZA catalysts.	46
Figure 13 CO ₂ -TPD profile of different pH of CZA catalysts.	47
Figure 14 The amounts of basic sites by CO ₂ -TPD of different pH of CZA catalysts.	48
Figure 15 NH ₃ -TPD profile of different pH of CZA catalysts.	49
Figure 16 The amounts of acid sites by NH ₃ -TPD of different pH of CZA catalysts.	50
Figure 17 Typical XPS spectra of CZA catalyst (for CZA-PH7).	51

Figure 18 Cu, Zn, Al species of different pH of CZA catalysts.....	53
Figure 19 CO ₂ conversion of different pH of CZA catalysts.....	55
Figure 20 methanol selectivity of different pH of CZA catalysts.....	55
Figure 21 methanol yield of different pH of CZA catalysts.....	56
Figure 22 XRD patterns of of CZA-PH8 catalyst with different promoters (CZA-PH8-X, X=Mn ,Si, and Zr) (●) CuO ; (Δ) ZnO ; (○) Zincian malachite, (Cu,Zn) ₂ (OH) ₂ CO ₃ ; (◆) Cu.....	57
Figure 23 N ₂ physisorption of loading metals of Cu/Zn/Al catalysts at boiling points at -196 °C liquid N ₂	59
Figure 24 Pore size distribution (BJH technique) of metals loading of CZA-PH8 catalysts.....	59
Figure 25 TPR profile of metals loading of CZA catalysts.....	60
Figure 26 CO ₂ -TPD profile of metals loading of CZA catalysts.....	61
Figure 27 The amounts of basic sites by CO ₂ -TPD of metals loading of CZA catalysts.....	62
Figure 28 NH ₃ -TPD profile of metals loading of CZA catalysts.....	63
Figure 29 the amounts of acid sites by NH ₃ -TPD of metals loading of CZA catalysts.....	64
Figure 30 Cu species of metals loading of CZA catalysts.....	65
Figure 31 CO ₂ conversion of loading metals of CZA catalysts.....	68
Figure 32 Methanol selectivity of loading metals of CZA catalysts.....	68
Figure 33 Methanol yield of loading metals of CZA catalysts.....	69
Figure 34 XRD patterns of fresh Cu/Zn/Al catalysts (CZA-PH8) and spent catalysts (sCZA-PH8) at pH 8 (●) CuO ; (Δ) ZnO ; (○) Zincian malachite, (Cu,Zn) ₂ (OH) ₂ CO ₃ ; (◆) Cu.....	70

Figure 35 XRD patterns of fresh Cu/Zn/Al catalysts of metals loading (CZA-X, X=Mn,Si) at pH 8 and spend catalysts (sCZA-X, X=Mn,Si), (●) CuO ; (Δ) ZnO; (○) Zincian malachite, $(\text{Cu,Zn})_2(\text{OH})_2\text{CO}_3$; (◆) Cu.....	71
Figure 36 SEM and EDX images of stability CZA-PH8, A; fresh CZA-PH8, B; spent sCZA-PH8.	73
Figure 37 Cu species of CZA-PH8 catalyst in fresh and spent catalyst.....	75
Figure 38 Chemicals species of CZA-PH8-Mn, sCZA-PH8-Mncatalyst in fresh and spent catalyst.....	76



CHAPTER 1

INTRODUCTION

1.1 Statement of problem

Presently, the untimed wants of population tend to increase while fossil source has been decreasing. The greenhouse gas such as CO₂ is the main environmental pollution for global warming. The effect of this problem leads to utilization of CO₂. Generally, the CO₂ and H₂ can react and convert into high value chemicals. Methanol is the main feedstock of many industries. Methanol can produce benefic products for wide application in clean energy field and industrially used in chemical process such as FAME (fatty acid methyl ester) processing, MTBE (Methyl Tertiary Butyl Ether), formaldehyde, acetic acid, methyl methacrylate, chloromethane, electrical power generation and light olefin by MTO process[1, 2].

Hydrogenation is a common process for methanol production. Normally, the methanol synthesis is operated at high pressure with high temperature (3.5-10 MPa, 200-300 °C) by conventional CO hydrogenation. For the next generation, the CO₂ is promoted 80% of mixed feed in methanol synthesis via CO hydrogenation. Currently, the pure CO₂ hydrogenation is widely studied for alternative CO₂ utilization. In the same way, CO₂ reactant can produce methanol by the two major reactions; (1) CO₂ hydrogenation, (2) reverse water gas shift (RWGS) reaction. The involved reactions are as follows;



To avoid the undesired product, a chosen catalyst should be neutral and basic function catalyst. The Cu-based catalyst is a way to industrially use. The CuO/ZnO/Al₂O₃ (CZA) is tertiary structure and conventional of general catalysts. The Cu is the main active site of tertiary, while ZnO can interact of H₂ adsorption and support a Cu active site. In common, Al₂O₃ is a third component of CZA used to

increase the stability and activity of Cu/Zn component. Therefore, CZA is appropriate for methanol synthesis.

In addition, the dropping of promoter significantly affects activity of CZA and stability at high temperature. The promoter of CZA can be divided into two categories. Firstly, noble metal (Pt, Au, Pd) can improve activity, as the little amount of Au tends to reduce CO side reaction by spillover of H₂ [3]. Whereas, noble metal is not approximate into economic and stability. Metal oxides (La, Mn, Ce, Zr, Mg, Y) are modifiers of CZA, the metal oxide is dropped into solution by a few weight ratios [4]. Zr is the most widely used for improving physical of CZA and increasing basicity. Mn has basic property, in which the relative major property results with decreasing of DME and Cu dispersion. In another way, the high surface area (SiO₂, TiO₂) can modify stability by strong interaction between CZA [5].

In this research, the main work is divided into 2 parts. Firstly, the tertiary catalyst was synthesized by adjusting the differences of pH during coprecipitation, and then tested in the reaction at suitable condition including various temperature ranges of 200-300 °C at atmospheric pressure. Secondly, the effect of Zr, Mn, Si will be studied on the suitable pH in first part of CZA catalysts. Furthermore, the characterization techniques such as X-ray diffraction (XRD), scanning electron microscope (SEM), energy-dispersive X-ray spectroscopy (EDX), N₂ physisorption, temperature-programmed reduction (TPR) and temperature-programmed desorption of carbon dioxide (CO₂-TPD), Temperature-programmed desorption of ammonia (NH₃-TPD) and X-ray Photoelectron spectroscopy (XPS) were conducted to determine the catalytic properties.

1.2. Objective of research

To study the effect of Zr, Mn, Si on catalytic properties of CZA catalyst in methanol synthesis via CO₂ hydrogenation.

1.3. Scope of research

1.3.1. Catalyst preparation

1.3.1.1. Preparation of CZA (40:40:20 wt.%) by co-precipitation with different pH (pH = 7,8,9).

1.3.1.2. Preparation of CZA-Zr, CZA-Mn, CZA-Si catalysts (Zr, Mn, Si = 0.3 wt.%) by co-precipitation.

1.3.2. Characterization of catalyst

1.3.2.1. X-ray diffraction (XRD)

1.3.2.2. Scanning electron microscopy (SEM)

1.3.2.3. Energy-dispersive X-ray spectroscopy (EDX)

1.3.2.4. N₂ physisorption

1.3.2.5. Temperature-programmed reduction (TPR)

1.3.2.6. Temperature-programmed desorption of carbon dioxide (CO₂-TPD)

1.3.2.7. Temperature-programmed desorption of ammonia (NH₃-TPD)

1.3.2.8. X-ray photoelectron spectroscopy (XPS)

1.3.2.9. H₂-Chemisorption (H₂-Chem)

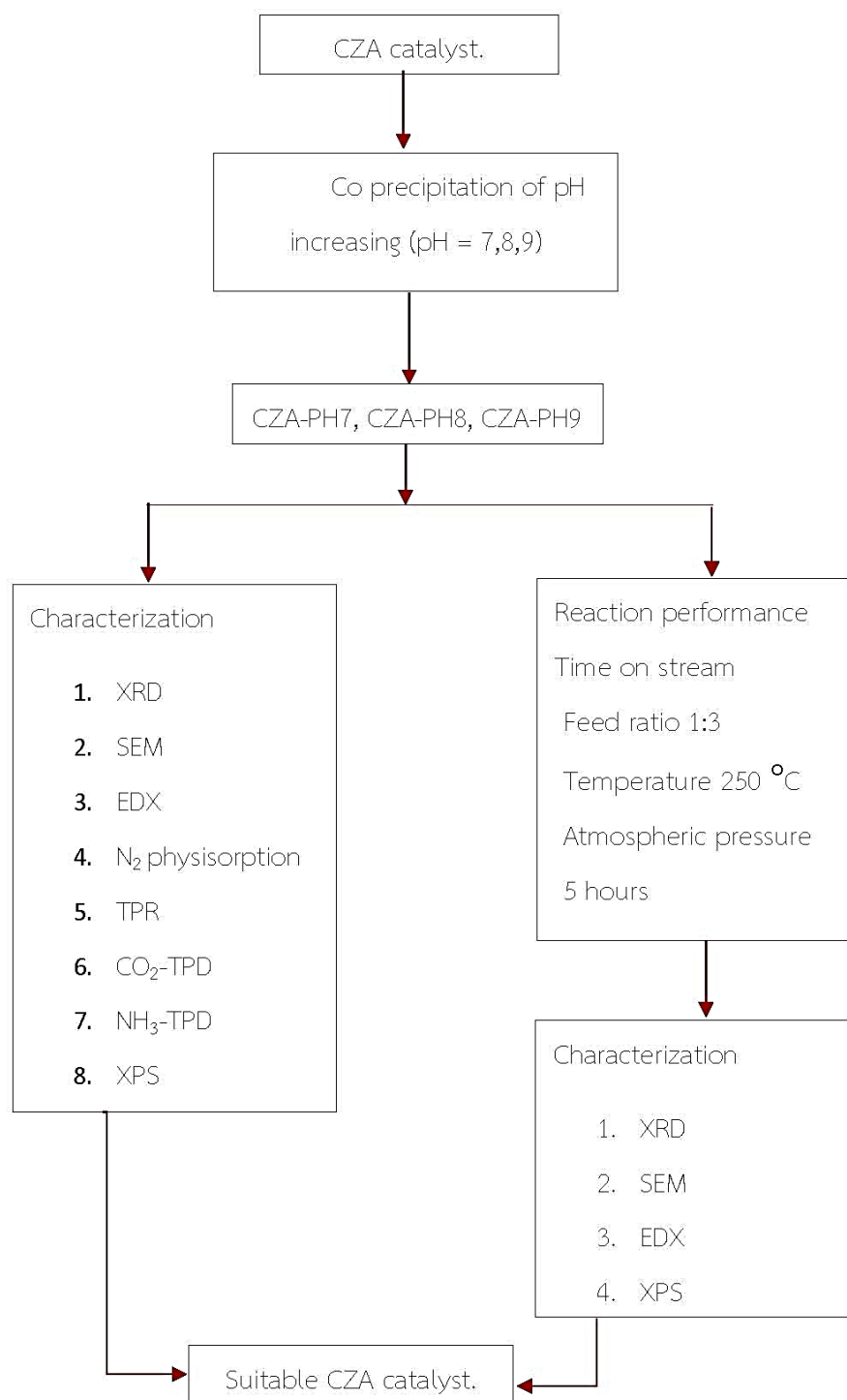
1.3.3 Activity Test

1.3.3.1 Settling the condition by feeding reactants of CO₂:H₂ = 1:3, T = 250 °C for CZA, P = 1 atm, 5 hours.

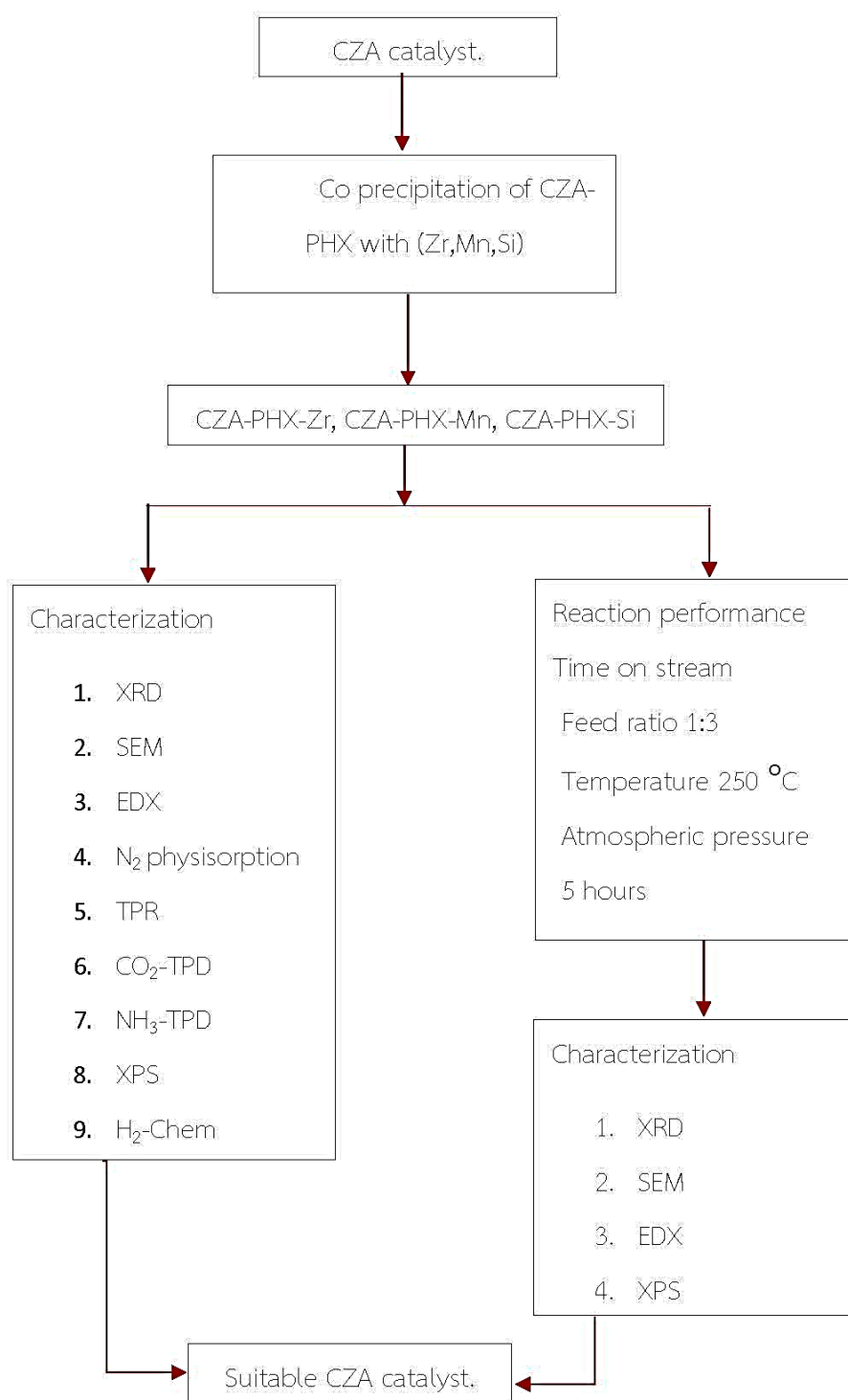
1.3.3.2 Analysis of data by CO₂ conversion and CH₃OH selectivity measured by gas chromatograph (GC).

1.4 Research methodology

Part 1: The suitable condition of differences pH of CZA catalyst.



Part 2: The effect of Zr, Mn, Si modification



1.5 Research plan

Topic	2018		2019	
	1	2	1	2
1. Literature review	→			
2. Lab scale construction	→			
3. Test Lab scale			→	
4. Preparation of differences pH CZA			→	
5. Characterization of differences pH CZA			→	
6. Test reaction of differences pH CZA				→
7. Preparation of CZA-Zr, CZA-Mn, CZA-Si				→
8. Characterization of CZA-Zr, CZA-Mn, CZA-Si				→
9. Test reaction of CZA-Zr, CZA-Mn, CZA-Si				→
10. Thesis writing				→

CHAPTER 2

BACKGROUND AND LITERATURE REVIEW

2.1 The reaction of methanol synthesis via CO₂ hydrogenation

The two major of CO₂ hydrogenation was followed by, (1) CO₂ hydrogenation and (2) Reverse water gas shift (RWGS) reaction. However, the side reaction is appeared by (3) Dehydration of Methanol to dimethyl ether by methanol reactant.



The methanol synthesis via CO₂ hydrogenation is exothermic reaction while RWGS is endothermic reaction. Therefore, the reaction should operate at high temperature for association of CO₂ and reaction with H₂. For another way of methanol synthesis, the CO hydrogenation was occurred by following (4). The high temperature in CO hydrogenation accelerates the deactivation of catalyst.



However, the methanol synthesis via CO₂ hydrogenation was presented in mainly two reaction at low temperature



2.2 Coke formation

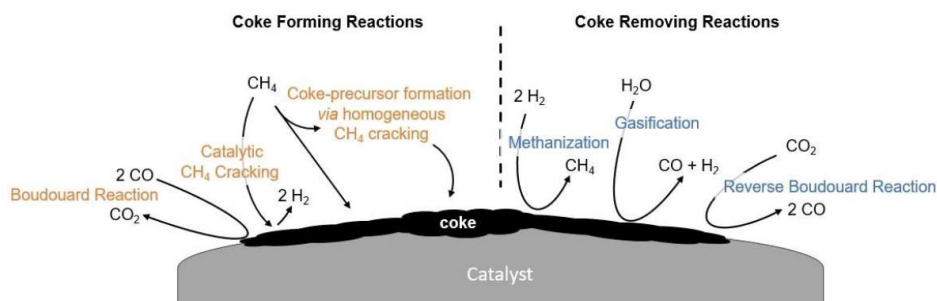
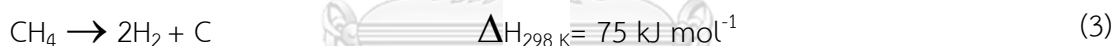
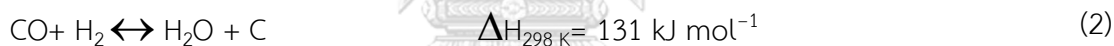
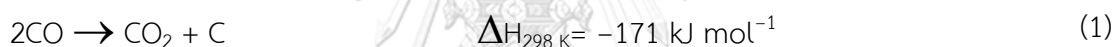


Figure 1 The coke formation and coke removing reactions [6].

Severally, coke appeared at high temperature by effect of reactant gas, such CO, CO₂, CH₃ into catalytic or non-catalytic. The coke formation was identified into three reaction as following, (1) The Boudouard reaction, (2) Reduction of CO, (3) Methane cracking.



The Boudouard reaction was formed at low temperature by approximated CO source, the CO was conversed to CO₂ and carbon graphite based on CO disproportionation. Next reaction, the CO reacted with H₂ at high H₂ feed content. Finally, methane cracking is the most evidence of side reaction of methanol synthesis by supporting of methanation in CO₂ hydrogenation.

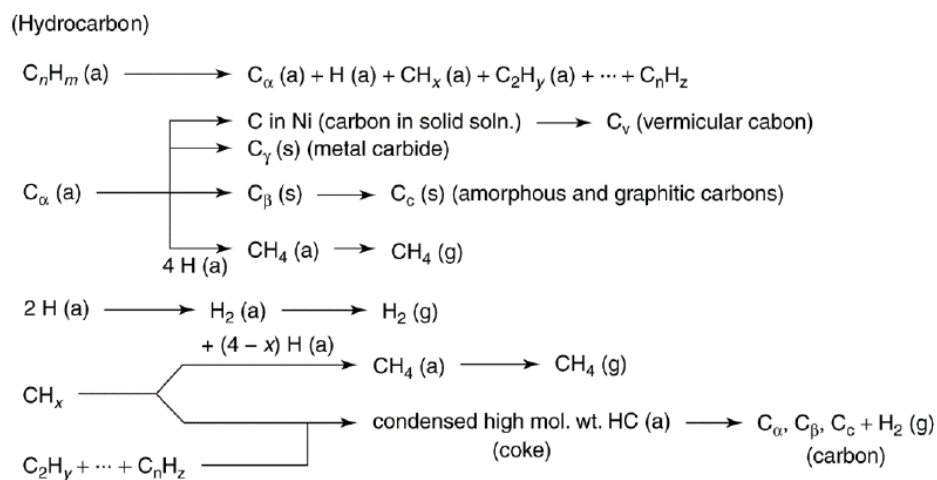


Figure 2 The coke formation from hydrocarbon [7].

In addition, coke formation from hydrocarbon such methane was show in **Figure 2**. The result can discuss undersign of reaction at high content of methane by product. The illustration was supported the type of C_α which property of the first coke development, surface carbine is the general coke on surface catalyst. The accumulation contributes to C_β formation, the amorphous film can develop into approximate temperature range. To avoid this way, the reaction should lowest hydrocarbon and CO, CO₂ limit source.

2.3 Methanol

จุฬาลงกรณ์มหาวิทยาลัย

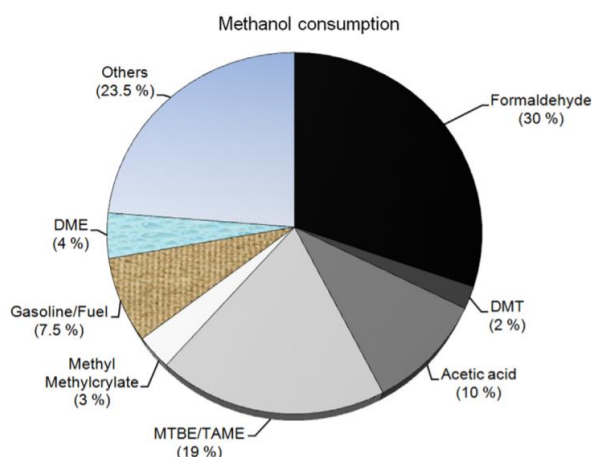
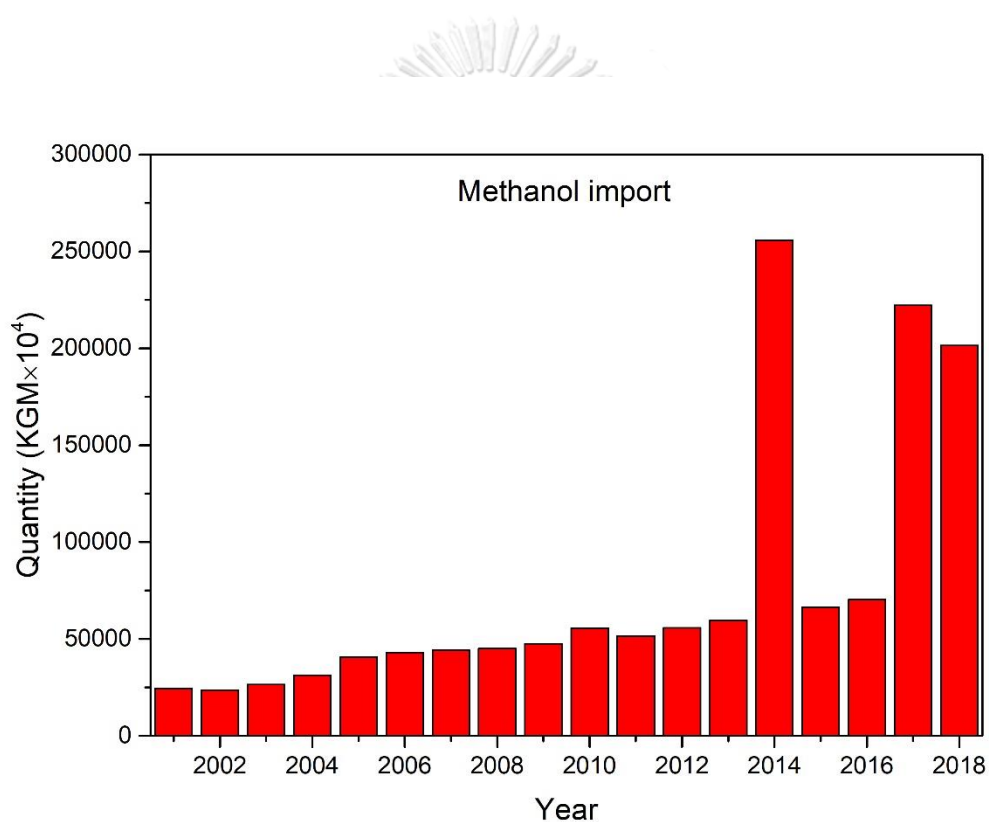


Figure 3 The application of methanol feed stock [8].

Methanol is the main feedstock of industrially. The commercial of methanol production is come from fossil source by CO and few CO₂ content at highly temperature and pressure. Also, the CO₂ hydrogenation can design at atmospheric pressure by suitable catalyst. The application of methanol was show in **Figure 3**, such as fatty acid methyl ester processing (FAME), methyl Tertiary Butyl Ether (MTBE), formaldehyde, acetic acid, methyl methacrylate, dimethyl ether (DME), dimethyltryptamine (DMT) or additive blending for gasoline.



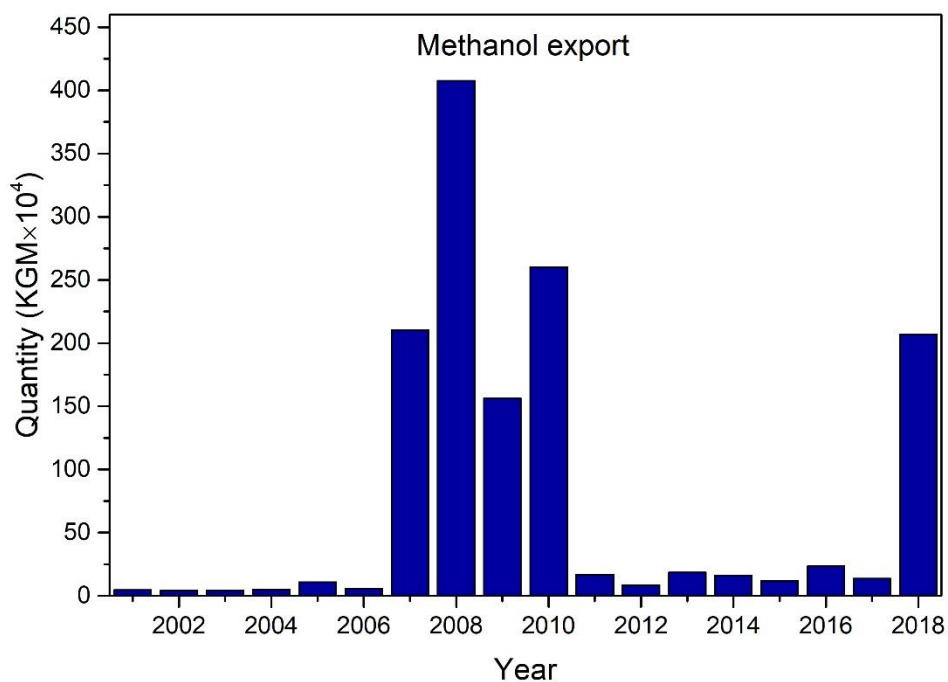


Figure 4 The Thai customer review of methanol importation and exportation.

For Thailand, the methanol importation and exportation were presented by Figure 4, the methanol importation show that the methanol is trend to increase in year 2017, 2018 extremely. The result lead to unlimiting of widely use in methanol application while the methanol exportation has low quantity production.

Table 1 Properties of methanol

Properties	Specification
Chemical formula	CH ₃ OH
Appearance	Colorless liquid
Molar mass	32.04 g/mol
Density	0.792 g/cm ³
Melting point	-97.60 °C
Boiling point	64.70 °C
Vapor pressure	13.02 kPa (at 20 °C)

2.4 Cu, Zn, Al oxide

The Cu-base catalyst was widely use in methanol synthesis. The Cu is the main active site. ZnO is the support of catalyst and promote H₂ adsorption. Al₂O₃ is a third component of CZA used to increase a stability and activity of Cu/ Zn component.

In addition, the CZA catalyst is a commercial catalyst that popular consider in industrial by following the **Table 2**,

Table 2 The review Cu-based in Manufacturer

Manufacturer	Cu	Zn	Al	Other
BASF K3-110	40	40	20	-
ICI 51-2	62	35	3	-
BASF	38.5	48.8	12.9	-
Dupont	50	19	31	-
Haldor Topsoe	>55	21 - 25	8 - 10	-
ICI	20 - 35	15 - 50	4 - 20	-
IFP	45 - 70	15 - 35	4 - 20	-
Lurgi	60 - 70	20 - 30	5 - 15	-
Shell	71	24	-	-
Sud Chemie	65	22	12	-
Alfa Aesar-Johnson Matthey	50.6	22.5	4.6	-
Alfa Aesar- HiFUEL R120	50	25	25	-
AIST & JKK Crop.	68 - 86	45 - 21	2 - 20	-
Hyundai Heavy Industries	40 - 60	25 - 35	5 - 20	-
Co & KR	40 - 60	25 - 35	5 - 20	Zr 1 - 10

2.5 Zirconium

The Zr is the main used in CZA catalyst or photocatalysis. The effect of Zr in methanol synthesis can improve physical property such as Cu dispersion, reduce

crystalline site and increase activity of CZA. The Zr is appeared in metal oxide form, the precursor that most choice for preparation and environment solvent friendly is *Zirconium nitrate*.

Table 3 Properties of Zirconium

Properties	Specification
Chemical formula	Zr(NO ₃) ₄
Appearance	Transparent plates
Molar mass	339.244 g/mol
Density	-
Melting point	°C
Boiling point	Decompose 100 °C
Solubility	Ethanol Hydrolysis with water,

2.6 Manganese

The Mn is the most use in promoter of general catalyst. The basicity of Mn can improve the production of many reaction. The catalyst that relative with basic site is the specially of alcohols such as methanol. By product such as DME, coke, methane is formed by significant acidity of catalyst. Generally, Mn is the favorite nitrate of precursor.

Table 4 Properties of Manganese

Properties	Specification
Chemical formula	Mn(NO ₃) ₂
Appearance	White powder
Molar mass	178.95 g/mol
Density	-
Melting point	37 °C
Boiling point	100 °C

Solubility	Water
------------	-------

2.7 Silica

The high surface area SiO_2 is the most use in support of catalyst. In addition, the Si metal oxide became to modifier of CZA catalyst. The strong interaction was selected to improve stability of catalyst at high temperature. The sintering is the most appearance of temperature effect. However, the SiO_2 can interacted with metal oxide active site of catalyst. The precursor of Si is TEOS in preparation promoter.

Table 5 Properties of Silica

Properties	Specification
Chemical formula	$\text{Si}(\text{OC}_2\text{H}_5)_4$
Appearance	Colorless liquid
Molar mass	208.33 g/mol
Density	0.933 g/mL
Melting point	-77 °C
Boiling point	168 °C
Solubility	Water, Ethanol

2.8 Literature reviews

Table 6 The conditions and significant review

No.	Catalyst, reactor type and reaction condition	Significant result	Reference
1. (2001)	<p>Catalyst : Cu/Zn/Al/Zr</p> <ul style="list-style-type: none"> - Co-precipitation method. - Cu/ZnO/ZrO₂/Al₂O₃ (40/30/25/5 wt.%) - Cu/ZnO/ZrO₂/Al₂O₃ - colloidal silica - Calcined at 600 °C for 2 h. <p>Reactor type : fixed-bed reactor</p> <p>Reaction condition : 250 °C, 50 bar, feed CO₂ (22%), CO (3%) and H₂ (75%)</p> <ul style="list-style-type: none"> - Reduced : gas mixture of H₂ (10%) and He (90%) at 300 °C for 2 h. pressure 50 bar. 	<ul style="list-style-type: none"> - Water produced during methanol synthesis from a CO₂-rich feed accelerated the crystallization of Cu and ZnO contained lead to deactivation of the catalyst. - The case of methanol synthesis from a CO-rich feed, the catalysts both with and without silica were deactivated very little. 	<p>The stability of Cu/ZnO-based catalysts in methanol synthesis from a CO₂-rich feed and from a CO-rich feed [9]</p>
2. (2003)	<p>Catalyst : Mg and Mn oxide additions Cu/ZnO/ZrO₂</p> <ul style="list-style-type: none"> - Decomposing the citrate complexes - Calcinated on air for 1 h at 100, 200, 250 and 300 °C. <p>Reactor type : fixed-bed reactor</p>	<ul style="list-style-type: none"> - The catalytic activity increase by CuZnZr < CuZnZrMg < CuZnZrMn. - Dispersion of Cu determined with the XRD line broadening method and from the reactive adsorption of N₂O increasing. 	<p>Effect of Mg and Mn oxide additions on structural and adsorptive properties of Cu/ZnO/ZrO₂ catalysts for the methanol synthesis from CO₂ [10]</p>

No.	Catalyst, reactor type and reaction condition	Significant result	Reference
3. (2007)	<p>Reaction condition : Pressure 80 bar, temperature 220 °C, GHVS 5400 h⁻¹, reactant mixture H₂:CO₂ = 1:3.</p> <p>- Reduced : 10% H₂ in N₂ at 200 °C under atmospheric pressure for 15 h.</p> <p>Catalyst : Cu/ZnO/Al₂O₃</p> <p>- Homogeneous precipitation using hydrolysis</p> <p>- pH 9.0 controlled by NaOH</p> <p>- Calcined at 300 °C for 3 h in air</p> <p>Reactor type : U-shaped Pyrex glass Reaction condition : CO/H₂O/H₂/CO₂/N₂ (0.77/2.2/4.46/0.57/30 ml min⁻¹) at 700 °C, atmospheric pressure.</p> <p>- Reduced with a mixed gas flow of H₂/N₂ (5/30 ml min⁻¹) at 200 °C for 30 min</p>	<p>- Hp-preparation, a significant Cu leaching was observed, but was effectively suppressed by lowering the aging temperature from 90 to 80 ° C. A main crystal phase in the precursor was always Cu/Zn bimetallic aurichalcite.</p> <p>- The formation of malachite caused a lowering in the activity probably due to its monometallic Cu property</p>	<p>Catalytic behavior of ternary Cu/ZnO/Al₂O₃ systems prepared by homogeneous precipitation in water-gas shift reaction [11]</p>

No.	Catalyst, reactor type and reaction condition	Significant result	Reference
4. (2007)	<p>Catalyst : Cu/Zn/Al/Zr</p> <ul style="list-style-type: none"> - co-precipitation. - calcined at 350 °C for 4 h - pH = 7 <p>Reactor type : fixed-bed reactor</p> <p>Reaction condition : T = 240 °C, P = 40 bar, Sv = 9742 h⁻¹, Feed gas: H₂:CO₂ = 3:1</p> <ul style="list-style-type: none"> - Reduced with a 5%H₂/ 95%N₂ mixture at atmospheric pressure 	<p>- 5 mole% Zr showed the best activity and thermal stability with a methanol STY that was 81% higher than a commercial industrial catalyst.</p>	<p>A Cu/Zn/Al/Zr Fibrous Catalyst that is an Improved CO₂ Hydrogenation to Methanol Catalyst [12]</p>
5. (2007)	<p>Catalyst : Cu-V-Al₂O₃, Cu-V-V-Al₂O₃</p> <ul style="list-style-type: none"> - co-precipitation method. - 12 wt.% Cu, V supported on V-Al₂O₃. - calcination at 500 °C for 4 h. <p>Reactor type : fixed-bed reactor</p> <p>Reaction condition : T =240 °C, P = 30 bar, GHSV = 3600 h⁻¹ and H₂:CO₂ = 3:1 (molar ratio).</p> <ul style="list-style-type: none"> - Pretreated by H₂ at a temperature of 300 °C for 3 h. 	<p>-After addition V, both the catalytic activity of Cu-based catalysts and the selectivity for methanol were improved.</p> <ul style="list-style-type: none"> - The best conditions for reaction for the hydrogenation of CO₂ were as follows: 240 °C, 3600 h⁻¹ and a molar ratio of H₂ to CO₂ of 3:1. 	<p>Study of CO₂ Hydrogenation to Methanol over Cu-V-V-Al₂O₃ Catalyst [13]</p>

No.	Catalyst, reactor type and reaction condition	Significant result	Reference
6. (2007)	<p>Catalyst : Cu/ZnO/ZrO₂</p> <ul style="list-style-type: none"> - Co precipitation - pH 7 - Calcined in air at 350 °C for 2 h. <p>Reactor type : fixed-bed reactor</p> <p>Reaction condition : pressure 30 bar, temperature 230–270 °C, mixing rate 1000 rpm, flow rate 50 mL/min, composition of reactant gas H₂:CO₂ = 3:1</p> <ul style="list-style-type: none"> - Reduced in situ at 300 °C with 50 mL/min of pure H₂ (99.9%) for 4 h under atmospheric 	<ul style="list-style-type: none"> - Increasing of ageing time, the sodium content of the catalyst decreases and finer crystallite structures are formed. - The lower sodium contents and finer crystallite structures the BET surface area and the pore volume in small pores increased and reduction of Cu was facilitated. 	<p>The effect of ageing time on co-precipitated Cu/ZnO/ZrO₂ catalysts used in methanol synthesis from CO₂ and H₂ [14]</p>
7. (2007)	<p>Catalyst : Cu–ZnO/ZrO₂</p> <p>(Zn/Cu at, 0–3 ; ZrO₂, 42–44 wt.%)</p> <ul style="list-style-type: none"> - Co precipitation - Reverse coprecipitation - pH 7.0–7.5 - calcined in air at 350 °C for 4 h. <p>Reactor type : fixed-bed reactor</p>	<ul style="list-style-type: none"> - Basic relationships among surface area, dispersion, and catalyst reducibility point to a strong promoting effect of ZnO on catalyst texture. - The negative effect of water on the rate of methanol formation 	<p>Synthesis, characterization and activity pattern of Cu–ZnO/ZrO₂ catalysts in the hydrogenation of carbon dioxide to methanol [7]</p>

No.	Catalyst, reactor type and reaction condition	Significant result	Reference
	<p>Reaction condition : 160–260 °C and 10–30 bar, CO₂/H₂/N₂ reaction mixture with molar ratio of 3/9/1 was fed at the rate of 40 stp mL/min (GHSV = 4400 NL/(h· kg cat)) or 80 stp mL/min (GHSV = 8800 NL/(h· kg cat))</p> <p>- Reduced at 300 °C for 1 h in H₂ flow (100 stp mL/min) at atmospheric pressure.</p>	<p>accounts for the poorer catalytic performance.</p>	
8. (2008)	<p>Catalyst : CuO/ZnO/Al₂O₃</p> <p>- Co-precipitation</p> <p>- Calcined at 300 °C under air for 3 h (heating ramp 2 °C/min)</p> <p>Reactor type : 49-channel parallel reactor</p> <p>Reaction condition : T = 245 °C, P = 45 bar, 70 vol% H₂, 24 vol% CO, and 6 vol% CO₂.</p> <p>equilibrated for 3 h.</p> <p>- Reduced with a 5% H₂/N₂ mixture at 245 °C</p>	<p>- The following “ preparation history” : precipitation temperature of 70 °C, pH of 6–8, aging time of 20 – 60 min, and calcination at 300 °C.</p> <p>- Calcination temperatures above 300 °C resulted in the formation of pure CuO phases.</p>	<p>Correlations between synthesis, precursor, and catalyst structure and activity of a large set of CuO/ZnO/Al₂O₃ catalysts for methanol synthesis [8]</p>

No.	Catalyst, reactor type and reaction condition	Significant result	Reference
9. (2011)	<p>Catalyst : Cu-MeO_x/Zr_aCe_bO₂ Me/Cu atomic ratio of 0.30–0.35</p> <ul style="list-style-type: none"> - Reverse co-precipitation. - Calcined in air at 350 °C (4 h). <p>Reactor type : fixed-bed reactor</p> <p>Reaction condition : 180–240 °C (P, 30 bar), GHSV = 8.8 ML g⁻¹ h⁻¹ or 80 stp mL/min</p> <ul style="list-style-type: none"> - Reduction temperature at 350 °C for 8 h. 	<ul style="list-style-type: none"> - The effects of ceria promoter and activation atmosphere on the CO₂-hydrogenation functionality of Cu catalysts have been addressed. - ZnO as promoter of both dispersion and catalytic functionality of the metal copper phase. 	<p>Role of the ceria promoter and carrier on the functionality of Cu-based catalysts in the CO₂-to-methanol hydrogenation reaction [9]</p>
10. (2011)	<p>Catalyst : Cu/ZrO₂ catalysts with various La loadings</p> <ul style="list-style-type: none"> - The urea-nitrate combustion method. - Calcined in air at 500 °C for 5 h. <p>Reactor type : fixed-bed reactor</p> <p>Reaction condition : a mixture (CO₂:H₂:N₂ = 22:66:12, molar), pressure to 30 bar, temperature 140 °C</p> <ul style="list-style-type: none"> - Reduce 10% H₂/N₂ 30 mL/min, 300 °C for 3 h. 	<ul style="list-style-type: none"> - The introduction of La, Zr⁴⁺ is substituted partially by La³⁺ and La₂Zr₂O₇ is formed. - Increasing of La loading, the density of basic site of La-ZrO₂ catalysts increase. - Maximum yield is obtained at the La loading of 5%. 	<p>The influence of La doping on the catalytic behavior of Cu/ZrO₂ for methanol synthesis from CO₂ hydrogenation [10]</p>

No.	Catalyst, reactor type and reaction condition	Significant result	Reference
11. (2011)	<p>Catalyst : Cu/ZnO/ZrO₂</p> <ul style="list-style-type: none"> - the urea-nitrate combustion method. - calcined in air at a certain temperature (400–800 °C) for 4 h. <p>Reactor type : fixed-bed reactor</p> <p>Reaction condition : gas mixture (CO₂:H₂ = 1:3, molar ratio), pressure 30 bar, temperature 140 °C.</p> <ul style="list-style-type: none"> - Reduced in a stream of 10% H₂/N₂ at 300 °C for 3 h under atmospheric pressure. 	<ul style="list-style-type: none"> - The physicochemical properties and catalytic activity of the catalysts are strongly influenced by the calcination temperature. - the phase transformation of zirconia from tetragonal to monoclinic occurs as the calcination temperature exceeds 600 °C. 	<p>CO₂ hydrogenation to methanol over Cu/ZnO/ZrO₂ catalysts prepared via a route of solid-state reaction [11]</p>
12. (2011)	<p>Catalyst : Cu-Zn-Zr</p> <ul style="list-style-type: none"> - Co precipitation by NaHCO₃ (CB). - Complexation by citric acid (CT). - Geloxalate co-precipitation (OX). <p>Reactor type : fixed-bed reactor</p> <p>Reaction condition : CO₂/H₂/N₂ = 3/9/1) in the temperature range 180–240 °C, 30 bar.</p>	<ul style="list-style-type: none"> - Irrespective of a high Cu loading (60 wt.%), the preparation conditions significantly affect structure, surface properties and redox behavior. 	<p>The changing nature of the active site of Cu-Zn-Zr catalysts for the CO₂ hydrogenation reaction to methanol [12]</p>

No.	Catalyst, reactor type and reaction condition	Significant result	Reference
13. (2011)	<p>Catalyst : CuO–ZnO–Al₂O₃ add TiO₂</p> <ul style="list-style-type: none"> - Co precipitation - (CuO/ZnO/Al₂O₃ = 5/4/1 with TiO₂ mass ratio x = 0, 2, 4, 6 and 8) - Calcined in air 50 °C for 4 h. <p>Reactor type : fixed-bed reactor</p> <p>Reaction condition : temperature 230 °C, H₂/CO₂ = 3, 26 bar</p> <ul style="list-style-type: none"> - Reduced by hydrogen (10% in nitrogen) at 260 °C and an atmospheric pressure for 2 h. 	<ul style="list-style-type: none"> - TiO₂ is improved CuO dispersion and enhanced the adsorption on the surface of catalyst, leading to easier reduction of CuO and lower concentration of strong acid sites. - TiO₂ can enhance the dispersion of CuO and ZnO in the catalyst, leading to better adsorption CO₂. 	<p>Effect of promoter TiO₂ on the performance of CuO–ZnO–Al₂O₃ catalyst for CO₂ catalytic hydrogenation to methanol [13]</p>
14. (2012)	<p>Catalyst : CuO/ZnO/Al₂O₃/M = 5/4/1/0.02 (M represents SiO₂, TiO₂ or SiO₂-TiO₂, SiO₂/TiO₂ = 1/1, mass ratio)</p> <ul style="list-style-type: none"> - Co-precipitation method - Calcined at 350 °C for 4 h <p>Reactor type : a tubular stainless steel, fixed-bed reactor</p> <p>Reaction condition : T = 260 °C, P = 26 bar,</p>	<ul style="list-style-type: none"> - CuO-ZnO-Al₂O₃ catalysts modified with SiO₂, TiO₂ or SiO₂-TiO₂ exhibited better catalytic performances than the catalyst without promoter. - SiO₂, TiO₂ or SiO₂-TiO₂ enhanced CuO dispersion in the catalyst body. 	<p>Effect of promoter SiO₂, TiO₂ or SiO₂-TiO₂ on the performance of CuO-ZnO-Al₂O₃ catalyst for methanol synthesis from CO₂ hydrogenation [5]</p>

No.	Catalyst, reactor type and reaction condition	Significant result	Reference
15. (2013)	<p>$H_2:CO_2 = 3:1$ (volume ratio) and $SV = 3600 \text{ hr}^{-1}$.</p> <ul style="list-style-type: none"> - Reduced at $270 \text{ }^\circ\text{C}$ and atmospheric pressure for 2 h by a hydrogen stream (10 vol.% H_2/N_2) <p>Catalyst : Hydrotalcite-like compounds with mol% ratios of $Cu:Zn:Al = 50:25:25$ and $Cu:Zn:Al:X = 50:25:22.5:2.5$ (X represents Mn, La, Ce, Zr and Y)</p> <ul style="list-style-type: none"> - co-precipitation method - The pH 10.0 ± 0.2. - Calcined in air at $500 \text{ }^\circ\text{C}$ for 4 h. <p>Reactor type : fixed-bed reactor</p> <p>Reaction condition : $230\text{--}270 \text{ K}$, $50 \text{ }^\circ\text{C}$, $H_2:CO_2 = 3:1$ (molar ratio), $GHSV = 12,000 \text{ mL gcat}^{-1} \text{ h}^{-1}$.</p> <ul style="list-style-type: none"> - Reduction at $300 \text{ }^\circ\text{C}$ for 8 h. 	<ul style="list-style-type: none"> - Promoter $SiO_2\text{-}TiO_2$ showed well performance than SiO_2 or TiO_2. <ul style="list-style-type: none"> - The modifier (Mn, La, Ce, Zr and Y) leads to higher BET specific surface area, Cu surface area and Cu dispersion. - The Mn, La, Ce, Zr and Y is favorable for the production of methanol. - The Y- and Zr-modified Cu/Zn/Al catalysts exhibit the highest CO_2 conversion and CH_3OH selectivity. 	<p>Influence of modifier (Mn, La, Ce, Zr and Y) on the performance of Cu/Zn/Al catalysts via hydrotalcite-like precursors for CO_2 hydrogenation to methanol [4]</p>

No.	Catalyst, reactor type and reaction condition	Significant result	Reference
16. (2013)	<p>Catalyst : Cu/Zn/Al/Zr</p> <ul style="list-style-type: none"> - The $\text{Cu}^{2+}:\text{Zn}^{2+}:(\text{Al}^{3+}+\text{Zr}^{4+})$ atomic ratio 2:1:1 $\text{Zr}^{4+}:\text{Al}^{3+}$ atomic composition 0:1 to 0.7:0.3. - co-precipitation method - pH 10.0 ± 0.2. - Calcined $500\text{ }^\circ\text{C}$ for 4 h. <p>Reactor type : fixed-bed reactor</p> <p>Reaction condition : $230\text{--}270\text{ }^\circ\text{C}$, 50 bar, $n(\text{H}_2):n(\text{CO}_2) = 3:1$, and GHSV = 4000 h^{-1}.</p> <ul style="list-style-type: none"> - Reduced in pure H_2 at a flow rate of 80 mL min^{-1} under atmospheric pressure. 	<ul style="list-style-type: none"> - The pure and crystalline Cu/Zn/Al/Zr hydrotalcite-like compounds can be formed by the replacement of Al^{3+} with Zr^{4+}. - Increasing of $\text{Zr}^{4+}:(\text{Al}^{3+}+\text{Zr}^{4+})$ atomic ratio, exposed Cu surface area and the dispersion of Cu. - The best performance is obtained with $\text{Zr}^{4+}/(\text{Al}^{3+}+\text{Zr}^{4+}) = 0.3$. 	<p>Influence of Zr on the performance of Cu/Zn/Al/Zr catalysts via hydrotalcite-like precursors for CO_2 hydrogenation to methanol [15]</p>
17. (2013)	<p>Catalyst : CuZnCe, CuZnZr, Cu-ZnO</p> <ul style="list-style-type: none"> - Reverse coprecipitation under ultrasound irradiation. - Varied calcine temperature. <p>Reactor type : fixed-bed reactor</p> <p>Reaction condition : $180\text{--}240\text{ }^\circ\text{C}$ and at 1–50 bar , $\text{CO}_2/\text{H}_2/\text{N}_2$ (23/69/8) mixture at a rate of 80–500</p>	<ul style="list-style-type: none"> - The suitable condition on Cu-ZnO/ZrO₂ system, at 10% of CO_2 conversion per pass ($T = 240\text{ }^\circ\text{C}$; P = 50 bar). 	<p>Effects of oxide carriers on surface functionality and process performance of the Cu-ZnO system in the synthesis of methanol via CO_2 hydrogenation [16]</p>

No.	Catalyst, reactor type and reaction condition	Significant result	Reference
18. (2013)	<p>Catalyst : CuZnCe, CuZnZr, CuZnAl</p> <ul style="list-style-type: none"> - Reverse co-precipitation under ultrasounds irradiation <p>Reactor type : fixed-bed reactor</p> <p>Reaction condition : 180–240 °C at 30–50 bar using a gas–liquid feed automated plant.</p> <p>CO₂/H₂/N₂ (23/69/8) mixture. (GHSV, 8800–55,000 NL kgcat⁻¹ h⁻¹) 80–500 STP mL/min.</p> <ul style="list-style-type: none"> - Reduced at 300 °C in H₂ flow (100 stp mL/min) at atmospheric pressure (1 h) 	<ul style="list-style-type: none"> - Oxide carrier controls texture and adsorption properties of the Cu–ZnO system. - Methanol is a primary reaction product at low temperature and extent of CO₂ conversion. - The catalytic activity depends on a synergism of metal and basic oxide sites, pointing to a dual-site reaction path. 	<p>How oxide carriers control the catalytic functionality of the Cu–ZnO system in the hydrogenation of CO₂ to methanol [17]</p>
19. (2013)	<p>Catalyst : Fluorine-modified Cu/Zn/Al catalyst</p> <ul style="list-style-type: none"> - co-precipitation method. - Cu²⁺:Zn²⁺:Al³⁺ = 2:1:1 - The pH 10.0 ± 0.2. - calcined in air at 500 °C for 4 h. <p>Reactor type : fixed-bed reactor</p> <p>Reaction condition : 230–270 K, 50 bar,</p>	<ul style="list-style-type: none"> - The pure and fluorine-modified Cu/Zn/Al catalysts were synthesized by calcination of the corresponding Cu/Zn/Al HTICs and tested for the CO₂ hydrogenation to methanol. - Fluorine-modified Cu/Zn/Al 	<p>Influence of fluorine on the performance of fluorine-modified Cu/Zn/Al catalysts for CO₂ hydrogenation to methanol [18]</p>

No.	Catalyst, reactor type and reaction condition	Significant result	Reference
	<p>n(H₂):n(CO₂) = 3:1, GHSV = 4000 h⁻¹ .</p> <p>- Reduce at 330 °C for 8 h.</p>	<p>catalyst had the higher CH₃OH yield compared with the fluorine-free catalyst.</p>	
20. (2014)	<p>Catalyst : Zr-doped Cu-Zn-Zr-Al (CZZA)</p> <p>CZA (Cu/ZnO/Al₂O₃ = 4/3/3), CZZA (Cu/ZnO/ZrO₂/Al₂O₃ = 4/3/1.5/1.5), CZZ (Cu/ZnO/ZrO₂ = 4/3/3) by weight.</p> <p>- Co-precipitation method</p> <p>- Final pH of 7</p> <p>- Calcined in air at 400 °C for 5 h.</p> <p>Reactor type : fixed-bed reactor</p> <p>Reaction condition : 30 bar; 230 °C; H₂/CO₂ = 3/1, W/F = 10 g cat• h/mol.</p> <p>- Reduced in the flow of 5% H₂ in nitrogen at 250 °C for 4 h</p>	<p>- The doped Zr in Cu-Zn based catalyst promoted the hydrogen reduction of oxidized Cu surface, generated by water vapor to increase the concentration of metallic Cu, which is the active site for the methanol formation.</p>	<p>Development of highly stable catalyst for methanol synthesis from carbon dioxide [19]</p>

No.	Catalyst, reactor type and reaction condition	Significant result	Reference
21. (2014)	<p>Catalyst : La-M-Cu-Zn-O (M = Y, Ce, Mg, Zr)</p> <ul style="list-style-type: none"> - Sol-gel method. - Calcined under air at 400 °C for 2 h <p>Reactor type : fixed-bed reactor</p> <p>Reaction condition : 250 °C, 50 bar, n(H₂):n(CO₂) = 3:1, GHSV = 3600 h⁻¹.</p> <ul style="list-style-type: none"> - Reduction at 350 °C for 8 h. 	<ul style="list-style-type: none"> - The addition of Ce, Mg and Zr, catalysts with smaller particles, lower reduction temperature, higher Cu dispersion, larger amount of hydrogen desorption at low temperature and higher concentration of basic sites. 	<p>Methanol synthesis from CO₂ hydrogenation over La-M-Cu-Zn-O (M = Y, Ce, Mg, Zr) catalysts derived from perovskite-type precursors [20]</p>
22. (2014)	<p>Catalyst : Cu-Zn-Al catalyst</p> <ul style="list-style-type: none"> - Reverse precipitation method. - Cu : Zn : Al = 6.75 : 2.25 : 1 - Calcined at 350 °C for 4 h - The pH = 7.0–7.5. <p>Reactor type : fixed-bed reactor</p> <p>Reaction condition : CO : H₂ : CO₂ : N₂ (volume ratio) = 14 : 76 : 5 : 5, 50 bar, 225 °C, and the space velocity of 10,000 h⁻¹.</p>	<ul style="list-style-type: none"> - The test results show that the modified ternary Cu-Zn-Al catalysts with binary Cu-Zn precursor exhibit higher space time yields. - The characterization results indicate that the addition of binary Cu-Zn precursor optimized the ratio of Cu⁰ to Cu⁺ in the modified ternary Cu-Zn-Al catalyst. 	<p>Promoting effect of a Cu-Zn binary precursor on a ternary Cu-Zn-Al catalyst for methanol synthesis from synthesis gas [21]</p>

No.	Catalyst, reactor type and reaction condition	Significant result	Reference
23. (2015)	<p>Catalyst : Au/Cu-Zn-Al, Cu-Zn-Al</p> <ul style="list-style-type: none"> - Cu-Zn-Al (2:1:1) - The target gold loadings were 0.5, 1 and 3 wt. % - Co-precipitation method - pH 10–10.5 by injecting the 0.5 M Na₂CO₃ solution <p>The target gold loadings were 0.5, 1 and 3 wt. %</p> <ul style="list-style-type: none"> - Deposition– precipitation (DP) method - Calcined at 350 °C for 12 h under static air. <p>Reactor type : stainless steel tube reactor</p> <p>Reaction condition : 200 °C, H₂/CO₂ = 3/1</p> <ul style="list-style-type: none"> - treated with hydrogen gas at 300 °C for 2 h 	<ul style="list-style-type: none"> - The CZA composition promoted by 1 wt.% gold showed the highest of CO₂ conversion (28.0% mass) and methanol yield (16.6% mass) at H₂:CO₂ = 6:1 and GHSV 7000 h⁻¹. - The cooperative behavior between copper and gold exists in the form of copper–gold interface. The hydrogen spillover and enhanced adsorption capacities for CO and H₂ 	<p>Studies on Au/Cu-Zn-Al catalyst for methanol synthesis from CO₂ [3]</p>
24. (2015)	<p>Catalyst : CuO/ZnO</p> <p>Filament-like ZnO and rod-like ZnO</p> <ul style="list-style-type: none"> - Cu/Zn atomic ratio of 2 <p>Reactor type : fixed-bed reactor</p> <p>Reaction condition : 240 °C, 30 bar, 0.54 mol/(g-cat h) and molar feed composition of CO₂/H₂ = 1/3.</p>	<ul style="list-style-type: none"> - The CZ-filament has stronger interactions between ZnO and Cu, and more oxygen vacancies due to more exposed polar (002) face in filament-like ZnO, which exhibits the higher activity 	<p>Hydrogenation of CO₂ to CH₃OH over Cu/ZnO catalysts with different ZnO morphology [22]</p>

No.	Catalyst, reactor type and reaction condition	Significant result	Reference
25. (2016)	<p>- Reduced in H₂ flow at 270 °C for 1 h under atmospheric pressure.</p> <p>Catalyst : CuO/ZnO/Al₂O₃ Cu/Zn/Al atomic ratio 60/25/15</p> <ul style="list-style-type: none"> - Mechanical milling and combustion method - The pH 7.5–8.0. <p>Reactor type : fixed-bed reactor</p> <p>Reaction condition : 240 °C, 30 bar, 3600 h⁻¹ and molar feed composition of CO₂/H₂ = 1/3.</p> <ul style="list-style-type: none"> - Reduced in H₂ flow at 270 °C for 1 h under atmospheric pressure. 	<ul style="list-style-type: none"> - It is found that the combustion processes and physicochemical properties of catalysts depend strongly on the type and amount of fuel. - CZA-C-1.25 catalyst shows the highest catalytic activity for the hydrogenation of CO₂ to methanol. 	<p>Hydrogenation of CO₂ to CH₃OH over CuO/ZnO/Al₂O₃ catalysts prepared via a solvent-free routine [23]</p>
26. (2016)	<p>Catalyst : CZZA/rGO (graphene oxide)</p> <ul style="list-style-type: none"> - Co-precipitation method. - CuO/ZnO/ZrO₂/ Al₂O₃ mass ratio of 4/3/1.5/1.5 - Calcined at 400 °C for 5 h in air - The pH 7 <p>Reactor type : fixed-bed reactor</p> <p>Reaction condition : temperature 200 to 280 °C,</p>	<ul style="list-style-type: none"> - The CZZA/rGO catalysts showed only Cu and Cu₂O diffraction peaks because rGO provided a reducing atmosphere during the catalyst preparation process. - The H₂ and CO₂ adsorption increased with the use of rGO. 	<p>A graphene-supported copper-based catalyst for the hydrogenation of carbon dioxide to form methanol [24]</p>

No.	Catalyst, reactor type and reaction condition	Significant result	Reference
	<p>pressure range from 10 to 20 bar, space velocity range from 6075 to 10935 h⁻¹ using CO₂/H₂ (1/3)</p> <ul style="list-style-type: none"> - Reduced in the flow of 10% H₂/N₂ [100 cm³ (STP)/min] at 250 °C for 2 h. 		
27. (2016)	<p>Catalyst : Cu/Zn/Al/Zr, fluorine-modified Cu/ZnO/ Al₂O₃/ZrO₂</p> <ul style="list-style-type: none"> - Co-precipitation method. - Cu:Zn:Al:Zr = 2:1:0.7:0.3 - Calcined in air at 500 °C for 4 h. - The pH = 10.0 ± 0.2. <p>Reactor type : fixed-bed reactor</p> <p>Reaction condition : 230 °C, 50 bar, GHSV= 8500 mL gcat⁻¹ h⁻¹ and H₂/CO₂/N₂ = 73/24/3.</p> <ul style="list-style-type: none"> - Reduced in situ in pure H₂ under atmospheric pressure at 280 °C for 6 h. 	<ul style="list-style-type: none"> - The fluorine-modified Cu/ZnO/Al₂O₃/ZrO₂ catalysts with different fluorine content were then obtained by calcination and reduction of fluorinated hydrotalcite. - Cu/ZnO/Al₂O₃/ZrO₂ catalysts greatly improved the fraction of strongly basic sites, and then dramatically increased the CH₃OH selectivity. When F/Al > 0.83. 	<p>Fluorinated Cu/Zn/Al/Zr hydrotalcites derived nanocatalysts for CO₂ hydrogenation to methanol [25]</p>

No.	Catalyst, reactor type and reaction condition	Significant result	Reference
28. (2017)	<p>Catalyst : $\text{Cu/ZnO/Al}_2\text{O}_3/\text{ZrO}_2$, $\text{Cu}^{2+}:\text{Zn}^{2+}:\text{Al}^{3+}:\text{Zr}^{4+}$ = 2:1:1.2:0.1</p> <ul style="list-style-type: none"> - Co-precipitation method at 293 K - pH range of 6.0–11.0 - Calcined in air at 500 °C for 5 h. <p>Reactor type : fixed-bed reactor</p> <p>Reaction condition : 190 °C, 50 bar, $\text{H}_2/\text{CO}_2/\text{N}_2$ = 73/24/3, GHSV = 4000 h^{-1}.</p> <ul style="list-style-type: none"> - Reduced in pure H_2 at a flow-rate of 80 mL min^{-1} under atmospheric pressure. 	<ul style="list-style-type: none"> - Zincian malachite was formed as the main phase at the low pH, and both zincian malachite and HTL phases detected at pH 8. - Compared with the material resulting for well-crystallized zincian malachite (pH 7.0), the BET specific surface area and Cu surface area from phase-pure hydroxalcite precursors (pH \geq 9). 	<p>Highly efficient Cu-based catalysts via hydroxalcite-like precursors for CO_2 hydrogenation to methanol [26]</p>
29. (2017)	<p>Catalyst : $\text{CuO/ZnO/Al}_2\text{O}_3$ catalysts</p> <ul style="list-style-type: none"> - ammonia deposition-precipitation (ADP) method - $\text{CuO/ZnO/ZrO}_2/\text{Al}_2\text{O}_3$ mass ratio of 4/3/1.5/1.5 - calcined at 350 °C in air for 4 h. - The pH of the suspension was 11–12 <p>Reactor type : fixed-bed reactor</p> <p>Reaction condition : 40 bar, $\text{H}_2/\text{CO}_2/\text{N}_2$ = 73/24/3, and WHSV= 1500 $\text{mL gcat}^{-1}\text{h}^{-1}$</p>	<ul style="list-style-type: none"> - The increasing of metal loading, the amount, size and thickness of layered particles increased - maximum for the catalyst with Cu and ZnO 33.61 wt.-%. - The CO_2 conversion and yield increased with the increase of the weight of Cu and ZnO. 	<p>Preparation and CO_2 hydrogenation catalytic properties of alumina microsphere supported Cu-based catalyst by deposition-precipitation method [27]</p>

No.	Catalyst, reactor type and reaction condition	Significant result	Reference
30. (2018)	<p>- Reduced at 240 °C under atmospheric pressure for 6 h in pure H₂ at a flow rate of 80 mL min⁻¹.</p> <p>Catalyst : CuO/ZnO/Al₂O₃</p> <p>- Co-precipitation.</p> <p>- Calcination at 320 °C for 3 h.</p> <p>- The pH = 7</p> <p>Reactor type : fixed-bed reactor</p> <p>Reaction condition : The feed gas (100 mL/min) consisted of 81.11 vol% H₂, 9.94 vol% CO, and 8.95 vol% CO₂. 50 bar and 250 °C.</p> <p>- Reducing gas mixture (5% H₂ in 95% N₂) at 240 °C and atmospheric pressure for 12 h.</p>	<p>- The most active catalyst was obtained at CuO/ZnO = 2.7 and CuO/Al₂O₃ = 9.</p> <p>- CuO/ZnO = 1.8 compared to the best synthesized sample, contains interwoven nano-twins consisting of four different species.</p>	<p>Component ratio dependent</p> <p>Cu/Zn/Al structure sensitive catalyst in CO₂/CO hydrogenation to methanol [28]</p>
31. (2019)	<p>Catalyst : CuO/ZnO/ZrO₂@SBA-15</p> <p>- Co-precipitation method at 20 °C</p> <p>- pH range of 6.0–11.0</p> <p>- Calcined in air at 500 °C for 5 h.</p> <p>Reactor type : fixed-bed reactor</p> <p>Reaction condition : (CO₂:H₂:N₂ = 22.5:67.5:10</p>	<p>- CuO/ZnO/ZrO₂@SBA-15 composites with good for methanol synthesis from CO₂ hydrogenation by impregnation-sol-gel auto combustion approach with different active</p>	<p>Highly efficient</p> <p>CuO/ZnO/ZrO₂@SBA-15 nano catalysts for methanol synthesis from the catalytic hydrogenation of CO₂ [29]</p>

No.	Catalyst, reactor type and reaction condition	Significant result	Reference
	<p>pressure at 30 bar.</p> <ul style="list-style-type: none"> - Reduced 10% v/v H₂/N₂ at 300 °C for 2 h under atmospheric pressure. 	<p>Cu/Zn molar ratio (1.0 and 2.5 mol mol⁻¹).</p> <ul style="list-style-type: none"> - The results of 50 h high performance and stability for CZZS_20_1 catalyst. 	
32. (2020)	<p>Catalyst : A Zr-modified CuO/ZnO/Al₂O₃ (CZZA) catalyst, CuO/ZnO/ZrO₂/Al₂O₃</p> <ul style="list-style-type: none"> - Co-precipitation - Calcined at 500 °C for 5 h <p>Reactor type : fixed-bed reactor</p> <p>Reaction condition : 200–260 °C, with pressure of 27.6 bar, 6 mL/min CO₂, 18 mL/min H₂, and space velocity of 823 h⁻¹. The long-term stability tests for methanol synthesis were conducted at 220 °C, 27.6 bar, 6 mL/min CO₂, 18 mL/min H₂, and 823 h⁻¹ space velocity.</p> <ul style="list-style-type: none"> - Reduced at 250 °C for 10 h, with 20 mL/min of pure H₂ 	<ul style="list-style-type: none"> - Zr modified CZA catalysts were synthesized by the co-precipitation method. The effects of Al and Zr loading were investigated in both methanol and DME synthesis from CO₂ hydrogenation. - The optimized catalyst composition for methanol and DME synthesis was 4:2:1:0.5 for an atomic ratio of Cu/Zn/Zr/Al. 	<p>Enhanced catalytic performance of Zr modified CuO/ZnO/Al₂O₃ catalyst for methanol and DME synthesis via CO₂ hydrogenation [30]</p>

Gao, Li et al. 2013. [4] studied the effect of Mn, La, Ce, Zr and Y promoter on CZA catalysts via CO₂ hydrogenation. The CO₂-TPD was suggested the surface basicity of CZA in three type of surface basic site.

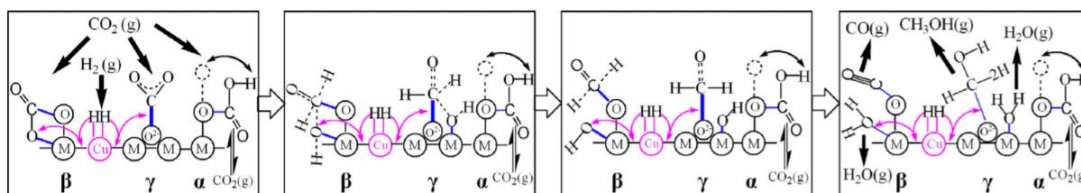


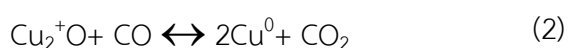
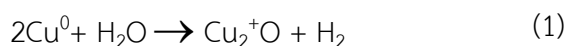
Figure 5 The reduced surface of the catalysts via hydrotalcite-like precursors and the functionality of the various surface sites for CO₂ hydrogenation to methanol.

Zhang, Zhang et al. 2012. [5] studied the addition of TiO₂, SiO₂, TiO₂-SiO₂ on CZA catalysts, the results showed that,

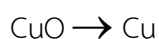
- (1) TiO₂-SiO₂ can improve dispersion of CuO, ZnO and well BET surface area. In the same way, the highly dispersion of ZnO has a benefit to CuO-ZnO interaction.
- (2) TiO₂-SiO₂ lead to increasing of CuO reduction temperature.

Baltes, C., et al. (2008). [8] investigated the “preparation history” of co-precipitation at 70 °C and pH of 6-8, aging time 20-60 min and calcination at 300 °C. The results showed that the postprecipitation can confirm in strong activity of catalyst and hydroxy carbonates is occur 20 min ca.

Atake, Nishida et al. 2007. [11] investigated the active sites on the homogeneous of CZA catalysts as following reduction-oxidation between Cu⁰ to Cu⁺



Li, Yuan et al. 2014. [19] studied the reducibility of CuO by TPR characterization. The main peak of CuO is appeared at 250 °C by following





In addition, the Zr promoter can improve the surface area of CZA catalyst by following the BET surface area $106.3 \text{ m}^2/\text{g}$ and small pore diameter 16.6 nm .

Wu, Saito et al. 2001 [31] studied the colloidal silica and metal oxide Mn, Ga, Zr. The addition of SiO_2 affected in physical properties such increasing of surface area and prevented deactivation of catalysts.

Wang, Zhao et al. 2011 [32] studied the CZA catalyst via decomposition preparation of $\text{M}(\text{Cu,Zn})$ -ammonia. The significant results show that the XRD of before calcination and after calcination have different phase by precursor show Aurichalcite and Malachite. While, the XRD after calcination show the CuO , ZnO . The evidence was conclusion in phase transformation in calcination process.

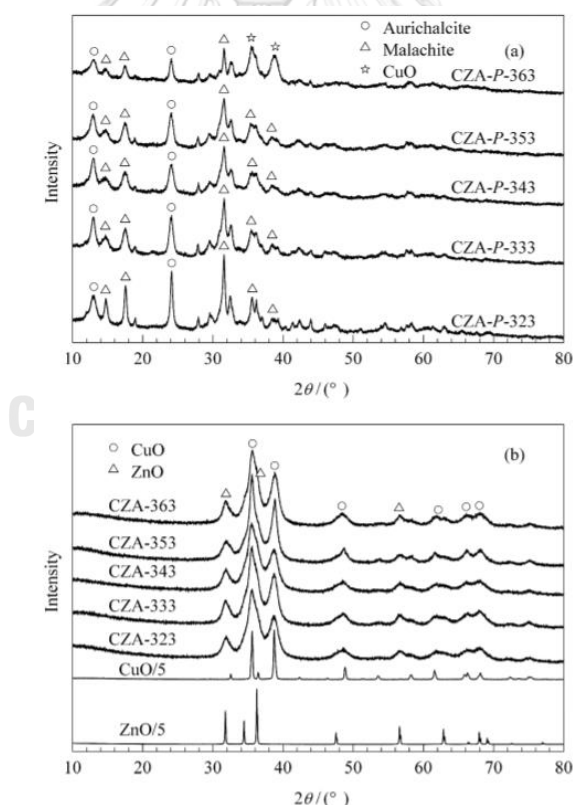


Figure 6 XRD patterns of $\text{Cu/ZnO/Al}_2\text{O}_3$ catalyst (a) before calcination, (b) after calcination

Chapter 3

EXPERIMENT

This chapter is divided into three sections. Firstly, the preparation is presented by different synthesis of CZA via co-precipitation method and promoting with Zr, Mn, Si metal oxide into CZA catalyst. After that, the physical and chemical properties of each catalyst was characterized by X-ray diffraction (XRD), scanning electron microscope (SEM), energy-dispersive X-ray spectroscopy (EDX), N_2 physisorption, temperature-programmed reduction (TPR, temperature-programmed desorption of carbon dioxide (CO_2 -TPD), temperature-programmed desorption of ammonia (NH_3 -TPD) for basicity or acidity, and X-ray Photoelectron spectroscopy (XPS) for chemical states. Finally, the performance of catalysts was determined by activity test. The results were presented in activity and stability of catalysts.

3.1 Catalysts preparation

Table 7 List of chemical prepared catalyst

Chemicals	Formula	Grade	Manufacture
Aluminum nitrate nonahydrate	$Al(NO_3)_3 \cdot 9H_2O$	$\geq 98\%$	Sigma- Aldrich
Zinc nitrate hexahydrate	$Zn(NO_3)_2 \cdot 6H_2O$	98%	Sigma- Aldrich
Copper(II) nitrate hemi(pentahydrate)	$Cu(NO_3)_2 \cdot 2.5H_2O$	98%	Sigma- Aldrich
Zirconium(IV) oxynitrate hydrate	$ZrO(NO_3)_2 \cdot xH_2O$	99%	Sigma- Aldrich
Manganese(II) nitrate tetrahydrate	$Mn(NO_3)_2 \cdot 4H_2O$	$\geq 97\%$	Sigma- Aldrich
Tetraethyl orthosilicate	$Si(OC_2H_5)_4$	$\geq 96\%$	TCl japan
Sodium hydrogen carbonate	$NaHCO_3$	-	Sigma- Aldrich

3.1.1 Preparation of different pH affected of CZA

The CZA was prepared by co-precipitation method. The metal oxide was synthesized by nitrate precursors including $Cu(NO_3)_2 \cdot 2.5H_2O$, $Zn(NO_3)_2 \cdot 6H_2O$,

$\text{Al}(\text{NO}_3)_3 \cdot 9\text{H}_2\text{O}$. The catalyst was prepared by mixing of DI water as solvent at 80 °C. The weight ratio of Cu:Zn:Al is 40:40:20. The NaHCO_3 was dropped into precursor solution for adjusting of different pH at 7,8, and 9. The mixture solution was stirred for 120 min. The precipitate solution was centrifuged and filtered DI water out. The cake in co-precipitation was dried overnight at 110 °C. The dried cake was calcined at 300 °C around 3 hours.

3.1.2 Preparation of modifier CZA-Zr, CZA-Mn, CZA-Si

The Zr, Mn, Si promoters were doped into approximate CZA in part 3.2.1. by co-precipitation method. Each precursor modifier was prepared using $\text{ZrO}(\text{NO}_3)_2 \cdot x\text{H}_2\text{O}$, $\text{Mn}(\text{NO}_3)_2 \cdot 4\text{H}_2\text{O}$, and $\text{Si}(\text{OC}_2\text{H}_5)_4$. The catalyst was prepared by mixing of DI water as solvent at 80 °C. The weight ratio of Cu:Zn:Al is the same weight ratio as mentioned above. The weight ratio of Zr, Mn, Si modifiers is 0.3. The NaHCO_3 was dropped into precursor solution for suitable pH. The mixture solution was stirred for 120 min. The precipitate solution was centrifuged and filtered DI water out. The cake in co-precipitation was dried overnight at 110 °C. The dried cake was calcined at 300 °C around 3 hours.

3.2 Catalysts characterizations

The physico-chemical property was identified by nine techniques as follows.

3.2.1. X-ray diffraction (XRD)

XRD is the technique to analyze crystal structure. The ternary structure was identified and shown the crystallite phase composition by X-ray diffraction with 2θ range of 20°- 80° with the wavelength of 0.15046 nm. The crystallite size is calculated using Scherrer's equation as follows:

$$D = \frac{K\lambda}{\beta \cos\theta}$$

The Scherrer's equation was used to calculate by K is unity constant factor, λ as wavelength, θ is the position of observe peak and β is X-ray diffraction broadening in half peak.

3.2.2. Scanning Electron Microscope (SEM)

Morphology was determined by SEM. The surface structure can be preferred with physical dispersion of CZA and the shape of agglomeration of metal species on catalyst surface.

3.2.3. Energy-dispersive X-ray spectroscopy (EDX)

EDX is an advantage of studied element dispersion on surface indicating the elemental distribution in the catalyst granules.

3.2.4. N₂ physisorption

The N₂ physisorption was used to determine the surface area by Brunauer-Emmett-Teller (BET) analysis.

3.2.5. Temperature-programmed reduction (TPR)

The technique of examine reduction behavior of oxide metal in catalyst. TPR can be preferred at approximation temperature of reduction. 0.05 g of catalyst was preheated to 300 °C and 1 hour. The reducing was conducted with 10% H₂/Ar between 30 – 500 °C.

3.2.6. Temperature-programmed desorption of carbon dioxide (CO₂-TPD)

This technique was used to analysis the basicity of catalysts by carbon dioxide gas. For this technique, the 0.10 g catalyst was loaded and pretreated with carrier flow 25 mL/min at 250 °C for 30 min and adsorbed CO₂ at 30 °C in 1 hour. Next step, the desorbed of CO₂ was heated to 500 °C by heating rate of 10 °C /min.

3.2.7. Temperature-programmed desorption of ammonia (NH₃-TPD)

This technique was used to analysis the acidity of catalysts by ammonia gas. The 0.10 g of catalyst was loaded and pretreated with carrier flow 25 mL/min at 250 °C for 30 min and adsorbed NH₃ analysis gas at 30 °C in 1 hour. Finally, the desorbed of NH₃ was heated to 500 °C by heating rate of 10 °C /min.

3.2.8. X-ray Photoelectron spectroscopy (XPS)

X-ray Photoelectron spectroscopy analysis technique was used to analyzed chemicals state of CZA catalysts by X-ray Photoelectron. Cu, Zn, Al, O, C species was detected between intensity and binding energy eV. CZA catalyst was determined in 0-1200 eV.

3.2.9. H₂-Chemisorption (H₂-Chem)

H₂-Chemisorption was used to analysis the active site of catalyst by H₂ adsorption between active site and support. Cu⁰ active site was detected and reported in form of pulse H₂ gas injection by 20 μ L.

Table 8 The characterization data equipment of this study

Technique	Characterization	Contact
XRD	Crystallinity	Department of Geology
SEM-EDX	Morphology, element of surface catalyst	Center of Excellence on Catalysis and Catalytic Reaction Engineering
BET	Single point: surface area Multi point: pore volume, pore diameter	Center of Excellence on Catalysis and Catalytic Reaction Engineering
H ₂ -TPR	Reducibility	Center of Excellence on Catalysis and Catalytic Reaction Engineering
CO ₂ -TPD	Basicity site	Center of Excellence on Catalysis and Catalytic Reaction Engineering
NH ₃ -TPD	Acidity site	Center of Excellence on Catalysis and Catalytic Reaction Engineering
XPS	Chemical states	Center of Excellence on Catalysis and Catalytic

		Reaction Engineering
H ₂ -Chem	Active site of catalyst	Center of Excellence on Catalysis and Catalytic

3.3 Activity test

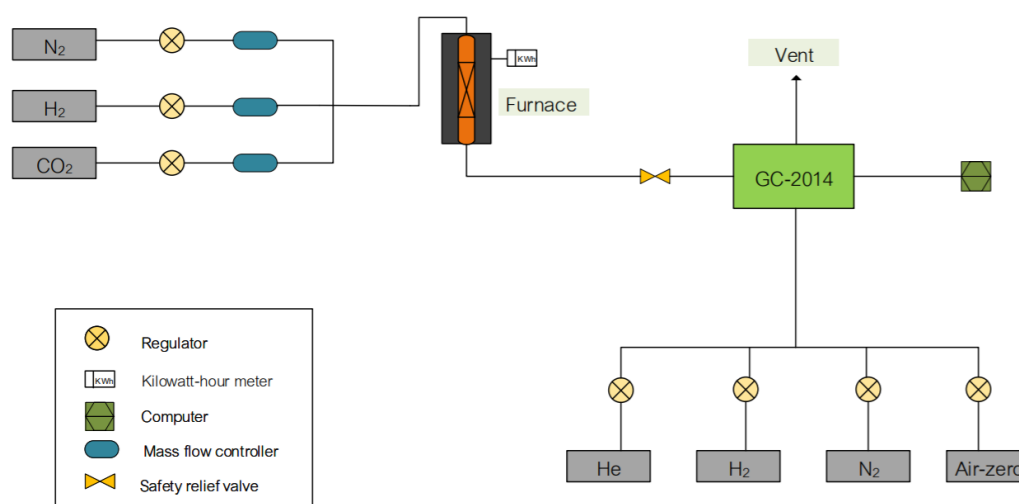


Figure 7 The Schematic of methanol synthesis via CO₂ hydrogenation.

In the first part, CZA 0.1 g catalyst having different pH during preparation (designated as CZA-PH7, CZA-PH8, and CZA-PH9) was loaded into the reactor with quartz wool. The reactor used is fix-bed microreactor (O.D. 12 mm, I.D. 10 mm, height 50 cm). Firstly, the catalyst was pretreated by N₂ for estimated moisture at 250 °C and 30 min. Secondly, the reduced condition was designed by 20% H₂ balance N₂ at 50 ml/min at 300 °C and 1 bar. Finally, the catalyst was test for methanol synthesis by temperature 250 °C and time on stream in 5 hours. the feed ratio of reaction test is 1:3 by volume of CO₂:H₂ at atmospheric pressure. The analysis gas was detected by multi detector TCD and FID GC-2014. The temperature giving high CO₂ conversion and high CH₃OH selectivity was chosen for second part.

In the second part, the effects of Zr, Mn, Si modification were determined by time on stream in suitable condition obtained from the first part. The condition was

as followed; in 4 hours for time on stream of stability. The analysis gas was measured by GC-2014 with the setting value as shown in **Table 9,10**.

Table 9 Condition of TCD detector

Gas Chromatograph	Shimadzu GC 2014
GC type	Multi-detector
Detector 1	TCD
Pack-bed reactor	Shincarbon
Carrier gas	Herium gas
Injector temperature	170 °C
Column temperature (Link FID)	Initial 150 °C Hold 240 °C Cool down 150 °C
Detector temperature	150 °C
Time analysis	15 min

Table 10 Condition of FID detector

Gas Chromatograph	Shimadzu GC 2014
GC type	Multi-detector
Detector 2	FID
Capillary column	Rtx-5
Carrier gas	Nitrogen gas Hydrogen gas Air zero gas
Injector temperature	170 °C
Column temperature (Link TCD)	Initial 150 °C Hold 240 °C Cool down 150 °C
Detector temperature	150 °C
Time analysis	1 min

CHAPTER 4

RESULTS AND DISCUSSION

This chapter is divided into 3 sections including 4.1 effect of pH on the catalyst preparation, 4.2 effect of promoters, and 4.3 stability of the chosen catalysts. Details of each section are as follows;

4.1. Effect of pH value in CZA catalyst preparation.

4.1.1 Characterization

4.1.1.1 X – ray diffraction (XRD)

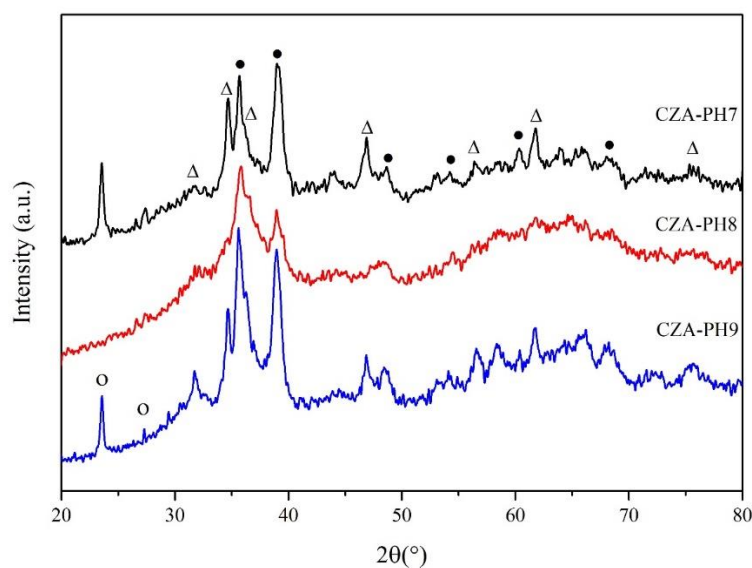


Figure 8 XRD patterns of different Cu/Zn/Al catalysts (●) CuO ; (▲) ZnO ; (○) Zincian malachite, $(\text{Cu,Zn})_2(\text{OH})_2\text{CO}_3$.

X – ray diffraction patterns of CZA catalysts with different pH in co-precipitation are presented in **Figure 8**. The results appeared a strong dispersion of CuO phase at $2\theta = 35.5^\circ, 38.5^\circ$ and $31.8^\circ, 48^\circ, 56.6^\circ, 62.8^\circ$ of ZnO phase on CZA catalysts. Moreover, it obtained zincian malachite or rassasite, $(\text{Cu,Zn})_2(\text{OH})_2\text{CO}_3$ at 23.6° and 27.5° , suggesting a precursor of nitrate solution at CZA-PH7 and CZA-PH9 in step of catalyst preparation. For this reason, CZA-PH8 tended to have well dispersion

of CuO active site more than CZA-PH7 and CZA-PH9. As a result, the residue of zincian malachite or rassasite can reduce at pH 8 of preparation condition. Crystalline sizes based on the Scherrer equation of all CZA catalysts are listed in **Table 11**. Therefore, the pH value only had only slight effect on the crystallite size of CuO. It was found that CZA-PH8 exhibited slightly smallest size among other catalysts. The dispersion of Al species was in the highly dispersed form. Thus, it was invisible in the XRD patterns.

Table 11 Crystalline size of CZA catalysts.

Samples	$D_{\text{avg,CuO}}$ (nm)
CZA-PH7	6.91
CZA-PH8	6.13
CZA-PH9	6.54

4.1.1.2. Scanning electron microscope (SEM) and energy-dispersive X-ray spectroscopy (EDX)

SEM and EDX were used to determine a surface property of different pH in CZA catalysts as shown in **Figure 9**. The effect of pH is shown by different morphology of each catalyst. The morphology of CZA-PH7 is presented as amorphous shape indicating that the precipitation was likely incomplete. However, CZA-PH8 and CZA-PH9 appear in spherical shape of catalyst. It is observed that CZA-PH8 is presented a fine crystalline granule compared to other catalysts.

EDX images are also presented showing all elemental distribution of CZA catalysts as seen in **Figure 9**. It was found that the distribution for all elements were similarly well distributed. As a result, the different pH in co-precipitation had an effect on morphology as seen from SEM images.

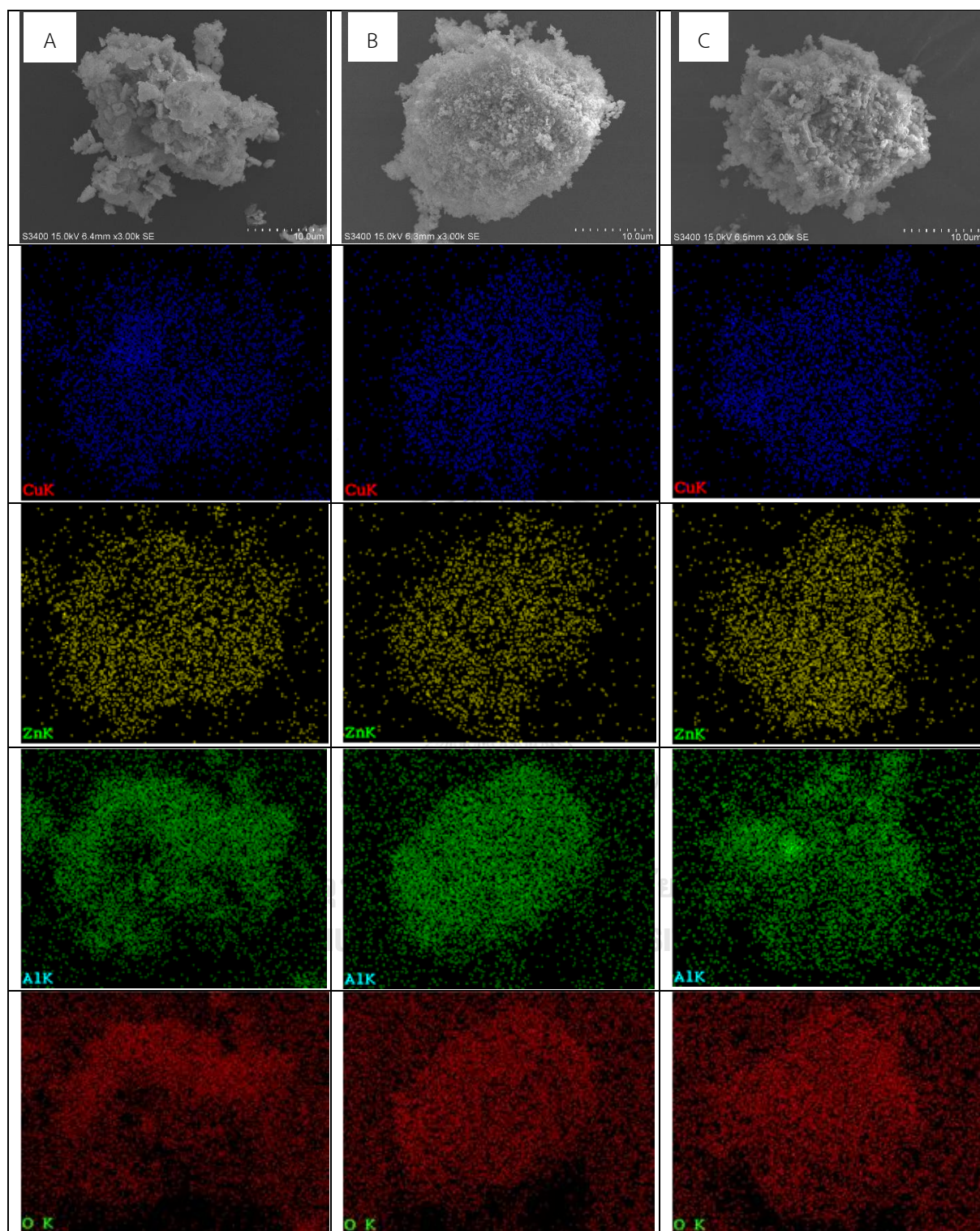


Figure 9 SEM and EDX images of different pH of CZA catalysts, A; CZA-PH7, B; CZA-PH8, C; CZA-PH9.

In addition, EDX was also used to determine an elemental distribution and amounts on near-surface of catalyst by scattering techniques and presented in

percent weight of all element as listed in **Table 12**. The element can present a component of catalyst in ratio of Cu:Zn:Al = ca.40:40:20

Table 12 EDX elemental analysis without O element on surface of different CZA catalysts (wt%).

Samples	Cu	Zn	Al
CZA-PH7	43.1	40.8	16.1
CZA-PH8	38.0	42.0	20.0
CZA-PH9	34.8	42.2	22.9

4.1.1.3. N₂ physisorption (BET)

N₂ physisorption is a technique which identifies surface area and pore structure of catalysts by multilayer point of N₂. Surface area and pore volume and pore size of catalysts are presented in **Table 13**. Surface area (SA) of catalysts with different pH value decreased at pH 9 during co-precipitation and being constant (ca. 36 m²/g) for CZA-PH7, CZA-PH8. Additionally, pore volume (PV) was found to be in range of 0.07-0.10 cm³/g. The pore size of different pH prepared CZA catalysts increased with increasing pH values.

Table 13 surface properties of catalysts

Sample	SA (m ² /g)	PV (BJH, cm ³ /g)	PS (nm)
CZA-7	35.52	0.07	08.04
CZA-8	35.95	0.10	11.37
CZA-9	21.62	0.07	12.28

For another, N₂ Physisorption isotherm of different pH value was followed in **Figure 10**. It shown that hysteresis loop of isotherm, it defined Type 4 of N₂ Physisorption isotherm, pore size is mesopores structure (2-50 nm) by comparison pore size of CZA-PH7, CZA-PH8, CZA-PH9 catalysts.

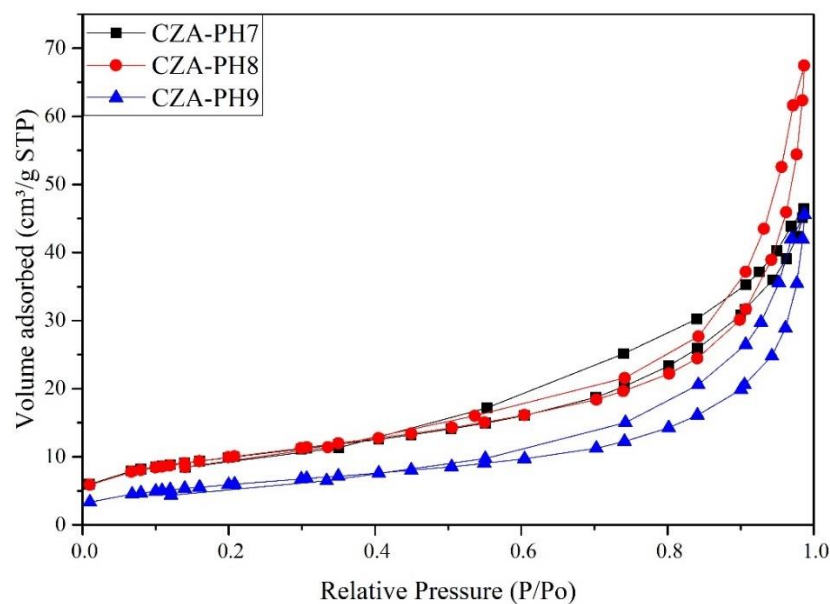


Figure 10 N₂ physisorption of different pH of Cu/Zn/Al catalysts at -196 °C liquid N₂.

In addition, pore size distribution is shown in **Figure 11**. It presented a pore diameter range of different pH values in catalysts by BJH method. The result revealed the broad pore size distribution in CZA-PH8. This property suggested the large pore volume to promote the good dispersion of high active metal on surface catalyst.

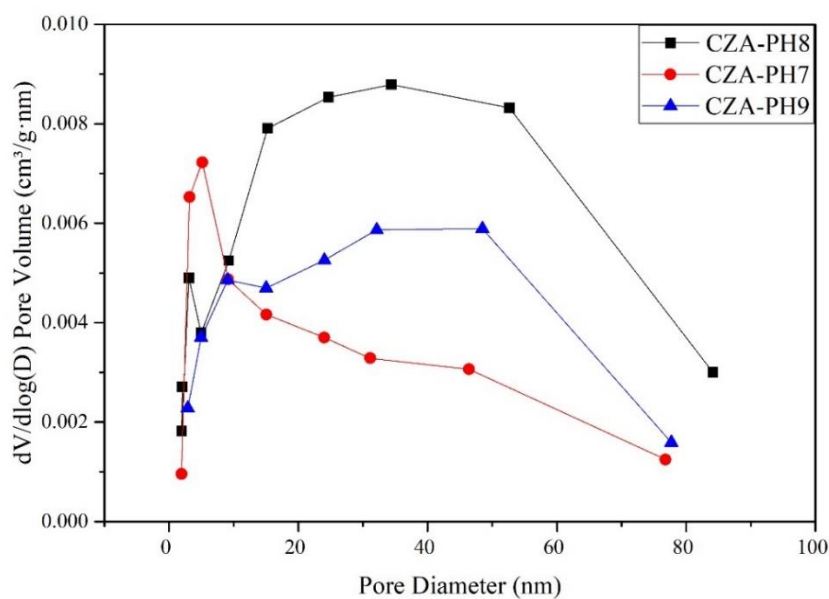


Figure 11 pore size distribution (BJH technique) of different pH of CZA catalysts.

4.1.1.4 Temperature-programmed reduction (TPR)

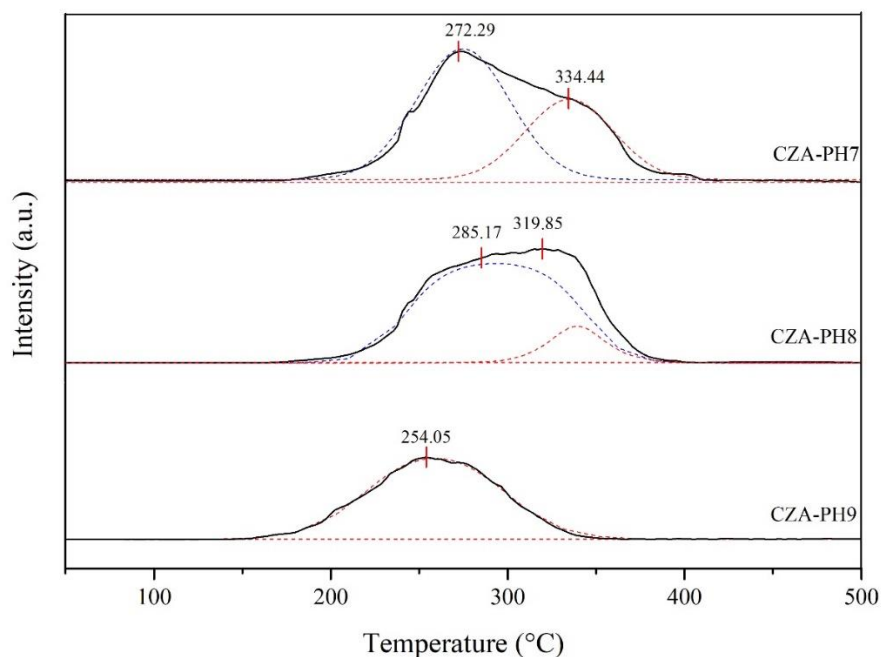
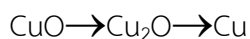
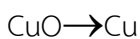


Figure 12 TPR profile of different pH of CZA catalysts.

From **Figure 12**, the H_2 -TPR peaks presented the reducibility of CuO species on different CZA catalysts. The phase of Cu oxide was reduced within a temperature peak range of 254-334 °C. It may refer to a type of Cu oxide active site of Cu^+ , Cu^{2+} by following peak of deconvolution. The pattern of reducibility was presented in 2 forms of 2 oxide species type as follows.



As a result of the first part, it showed interaction of Cu^+ and Cu^{2+} on ZnO support. The ability of reduction was easy and occurred at low temperature in the range that $CZA-PH9 > CZA-PH8 > CZA-PH7$. However, CZA-PH9 was found to have lower surface

area than CZA-PH7, CZA-PH8. This led to lower reducibility of CuO species on CZA-PH9 than other catalysts.

The reduction of Zn oxide species did not appear of this experimental condition because it occurred at very high temperature [19]. The deconvolution peak at 285 °C inhibited the interaction between Al₂O₃ and CuO. Thus, CZA-PH7 exhibited higher interaction of Al₂O₃ and CuO.

4.1.1.5 Temperature-programmed desorption of carbon dioxide (CO₂-TPD)

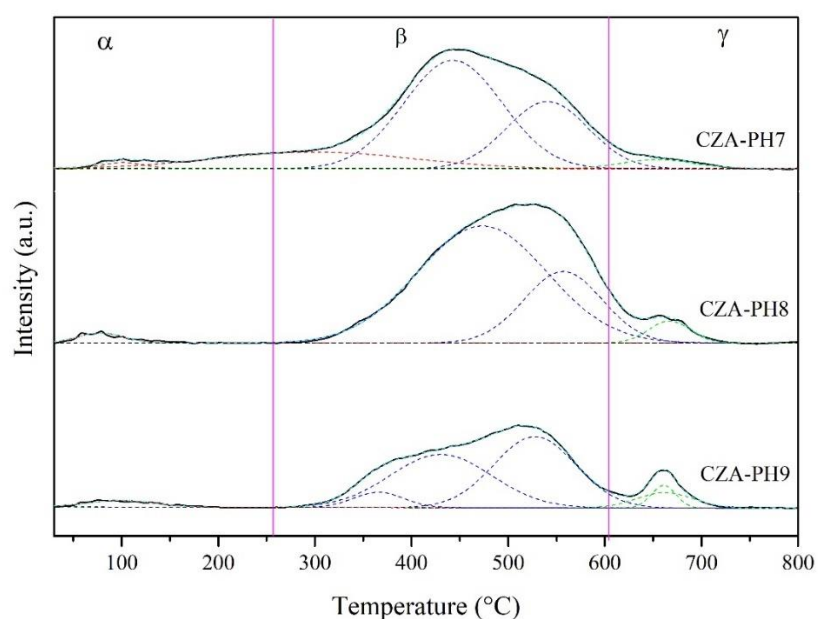


Figure 13 CO₂-TPD profile of different pH of CZA catalysts.

This technique was performed to determine the basicity of catalyst, which can facilitate the adsorption of CO₂. Firstly, the CO₂-TPD patterns are shown in **Figure 13**. It presented the three CO₂ desorption peaks of α , β , γ peaks, which refer to weak, moderate, and strong basic site of CZA catalysts. It can be observed that weak basic site was dominant for all CZA catalysts in this study. For weak basic site [33], they investigated the basicity of bicarbonate on surface of CZA. The moderate peak was presented interaction between metal and oxygen pair and adsorption of bidentate

carbonated and strong basic site was shown the adsorption of unidentate carbonates. In addition, the number of basis sites is shown in **Figure 14** by deconvolution of CO₂-TPD profiles. It showed the higher strong basic site increased in the following; CZA-PH8 > CZA-PH9 > CZA-PH7, whereas the total basic sites were as follows; CZA-PH8 ~ CZA-PH7 > CZA-PH9.

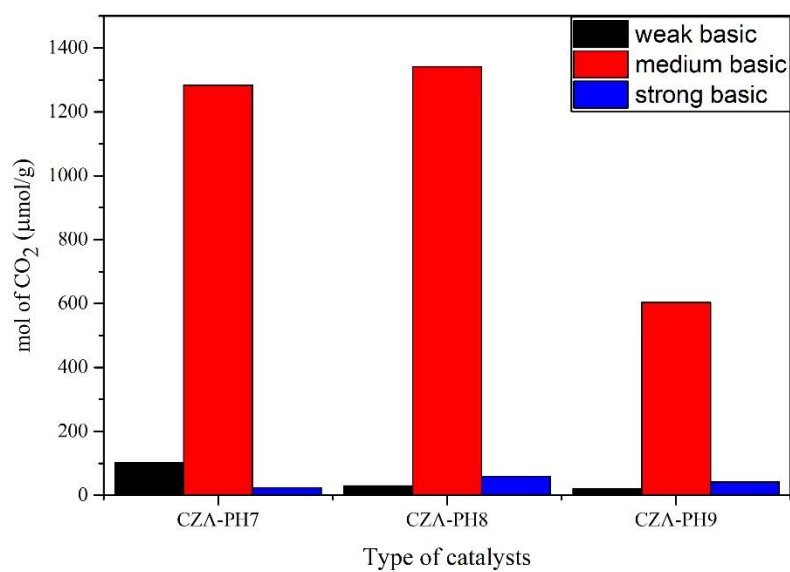


Figure 14 The amounts of basic sites by CO₂-TPD of different pH of CZA catalysts.

Table 14 The amounts of basic sites of all CZA catalysts.

Samples	Number of total basic sites (μmolg ⁻¹)	Number of basic sites (μmolg ⁻¹)		
		site α	site β	site γ
CZA-PH7	1408.19	101.62	1282.83	23.74
CZA-PH8	1428.39	29.11	1340.59	58.69
CZA-PH9	664.66	20.26	603.2	41.20

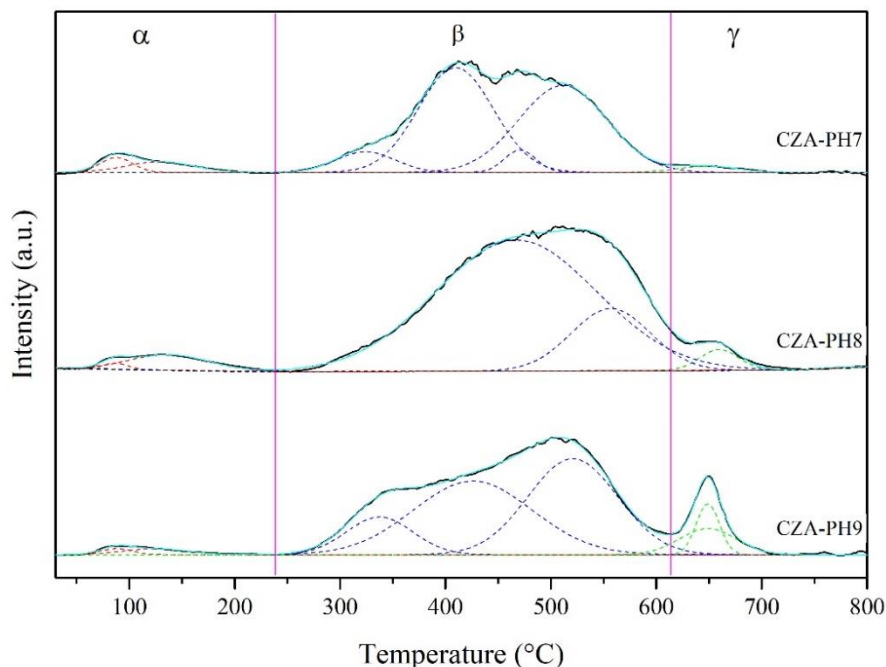
4.1.1.6 Temperature-programmed desorption of ammonia (NH₃-TPD)

Figure 15 NH₃-TPD profile of different pH of CZA catalysts.

The NH₃-TPD profile is presented in **Figure 15** of different pH values of CZA catalysts. The peaks were separated into 3 peaks of desorption, which denoted acid site of weak acid, moderate or medium acid and strong acid site (denote: α, β, γ), respectively. The number of amount acid site suggested with deconvolution of three-character acidity in NH₃-TPD profile. Zhang et al.[33] suggested that the moderate or strong acidity site became weakly peak led the catalyst had a well amount of basicity on CO₂ hydrogenation to methanol synthesis. It suggested that CO₂ can adsorb on surface of CZA catalyst with the lowest amount of acid site or decreasing of moderate strong acid site. This evidence supported that the lowest of acidity is essentially suitable for CO₂ hydrogenation reaction via CZA catalysts.

For one thing, the effect of pH condition can be explained by deconvolution of α, β, γ peak. The results revealed that CZA-PH7 had low amount acid site and not appear of γ peak. CZA-PH9 was found to have the lowest total amount of acid site.

However, γ peak was the highest for all CZA catalysts. The results of low amount of acid site are shown with the order of CZA-PH7>CZA-PH9>CZA-PH8 and lowest γ peak is in the order of CZA-PH7>CZA-PH8>CZA-PH9. It should be noted that CZA-PH8 exhibited the highest total number of basicity among CZA catalysts, which can be presumed that it exhibits the highest activity for CO₂ hydrogenation. As a result, CZA-PH8 catalysts were selected to promote with different metals in the next part.

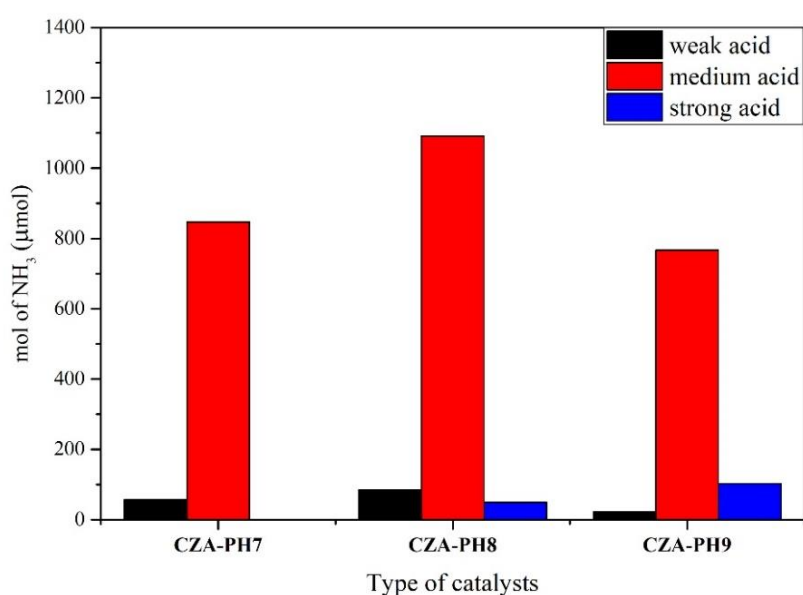


Figure 16 The amounts of acid sites by NH₃-TPD of different pH of CZA catalysts.

Table 15 the amounts of basic sites of all CZA catalysts.

Samples	Number of total acid sites (μmolg^{-1})	Number of acid sites (μmolg^{-1})		
		site α	site β	site γ
CZA-PH7	904.02	56.53	847.49	-
CZA-PH8	1527.01	85.58	1091.33	49.57
CZA-PH9	891.54	22.09	766.64	102.80

4.1.1.7 X-ray photoelectron spectroscopy (XPS)

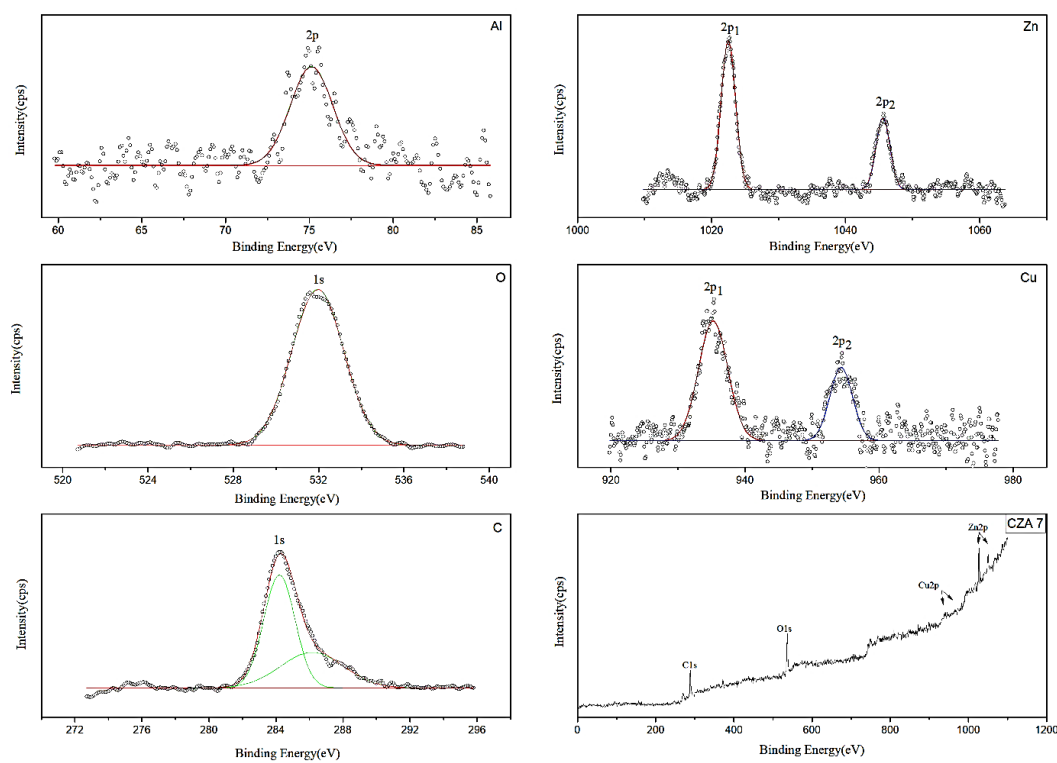


Figure 17 Typical XPS spectra of CZA catalyst (for CZA-PH7).

The XPS technique was performed to analyze a chemical state of CZA catalysts as shown in **Figure 17** (see all XPS spectra in **APPENDIX.D**). The XPS spectra presented Cu species at 935.3 and 954.5 eV of binding energy. Xiao et al.[26] reported a Cu^{2+} species on catalyst surface of CZA and suggested the presence of Cu^{2+} ions of cupric oxide in CZA catalyst. Additionally, $\text{Cu}2p_{1/2}$ was found in a part of different pH values. This suggested the existence of Cu^{2+} on CZA catalyst.

The deconvolution was used to determine a shape of XPS spectra by estimating the area of intensity of XPS signal and binding energy. Data are presented in Table 6. As a result, the different pH values were found to have a main peak of Cu^{2+} in state of $\text{Cu}2p_{3/2}$ and $\text{Cu}2p_{1/2}$ as the state of Cu^{2+} in excite state in form Cu^0 ($\text{Cu}^{2+} \rightarrow \text{Cu}^0$). The effect of different pH can increase Cu^{2+} on surface catalyst by following a peak of $\text{Cu}2p_{1/2}$ and $\text{Cu}2p_{3/2}$ in case of pH 7 and 8 as seen in **Figure 18**. In addition, Cu^{2+} on CZA-PH9 tended to decrease. This phenomenon was related with

the lowest surface properties on pH 9 condition. In addition, the peaks of ZnO and AlO were located at 1022.6, 1045.7 eV for ZnO and 74.9 eV for AlO. These peaks represented Zn^{2+} and Al^{3+} that being dispersed on surface of CZA catalysts.

In case of different pH value, it discovered only a slight change of XPS spectra by following a deconvolution of XPS profiles. It showed that the main Cu^{2+} species on surface catalyst became main active site of CZA catalysts, whereas CZA-PH9 was found to have the lowest Cu^{2+} active site on ZnO support.

Table 16 Property of XPS spectra and mass of Cu,Zn,Al,O species.

Samples	Position of binding energy(eV)					Mass (%)			
	Cu2p _{3/2}	Cu2p _{1/2}	Zn2p _{3/2}	Zn2p _{1/2}	Al2p	Cu	Zn	Al	O
CZA-PH7	935.3	954.5	1022.6	1045.7	74.9	13.01	31.40	7.33	48.27
CZA-PH8	935.3	954.5	1022.6	1045.7	74.9	16.66	27.79	6.43	49.11
CZA-PH9	935.3	954.5	1022.6	1045.7	74.9	10.22	33.77	6.63	49.40

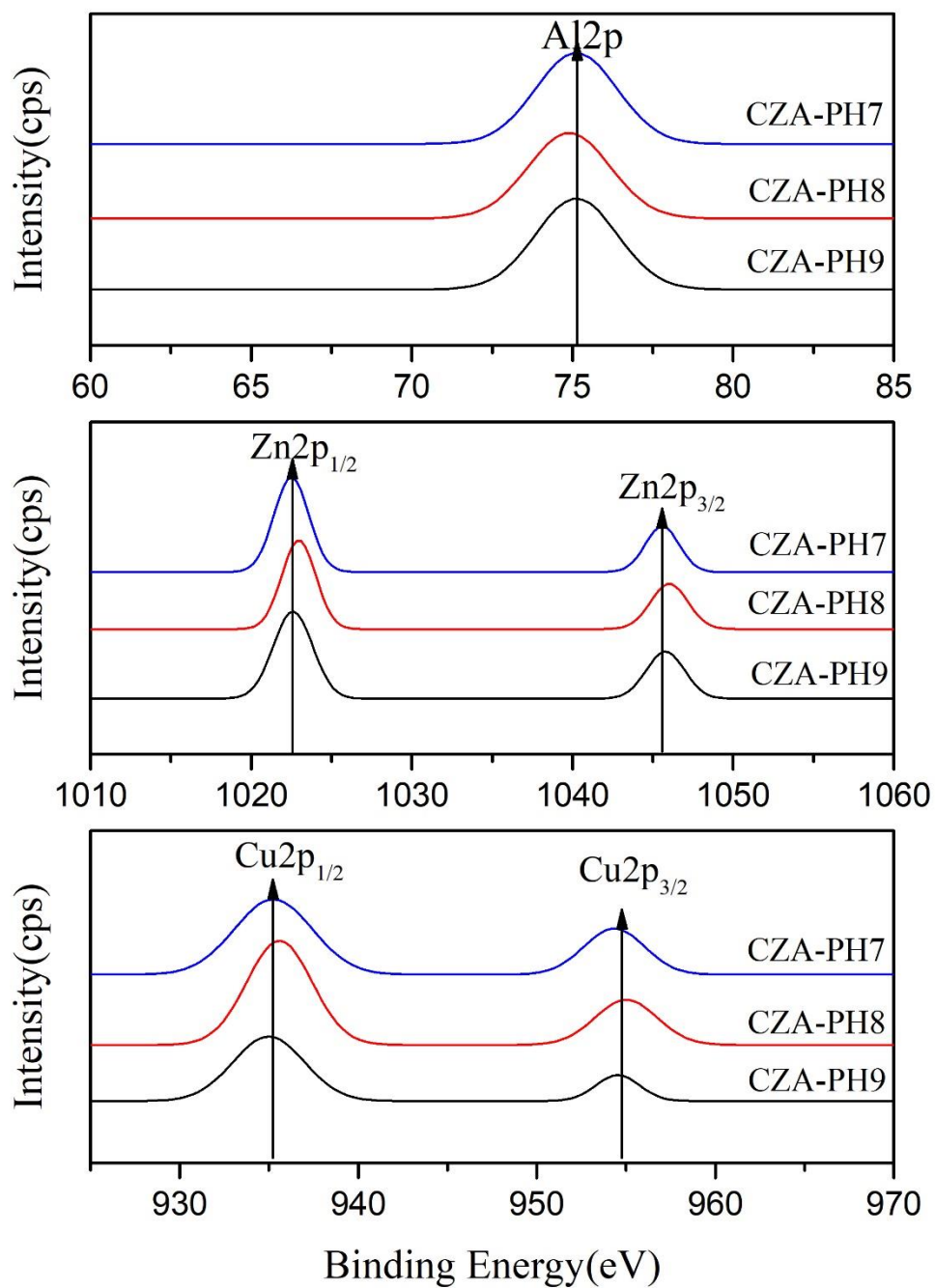


Figure 18 Cu, Zn, Al species of different pH of CZA catalysts.

The chemical state depending on pH value after reaction test was investigated in **Figure 18**. The results showed a decreasing of deconvolution peak in $\text{Cu}2p_{1/2}$ and $\text{Cu}2p_{3/2}$. The chemical state of CZA-PH8 and CZA-PH9 was found a changing of Cu^{2+} by physical property.

4.1.2 Reaction performance

The reaction performance of $\text{CuO}/\text{ZnO}/\text{Al}_2\text{O}_3$ (CZA) catalysts was followed by time on stream in 5 hours. The effects of increasing pH value (7,8,9) in catalysts preparation were explained in this part. The activity test of CZA catalyst expressed with CO_2 conversion, methanol selectivity and methanol yield by calculation of mol reactant and methanol product in CO_2 hydrogenation to methanol synthesis.

Firstly, the effects of increasing pH value were shown by following CO_2 conversion of CZA-PH7, CZA-PH8, CZA-PH9 in **Figure 19**, respectively. The result showed that CZA-PH9 had the lowest CO_2 conversion at 0.84% as seen from Table 6 due to its lowest surface area and basic sites. In addition, CZA-PH7 and CZA-PH8 had similar CO_2 conversion and higher than CZA-PH9. The percent conversion is expressed in a best of CO_2 converted into CH_3OH or CO . As a result, the effects of pH at 7 and 8 is not significantly different with CO_2 conversion.

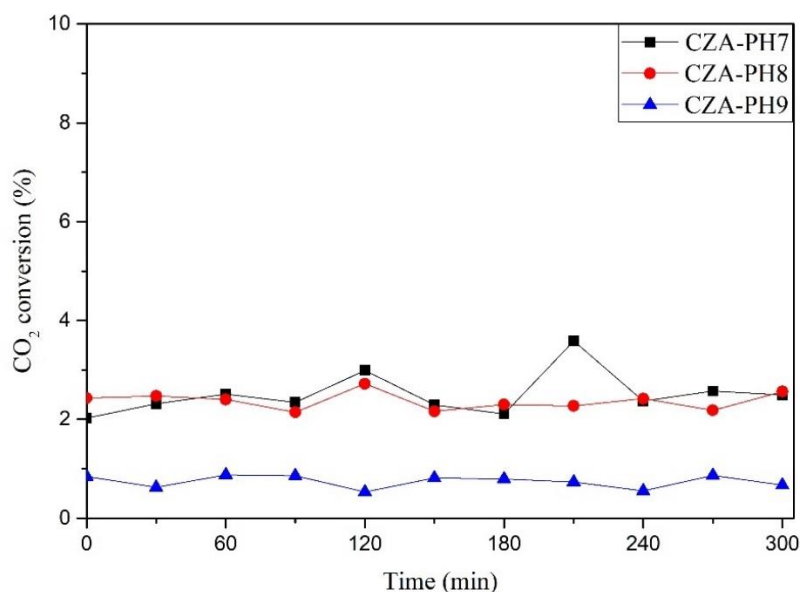


Figure 19 CO₂ conversion of different pH of CZA catalysts.

The methanol selectivity is shown in Fig.16. It was found the similar value in all catalysts in the part of different pH values at 9-11% for methanol selectivity by **Table 17**. The yield of methanol is illustrated in **Figure 21**. The catalysts activity can be compared by high methanol yield by following CZA-PH7 and CZA-PH8. As a result, the highest methanol yield was supported a suitable pH of catalyst. For the next part, CZA-PH8 was considered to promote with Zr, Mn, Si by the result of highest CuO dispersion, highest basicity and high methanol yield.

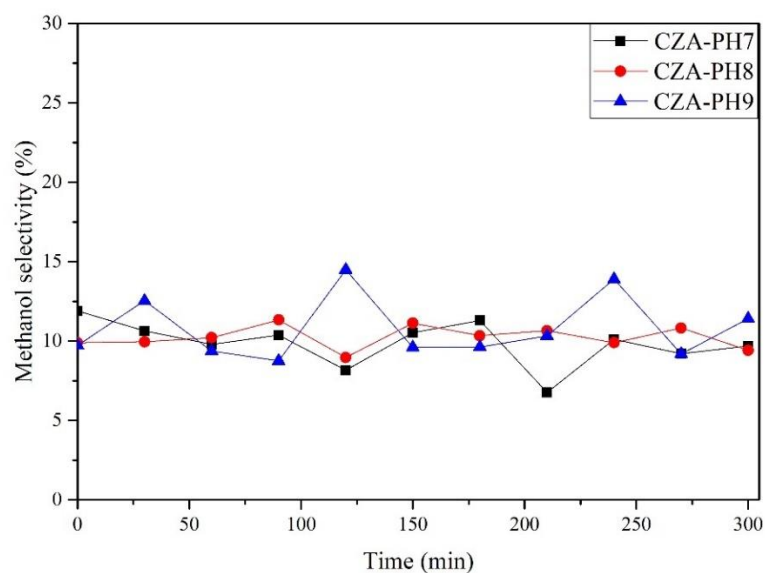


Figure 20 methanol selectivity of different pH of CZA catalysts.

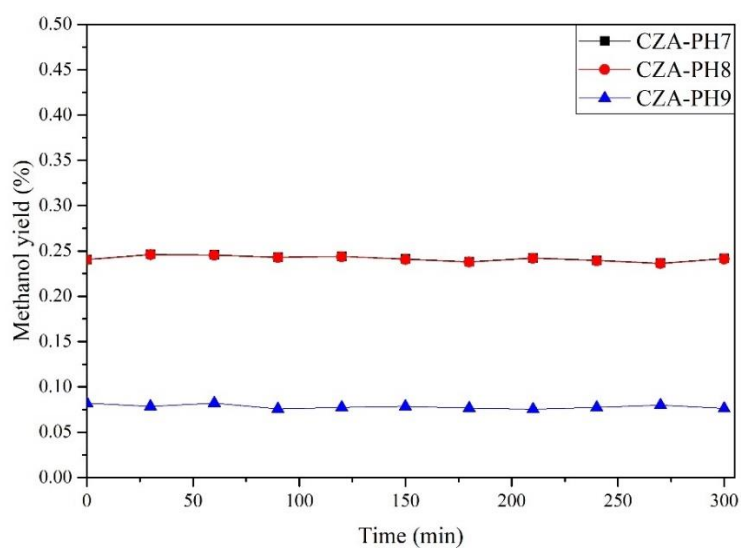


Figure 21 methanol yield of different pH of CZA catalysts.

Table 17 Catalyst activity of CZA catalysts (0 h = initial after proceeding of mixing reactant 30 min)

Samples	CO ₂ conversion (%)		CH ₃ OH selectivity (%)		CO selectivity (%)		CH ₃ OH yield (%)	
	0 h	5 h	0 h	0 h	0 h	5 h	0 h	5 h
CZA-PH7	2.03	2.49	11.89	9.69	88.11	90.31	0.24	0.24
CZA-PH8	2.43	2.56	9.89	9.42	90.11	90.58	0.24	0.24
CZA-PH9	0.84	0.67	9.715	11.41	90.29	88.59	0.08	0.08

4.2 The effect of Zr, Mn, and Si promoters.

4.2.1 Characterization

4.2.1.1 X – ray Diffraction (XRD)

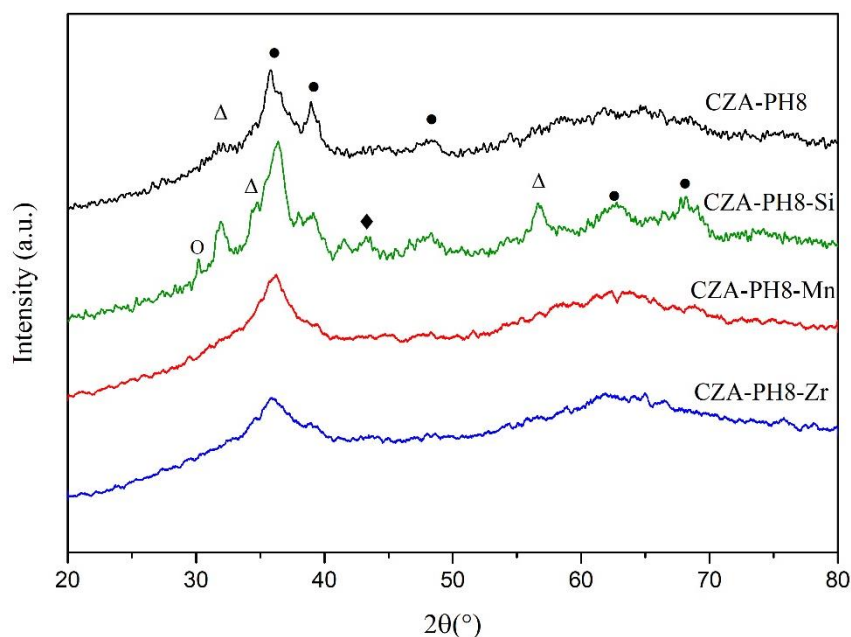


Figure 22 XRD patterns of CZA-PH8 catalyst with different promoters (CZA-PH8-X, X=Mn, Si, and Zr) (●) CuO ; (Δ) ZnO ; (○) Zincian malachite, $(\text{Cu,Zn})_2(\text{OH})_2\text{CO}_3$; (◆) Cu.

For XRD patterns in second part, the effects of metal promoter on crystal structure of catalyst are shown in **Figure 22**. It obtained a significant result of development in CZA-PH8. The XRD pattern presented a well dispersion of Cu and Zn oxide metal in CZA-PH8-Mn as mentioned earlier and CZA-PH8-Si. Nevertheless, Si species tended to increase agglomeration of CZA-PH8 resulting in the presence of higher peak of CuO and ZnO. However, the promotion of Mn and Zr led to a decreasing of crystallite size from 6.13 to 4.42 and 4.08 nm, respectively, whereas the Zr, Mn, Si oxide phases were not detected in XRD patterns [4]. This is because they were introduced in small quantity and being in the highly dispersed forms.

Table 18 Crystalline size of CuO in CZA catalysts.

Samples	$D_{\text{avg,CuO}}$ (nm)
CZA-PH8	6.13
CZA-PH8-Si	6.42
CZA-PH8-Mn	4.42
CZA-PH8-Zr	4.08

4.2.1.2 N₂ physisorption (BET)

For metal promoters of CZA-PH8, it is shown that the effect of metals can improve surface area and pore volume of catalyst as seen in **Table 23**. Mn and Si promoters had a significant effect with increasing of SA (89.8 and 40.8 m²/g, respectively). As a result, Mn and Si metals improved surface area, pore volume and high pore size of CZA-PH8 catalyst leading to increased dispersion of CuO species.

Table 19 surface properties of catalysts

Sample	SA (m ² /g)	PV (BJH, cm ³ /g)	PS (nm)
CZA-PH8	35.9	0.10	11.4
CZA-PH8-Si	40.8	0.23	16.8
CZA-PH8-Mn	89.8	0.33	10.8

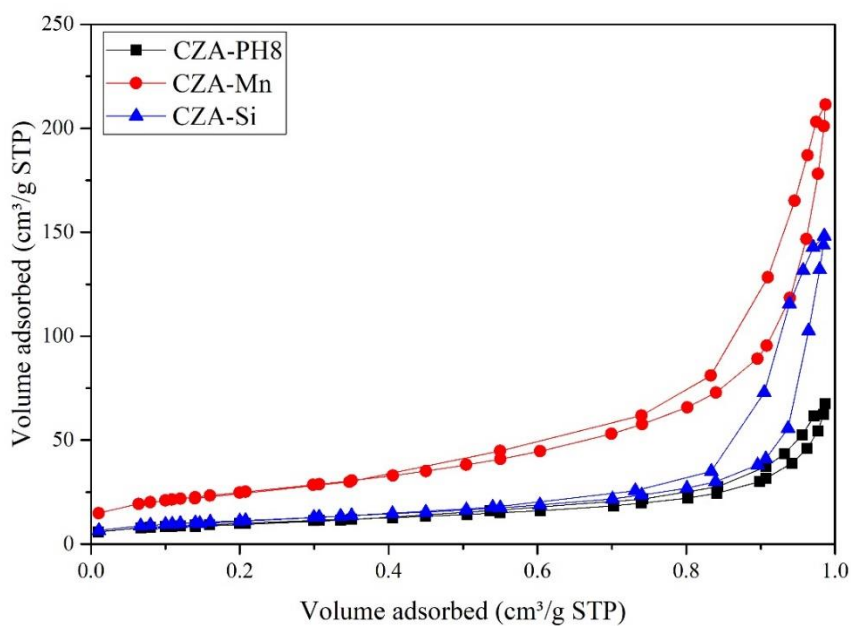


Figure 23 N_2 physisorption of loading metals of Cu/Zn/Al catalysts at boiling points at -196°C liquid N_2 .

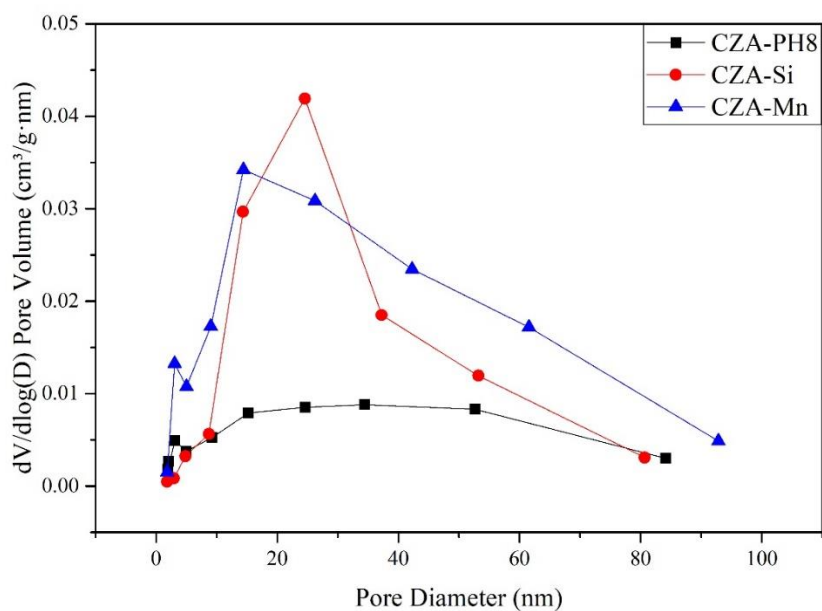


Figure 24 Pore size distribution (BJH technique) of metals loading of CZA-PH8 catalysts.

4.2.1.3 Temperature-programmed reduction (TPR)

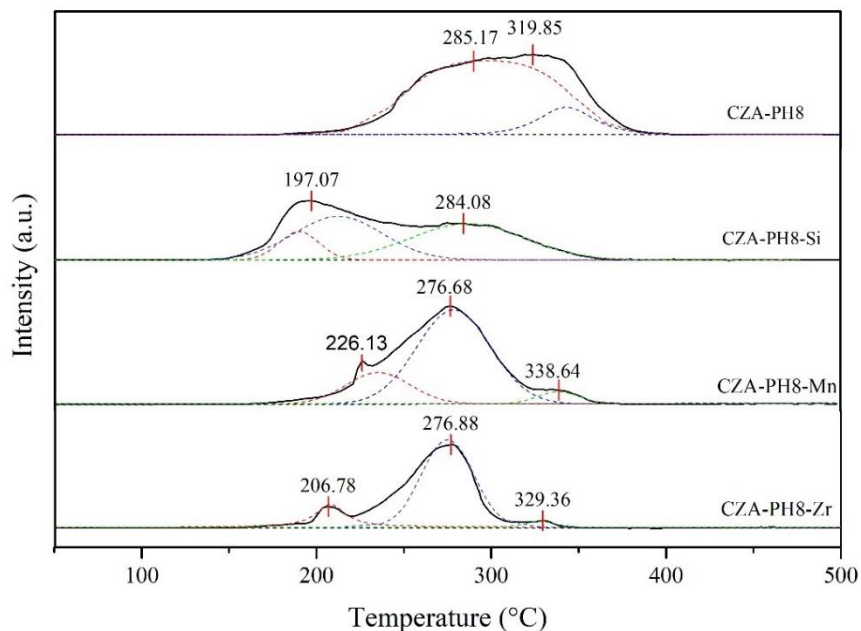


Figure 25 TPR profile of metals loading of CZA catalysts.

TPR profile was used to examine a reducibility of increasing temperature at room temperature up to 500 °C. The effect of metal promoter is presented in **Figure 25**. The deconvolution was divided into 3 peaks of reduction type. The development of metal promoter was observed relating to an effect of decreased interaction between metal-oxide on support catalyst. The promotion with metal facilitated the reduction by shift $\text{CuO} \rightarrow \text{Cu}^0$ metals which shows description in first peak. In addition, the proper CuO interaction of CuO and Al_2O_3 tends to easily shift to low temperature by following at second peak. The third peak was identified as reduction of metal promoter. CZA-PH8-Si tended to easily reduce at 300 °C of reaction. However, Mn and Zr was not reduced at experimental condition. This may refer to the oxide form interaction on CZA surface catalyst. The result was shown a development of metal in reducibility property by a shift of temperature to lower than CZA-PH8 catalysts. It related with MnO on surface catalyst had ability to increasing of CO_2 adsorption. This reason can be explained as well as description in

ZnO case. Nevertheless, Si modifier had a lower total amount of basic sites. Perhaps, the increasing of acid site was suggested to explain NH₃-TPD part.

4.2.1.4 Temperature-programmed desorption of carbon dioxide (CO₂-TPD)

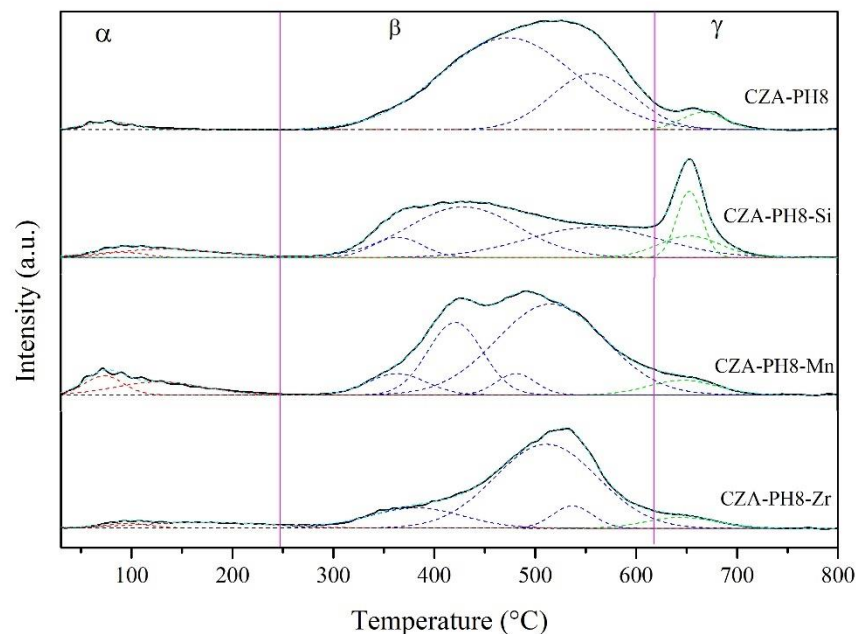


Figure 26 CO₂-TPD profile of metals loading of CZA catalysts.

The CO₂-TPD profiles of loading metals are shown in **Figure 26**. Gao et al. [4] reported a peak of basic site in a part of interaction between surface of catalyst and metal promoter. The moderate peak (β) related with metal-oxygen interaction. Therefore, CZA-Si catalyst had the lowest interaction of metal by easily increasing of strong basic sites. As a result, Mn promoter presented a highest total amount of basicity sites, while Zr had a total number of basic sites than CZA-PH8. The Mn promotion on CZA catalyst can adsorb CO₂ gas by relation of the highest total number of basic sites on surface area.

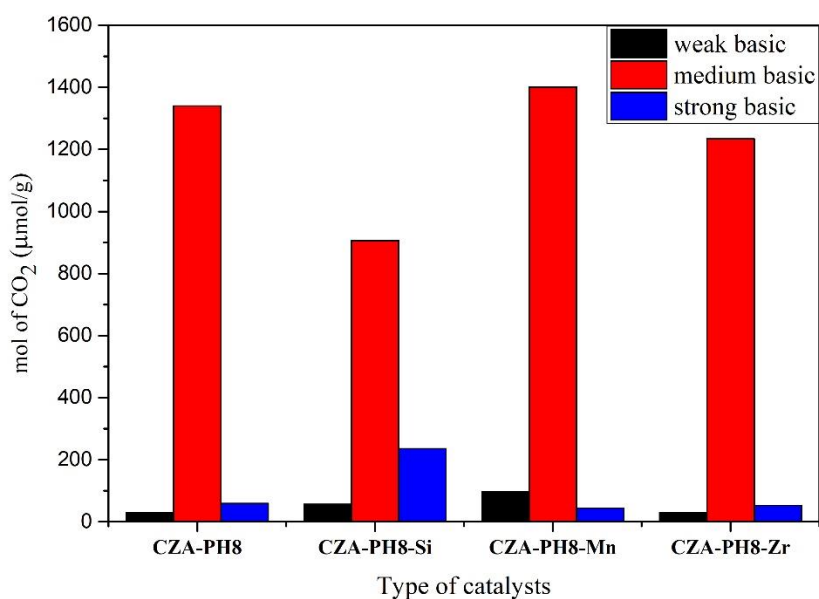


Figure 27 The amounts of basic sites by CO₂-TPD of metals loading of CZA catalysts.

Table 20 The amounts of basic sites of metals loading of CZA catalysts.

Samples	Number of total basic sites (μmolg^{-1})	Number of basic sites (μmolg^{-1})		
		site α	site β	site γ
CZA-PH8	1428.39	29.11	1340.59	58.69
CZA-PH8-Si	1197.81	56.12	905.82	235.87
CZA-PH8-Mn	1542.34	97.35	1401.2	43.79
CZA-PH8-Zr	1316.54	29.98	1233.7	52.86

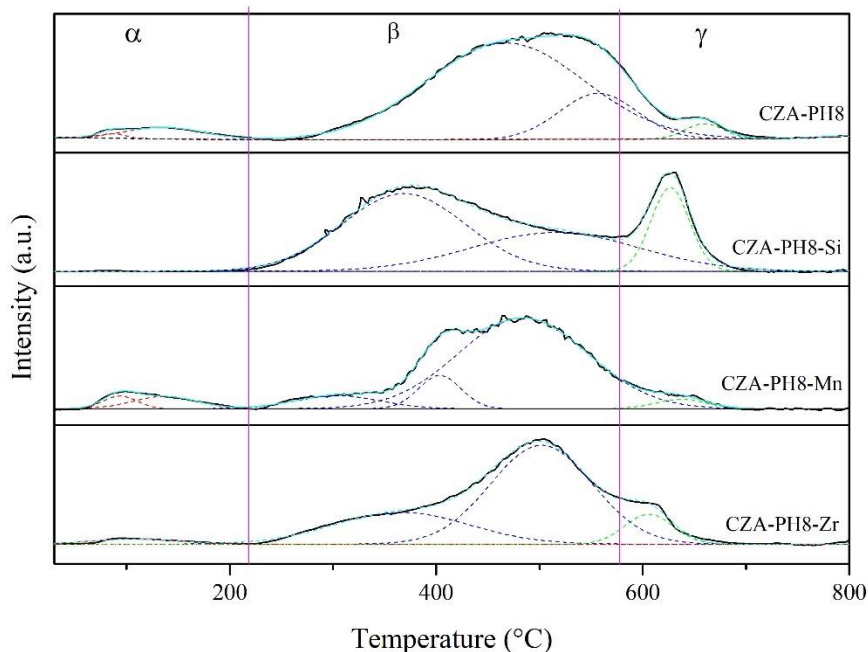
4.2.1.5 Temperature-programmed desorption of ammonia (NH₃-TPD)

Figure 28 NH₃-TPD profile of metals loading of CZA catalysts.

The effect of Si, Mn and Zr promoters developed a basicity of CZA-PH8 catalyst. As seen, **Figure 28** presented the three peaks of acid character type. The Mn promoter was observed a lower strong and modulate peak than CZA-PH8 and showed a high α peak of weakly acid site. The results related with evidence of temperature shift to lower in strong and moderate base of CZA-PH8-Mn. Nevertheless, Zr and Si promoters were shown the increasing of γ peak when compared with CZA-PH8 in **Table 22**.

The Mn promoter can reduce β, γ peaks of CZA-PH8 and become to weak acid site by shifting of lower temperature of β, γ peaks or increasing of α peak by deconvolution of NH₃-TPD profile. The result denoted that CO₂ adsorption in reaction test promoted with acid site at weak acid. The increasing of acid site related with H interaction on surface of CuO [34]. As a result, the accumulation of H may lead to undesirable of H₂O product.

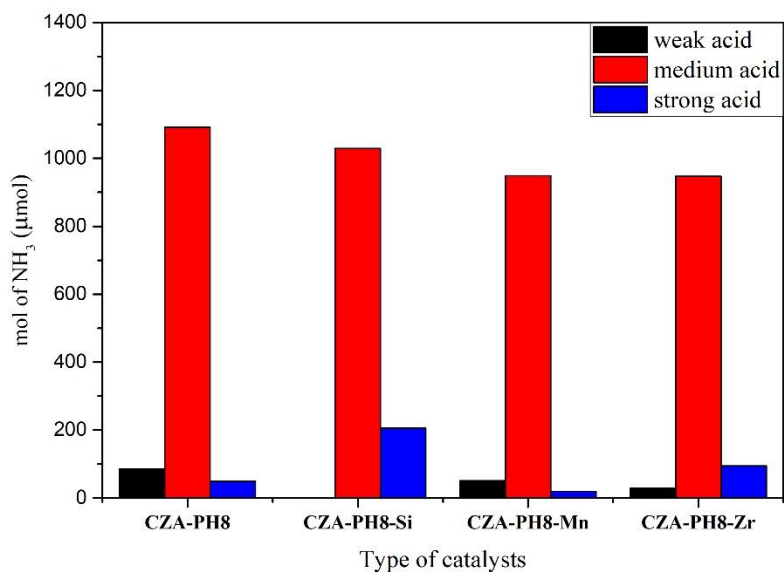


Figure 29 the amounts of acid sites by NH₃-TPD of metals loading of CZA catalysts.

Table 21 the amounts of basic sites of metals loading of CZA catalysts.

Samples	Number of total acid sites (μmolg^{-1})	Number of acid sites (μmolg^{-1})		
		site α	site β	site γ
CZA-PH8	1527.01	85.58	1091.33	49.57
CZA-PH8-Si	1234.98	-	1029.37	205.61
CZA-PH8-Mn	1020.18	51.15	948.94	20.09
CZA-PH8-Zr	1070.40	28.48	946.95	94.99

4.2.1.6 X-ray photoelectron spectroscopy (XPS)

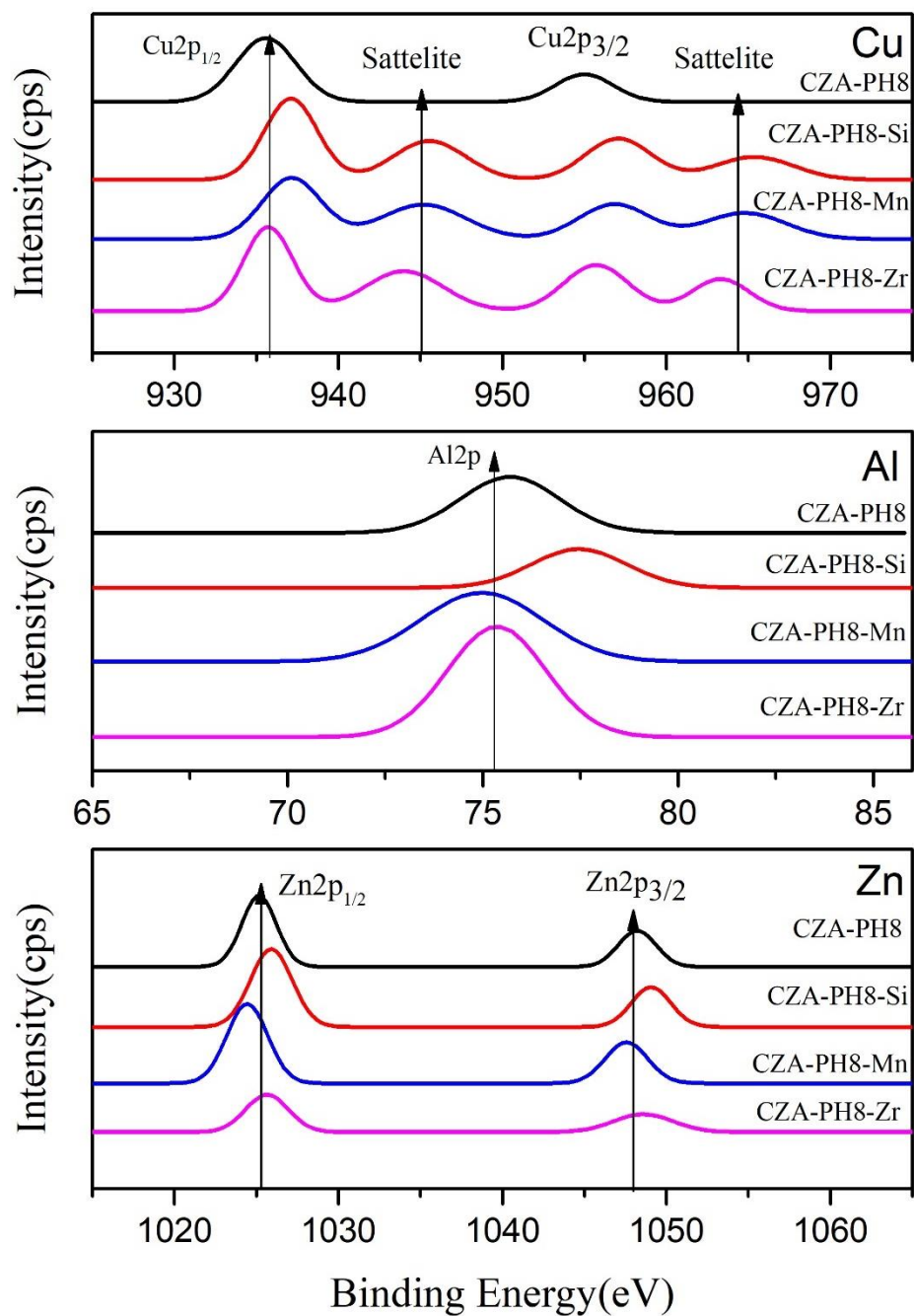


Figure 30 Cu species of metals loading of CZA catalysts.

The effects of metals loading are presented in **Figure 30**. Mn^{2+} , Si^{4+} , and Zr^{4+} were observed in binding energy at 634.9, 104.3, 184.3 eV, respectively. The position of predominantly peak was observed at 935.3 eV suggesting Cu^+ at surface area of

CZA catalyst promoted with metals. However, Mn and Si metals were observed a singly derivation of center position peak. The result was suggested that all catalysts consisted of Cu^{2+} at 945.6 eV. The satellite was identified of XPS spectra and it remained the existed in the form of Cu(I) and Cu(II) oxidation states in CZA catalyst which was modified with metals [35]. As a result, Mn, Zr and Si had ability to reduce in form between Cu^+ and Cu^{2+} . Additionally, effect of metal promoters was prompted the shifting of peak to 79.1 eV. The results lead to Al oxide interaction of Si or Si species covered on Al oxide. For another, the deconvolution of Zn was singly shift of binding energy. However, it was observed that Zn^{2+} form decreasing on CZA-Zr.

Table 22 The property of XPS spectra and mass of Cu, Zn, and Al₂O species of the effect of Zr, Mn, and Si promoters in CZA catalysts by X=Si, Mn, and Zr.

Samples	Position of binding energy(eV)							
	Cu^{2+}		Satellite		Zn^{2+}		Al^{3+}	X^x
	$\text{Cu}2p_{3/2}$	$\text{Cu}2p_{1/2}$	$\text{Cu}2p_{3/2}$	$\text{Cu}2p_{1/2}$	$\text{Zn}2p_{3/2}$	$\text{Zn}2p_{1/2}$	$\text{Al}2p$	$\text{X}2p$
CZA-PH8	935.3	954.5	-	-	1022.6	1045.7	74.9	-
CZA-PH8-Si	938.2	955.5	945.6	966.2	1023.3	1046.4	75.5	104.3
CZA-PH8-Mn	937.2	957.1	945.6	964.0	1025.6	1047.8	79.1	634.9
CZA-PH8-Zr	935.7	956.4	944.0	963.6	1023.1	1046.0	76.9	184.3

4.2.1.7 H₂-Chemisorption (H₂-Chem)

H₂-chemisorption was used to measure the Cu⁰ metal active site by pulse of H₂ gas 20 μL . The results are shown in Table 28. The Cu⁰ active sites of CZA-PH8 remarkably increased with Mn promoter. However, H₂ gas was poorly adsorbed CuO (1 1 1) main peak in XRD patterns (at 35.5°, 38.5°) at room temperature [36]. Therefore, Mn can promote Cu⁰ metal active site by increasing H₂ adsorption between CuO and Cu₂O.

Table 23 H₂-adsorption and Cu⁰ dispersion of CZA catalyst.

Sample	H ₂ adsorption ($\mu\text{mol/g}_{\text{cat}}$)	Cu ⁰ dispersion ($\times 10^6$)	Cu ⁰ dispersion (%)
CZA-PH8	7.11	0.27	27
CZA-PH8-Mn	16.28	0.64	64

4.2.2 Reaction performance

In second part, the selection of pH 8 (CZA-PH8) was introduced for promoting of different metals in part 2 by following the appropriate characterization of CZA catalyst in a topic of different pH value. Next step, the CZA-PH8 was promoted with Zr, Mn, and Si for studying the effect of metals to CZA-PH8. As a result, CO₂ conversion in part of metals loading was observed in **Figure 32**. The development of metals loading can improve CO₂ conversion of CZA-PH8 and show the highest increasing by CZA-PH8-Mn > CZA-PH8-Zr, > CZA-PH8-Si, respectively. In conclusion, the effect of metals can improve CZA catalysts by expression of different CO₂ conversion.

However, the results of various metals did not significant change the methanol selectivity by following in **Figure 32**. As a result, methanol selectivity of CZA-PH8 was almost consistent by adding of Si, Mn, and Zr. In addition, the suitable result of part 1 can explain as same as activity of CZA-PH7, CZA-PH8 and highest activity of CO₂ reaction in Mn metal loading.

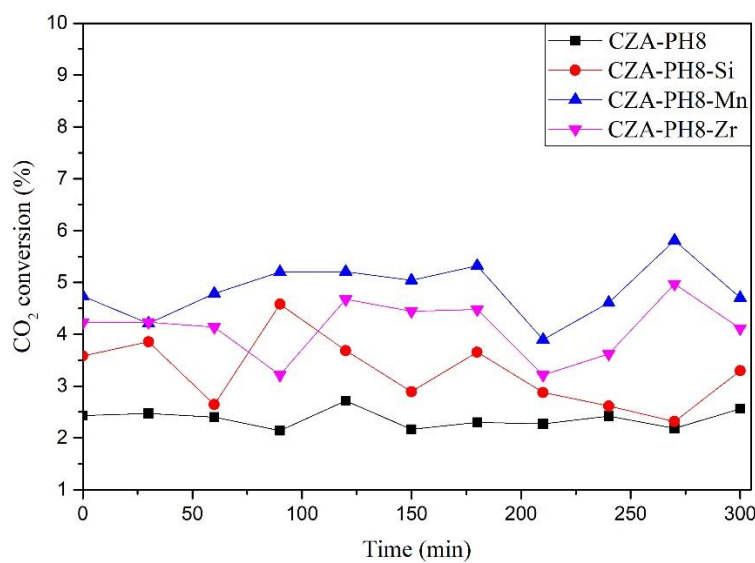


Figure 31 CO₂ conversion of loading metals of CZA catalysts.

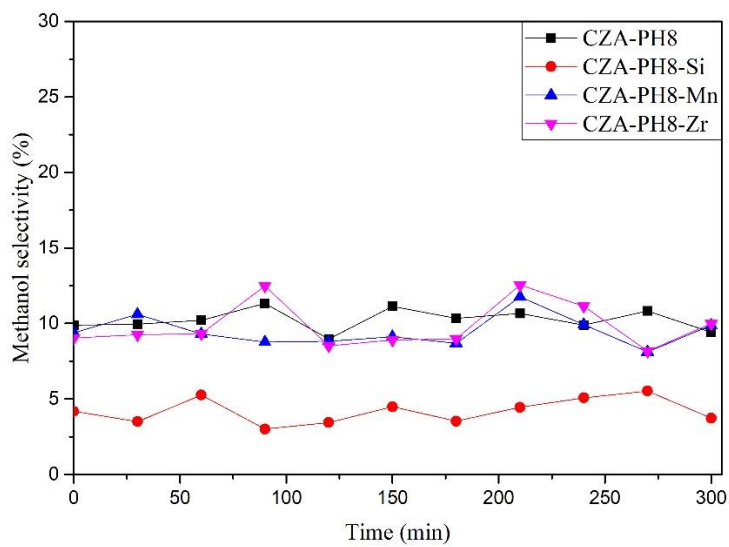


Figure 32 Methanol selectivity of loading metals of CZA catalysts.

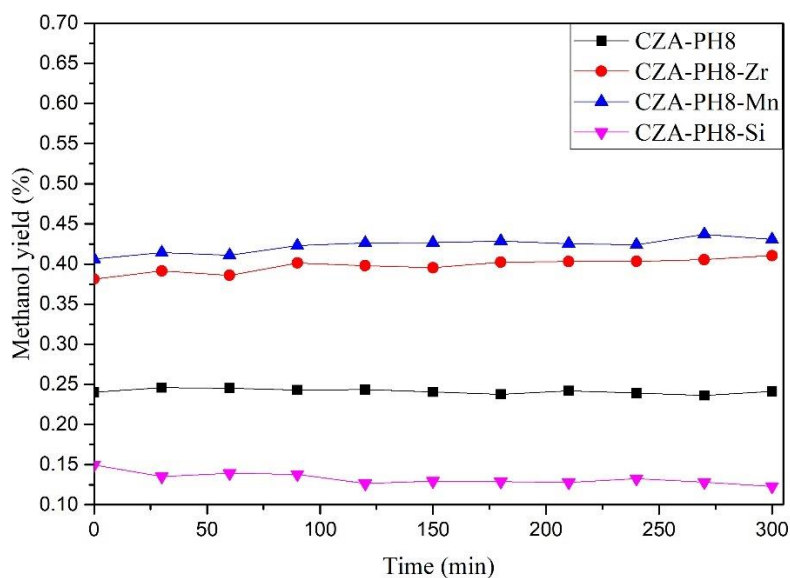


Figure 33 Methanol yield of loading metals of CZA catalysts.

Table 24 reaction test of CZA-PH8-X (X=Si, Mn, Zr) catalysts. (0 h = initial after proceeding of mixing reactant 30 min)

Samples	CO ₂ conversion (%)		CH ₃ OH selectivity (%)		CO selectivity (%)		CH ₃ OH yield (%)	
	0 h	5 h	0 h	0 h	0 h	5 h	0 h	5 h
CZA-PH8	2.43	2.56	9.89	9.42	90.11	90.58	0.24	0.24
CZA-PH8-Si	3.58	3.30	4.18	3.73	95.82	96.27	0.15	0.12
CZA-PH8-Mn	4.74	4.70	9.38	9.86	90.62	90.14	0.44	0.46
CZA-PH8-Zr	4.22	4.11	9.03	9.99	90.97	90.01	0.38	0.41

4.3 The stability of CZA catalyst

4.3.1 Characterization

4.3.1.1 X – ray diffraction (XRD)

XRD patterns of the fresh (CZA-PH8) and spent (sCZA-PH8) catalysts are illustrated in **Figure 34**. sCZA-PH8 catalyst showed a high agglomeration of crystallite size. It suggested high intensity of CuO, ZnO and Zincian malachite by CZA-PH8 reference. However, Cu metals phase at $2\theta = 43.4^\circ$ is shown approximate of reaction. It presented a success of some surface to change Cu^{2+} to Cu^0 . As a result, this reason investigated of CO_2 hydrogenation to methanol synthesis by increasing H_2 reactant adsorption.

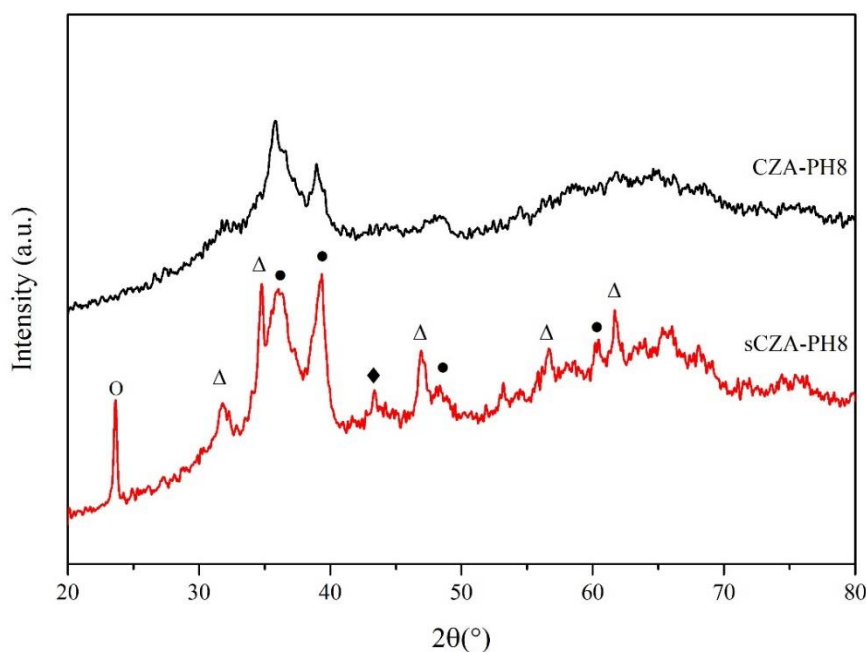


Figure 34 XRD patterns of fresh Cu/Zn/Al catalysts (CZA-PH8) and spent catalysts (sCZA-PH8) at pH 8 (●) CuO ; (Δ) ZnO ; (○) Zincian malachite, $(\text{Cu,Zn})_2(\text{OH})_2\text{CO}_3$; (◆) Cu.

After reaction test, sCZA-PH8-Mn is presented a small increasing of ZnO and CuO phase in XRD patterns. Cu metal is also presented in sCZA-PH8-Mn as seen in **Figure 35**. The Cu^0 of spent sCZA-PH8-Mn catalyst was detected the highest peak.

This result can support a higher reducibility to promote the reaction. Thus, Mn promoter can inhibit an agglomeration of CZA-PH8 by well dispersion of CuO and ZnO resulting increased catalytic activity.

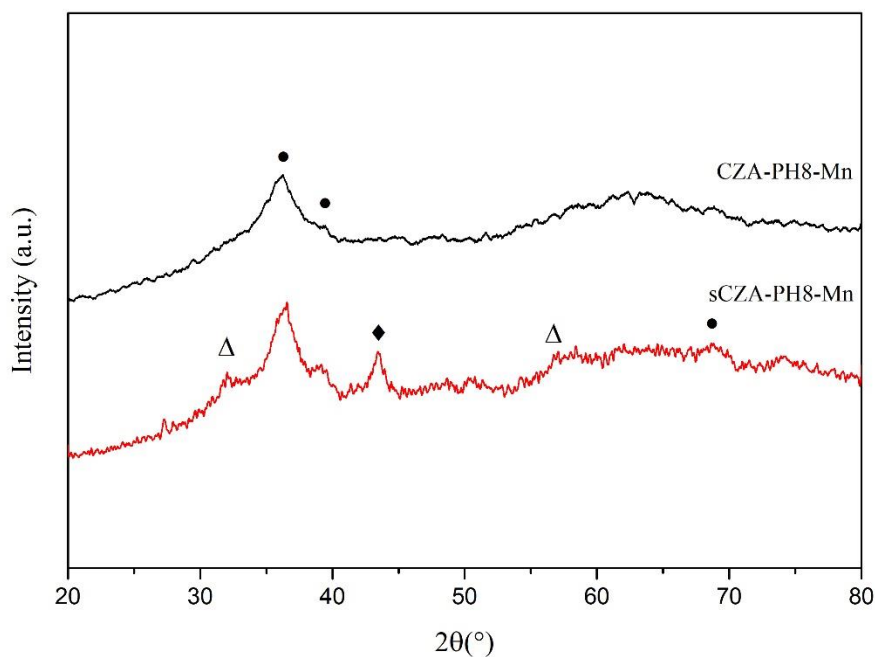


Figure 35 XRD patterns of fresh Cu/Zn/Al catalysts of metals loading (CZA-X, X=Mn,Si) at pH 8 and spent catalysts (sCZA-X, X=Mn,Si), (●) CuO ; (Δ) ZnO; (○) Zincian malachite, $(\text{Cu,Zn})_2(\text{OH})_2\text{CO}_3$; (◆) Cu.

Finally, the crystallite size of spent sCZA-PH8 was lower than fresh catalysts CZA-PH8 by a partial ZnO large crystallite size and cover in some surface of CuO. In addition, the result of spent Mn promoter was observed a singly changing of large crystallite size. As a result, Mn promoter had a significant effect to prevent a large crystallite size of metal active site.

Table 25 Crystalline size of CZA catalysts.

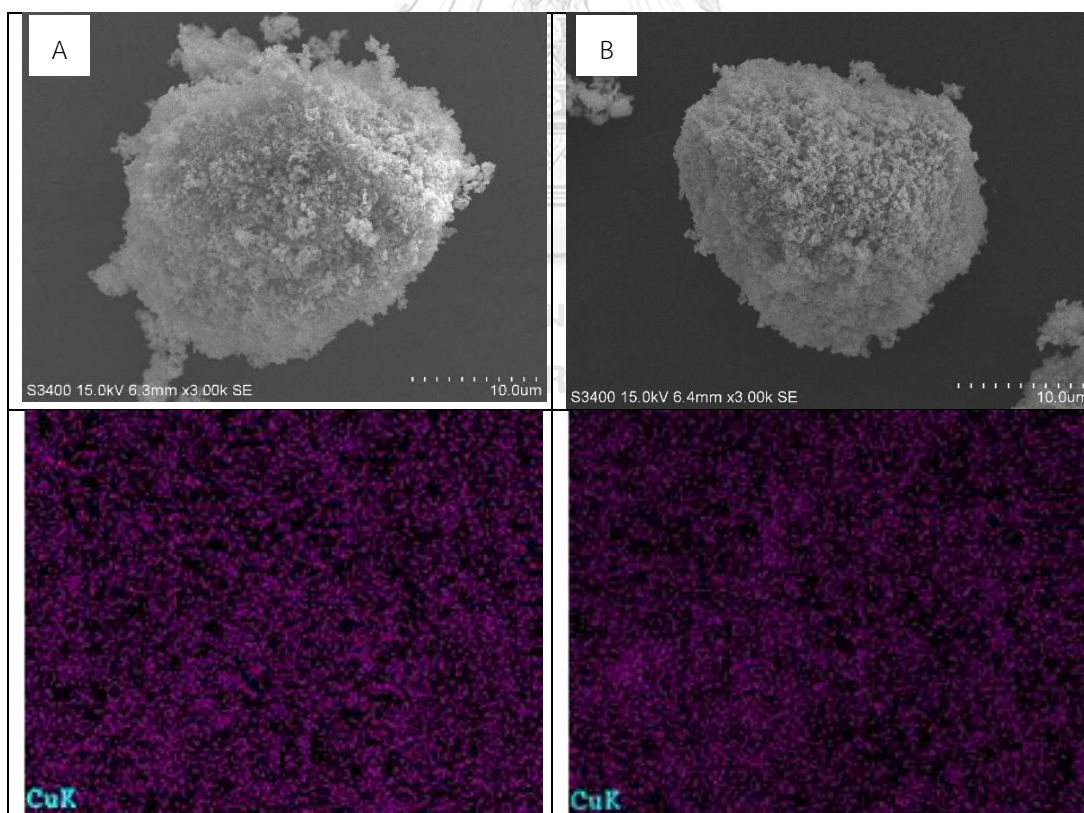
Samples	$D_{\text{avg,CuO}}$ (nm)
CZA-PH8	6.13
CZA-PH8-Mn	4.42

sCZA-PH8	5.11
sCZA-PH8-Mn	4.83

4.3.1.2 Scanning Electron Microscope (SEM) and energy-dispersive X-ray spectroscopy (EDX)

SEM and EDX determined a surface property of CZA catalysts during stability test as shown in **Figure 36**. The effect of morphology after stability test is shown by the similar morphology of catalysts by comparison of CZA-PH8 and sCZA-PH8.

EDX images is presented for all important elements of CZA catalysts in **Figure 36**. It was found that amount of all elements was similar. As a result, the activity test of catalyst in before and after reaction had a similar shape of spherical catalysts. On the other words, the morphology of CZA catalyst did not significantly change up on reaction condition after 5 h.



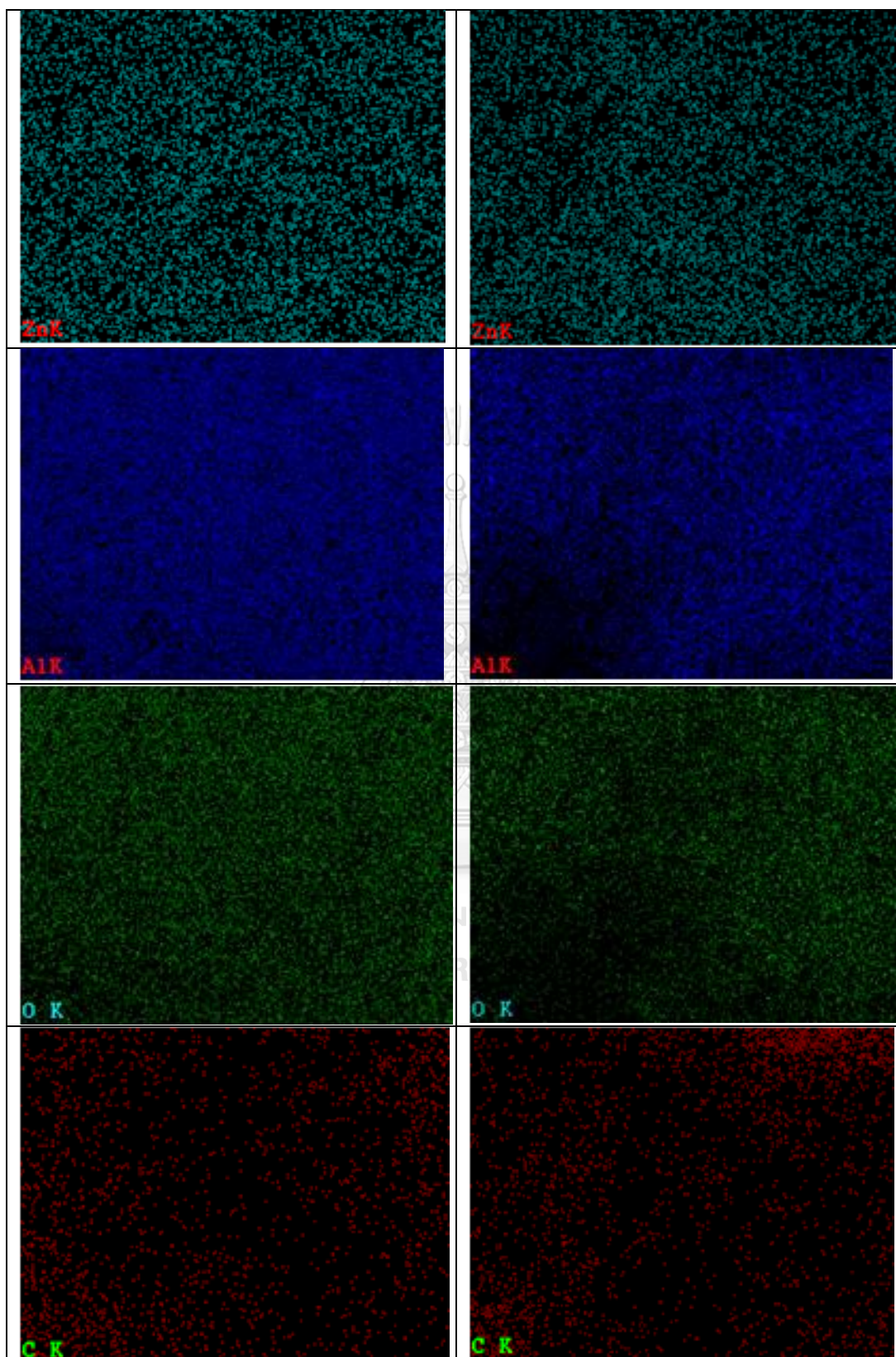


Figure 36 SEM and EDX images of stability CZA-PH8, A; fresh CZA-PH8, B; spent sCZA-PH8.

For another, EDX was used to determine an elemental distribution on surface catalyst by scattering techniques and presented in percent weight of each element in **Table 25**. The element can presented a component of catalyst in weight ratio of Cu:Zn:Al = 40:40:20 by following before and after reaction test in CZA-PH8. It was observed that Cu content had tended to increase. This fact related with XRD patterns, which promoted an agglomeration of CuO. Additionally, carbon (C) content was slightly increased from spent catalyst. C was identified the C in precursor of carbonated. However, the sCZA-PH8 was found an increasing of C contents form fresh catalyst. It referred to a coke in catalyst.

Table 26 EDX elemental analysis Cu, Zn, Al, O, and C element on surface of fresh CZA catalysts (CZA-PH8) and spent catalyst (sCZA-PH8)

Samples	Cu	Zn	Al	O	C
CZA-PH8	28.7	39.1	11.6	17.23	3.4
sCZA-PH8	31.9	34.5	14.0	14.4	5.2

4.3.1.3 X-ray photoelectron spectroscopy (XPS)

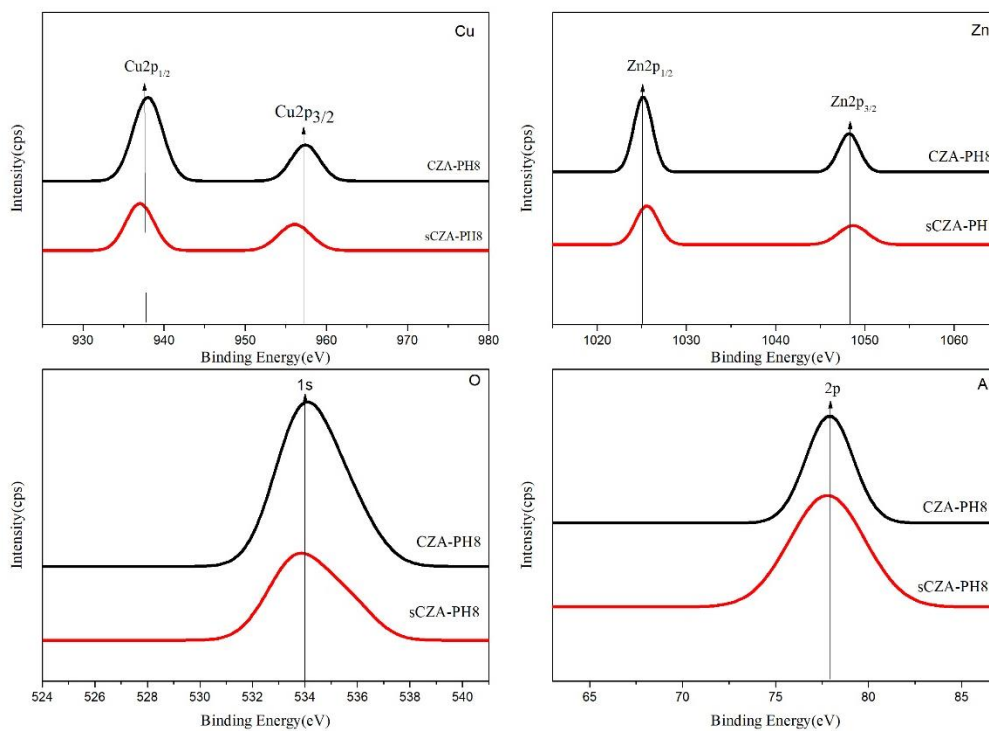


Figure 37 Cu species of CZA-PH8 catalyst in fresh and spent catalyst.

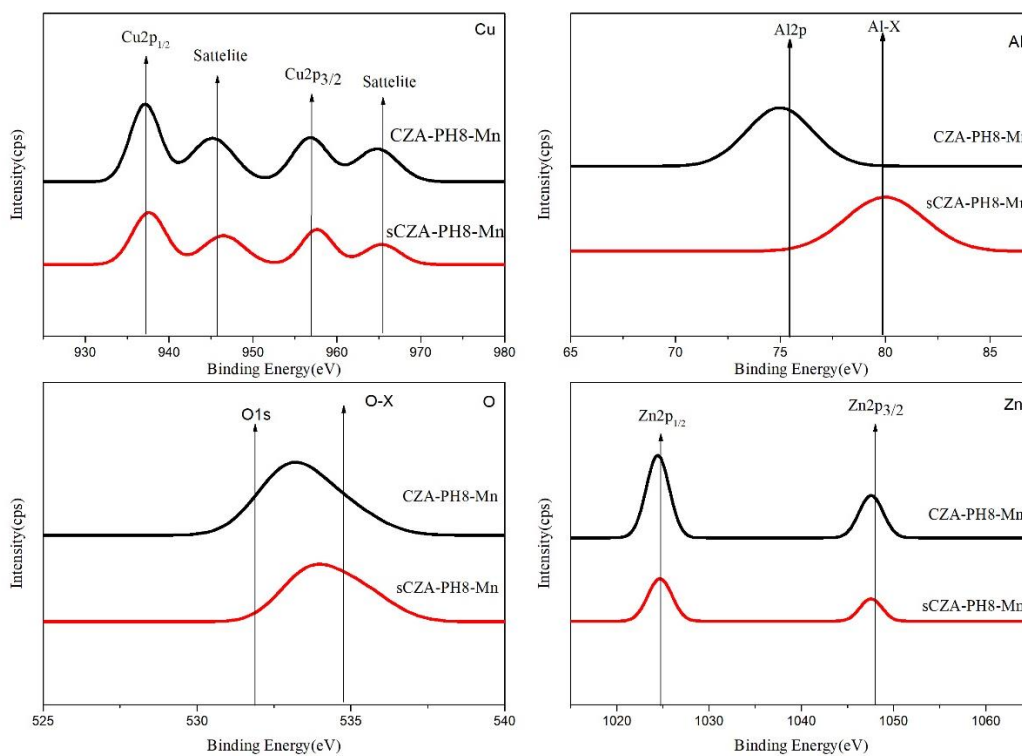


Figure 38 Chemicals species of CZA-PH8-Mn, sCZA-PH8-Mncatalyst in fresh and spent catalyst.

XPS spectra was used to determine a difference of before and after stability test as seen in **Figure 37**. The result suggested a specious by the same in first and second part of CZA catalyst. Kattel et al. [37] suggested the effect of accumulation of O species. It can dissociate to CO and O intermediates on ZnO or Cu⁰ metal site. This fact promoted mechanism of HCOO and O intermediate of changing methanol. Therefore, CZA-PH8 was selected to promote with O species decreasing on catalyst. However, the Cu²⁺ and Zn²⁺ were higher decreasing. This result led to inactive form of CuO and ZnO on surface catalyst with largely active site.

For a part of after reaction test by following a high methanol yield and CO₂ conversion of CZA-PH8-Mn, it was observed a specious property to CZA catalysts. The Mn promoter was shifted to high binding energy. This result was denoted in Mn-Al interaction or MnO contamination on Al²⁺. The proposal was identified by O

species. For another, O species was observed singly changing of binding energy. It promoted MnO interaction of CZA catalyst and Cu^{2+} was not observed a changing of deconvolute peak. This reason suggested to stability of Cu^{2+} active site to Cu^0 .

Table 27 The property of XPS spectra and mass of Cu,Zn,Al,O species of the effect of activity test, before activity test; CZA-PH8 and after activity test; sCZA-PH8

Samples	Position of binding energy(eV)					Mass (%)			
	Cu2p _{3/2}	Cu2p _{1/2}	Zn2p _{3/2}	Zn2p _{1/2}	Al2p	Cu	Zn	Al	O
CZA-PH8	935.3	954.5	1022.6	1045.7	74.9	16.66	27.79	6.43	49.11
sCZA-PH8	937.2	957.1	1025.6	1047.8	76.9	14.82	25.59	15.02	44.57

Table 28 The property of XPS spectra and mass of Cu,Zn,Al,O species of the effect of Zr,Mn promoter of the effect of activity test, before activity test; CZA-PH8-Mn and after activity test; sCZA-PH8-Mn

Samples	Position of binding energy(eV)							
	Cu^{2+}		Satellite		Zn^{2+}		Al^{3+}	X^x
	Cu2p _{3/2}	Cu2p _{1/2}	Cu2p _{3/2}	Cu2p _{1/2}	Zn2p _{3/2}	Zn2p _{1/2}	Al2p	X2p
CZA-Mn	937.2	957.1	945.6	964.0	1025.6	1047.8	79.1	634.9
sCZA-Mn	937.8	957.3	946.8	965.6	1026.0	1048.5	78.3	647.1

CHAPTER 5

CONCLUSIONS AND RECOMMENDATIONS

In conclusion, the effect of pH value in suitable catalyst and effect of metals loading was identifying into 3 part

Part 1: The effect of increasing pH value in CZA catalyst preparation.

From this first part, the effect of different pH during co-precipitation can be elucidated up on physical and chemical properties of CZA catalysts. It can be concluded that;

- (1) CZA-PH8 was found to have higher dispersion of CuO based on the XRD results resulting in small crystallite size of CuO and ZnO.
- (2) BET surface area was proposed a slight change of for CZA-PH7 and CZA-PH8. However, CZA-PH9 was found to have the lowest surface area.
- (3) The main active site of Cu is reported in form Cu^0 and the CZA-PH8 exhibited the highest reducibility among other catalysts.
- (4) CZA-PH8 and CZA-PH9 exhibited high amount of basic site. This property can improve the adsorption of CO_2 gas by carbonate group on surface. However, CZA-PH9 had lower surface area.
- (5) NH_3 -TPD was investigated and high acidity was denoted decreasing of activity of CZA catalyst.
- (6) XPS revealed that Cu^{2+} species is mainly in all CZA catalysts.

Part 2: The effect of Mn, Zr, and Si promoters on CZA-PH8 catalyst.

In conclusion, relation of characterization and reaction test is summarized the part of the effect of Zr, Mn, and Si promoters as follows;

- (1) The modification of Zr, Mn, and Si can decrease crystallite size to 3.43-4.42. The Mn and Zr was found to have a well dispersion of CuO, ZnO. Leading to low agglomeration as seen by XRD patterns.

- (2) Mn promoter was found to exhibit the highest surface area. It had relation with high CuO, ZnO dispersion in XRD part and Mn promoter improve Cu⁰ dispersion as measured by H₂-Chemisorption.
- (3) The shifting of moderate acidity site became to weak acid is an important property for not promoting H₂ saturation to undesirable H₂O product. This phenomenon was appeared with Mn promotion. This reason introduced basicity of Mn promotion.
- (4) Reaction test showed a good activity by Mn promoter. It can improve CZA-PH8 expressing the highest CO₂ conversion and methanol yield at 4.70% and 0.46%, respectively. The Mn promoter was selected to study the stability test in next part.

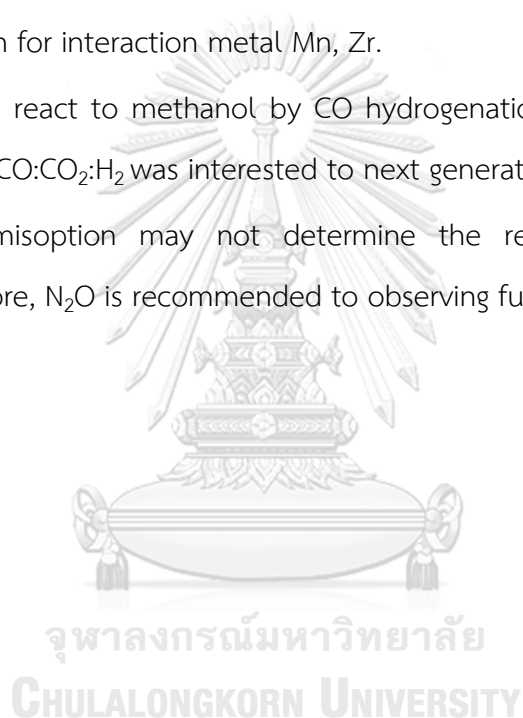
Part 3: The stability of CZA catalyst

In conclusion, the effect of stability can be explained in the different of previous part.

- (1) sCZA-PH8 was detected an accumulation of CuO and ZnO in XRD pattern. The Mn promotion was found a successful development of active site, which related to prevent active site sintering.
- (2) Mn promoter had an effect to promote Cu⁰ metal on XRD pattern and it facilitated reducibility, which was corresponding to high activity of CZA catalyst.
- (3) The promotion of Mn can increase CO₂ conversion and methanol yield by stability of Cu²⁺ on reaction condition.

Recommendations

- (1) C contents in CZA surface was found a stable in catalyst. It could to using and identified that C content in fresh catalyst is carbonates or coke species by TGA.
- (2) Mn, Zr and Si can load with various contents, at experiment the Mn is the best of this reaction condition.
- (3) The effect of reduction could to study by relative with temperature reaction for interaction metal Mn, Zr.
- (4) CO can react to methanol by CO hydrogenation. Therefore, the ratio of mixing CO:CO₂:H₂ was interested to next generation.
- (5) H₂-chemisoption may not determine the real total Cu⁰ active site. Therefore, N₂O is recommended to observing fully Cu⁰ metal.



APPENDIX

APPENDIX.A CALCULATION OF CATALYSTS PERFORMANCE

A.1 CO₂ Conversion by C balance

$$\text{CO}_2 \text{ Conversion}(\%) = \frac{CO_2^{\text{initial mole}} - CO_2^{\text{final mole}}}{CO_2^{\text{initial mole}}} \times 100$$

A.2 Methanol selectivity

$$\text{CH}_3\text{OH selectivity}(\%) = \frac{MeOH^{\text{final mole}}}{CO_2^{\text{initial mole}} - CO_2^{\text{final mole}}} \times 100$$

A.3 Methanol Yield

$$\text{CH}_3\text{OH yield}(\%) = \text{CH}_3\text{OH selectivity} \times \text{CO conversion}$$

A.4 CO₂ reaction rate

$$\text{CO}_2 \text{ reaction rate} = \frac{CO_2^{\text{initial mole}} - CO_2^{\text{final mole}}}{gCat \times time(\text{min})} \times 100$$

A.5 CH₃OH production rate

$$\text{CH}_3\text{OH production rate} = \frac{MeOH^{\text{final mole}}}{gCat \times time(\text{min})} \times 100$$

A.6 CO₂ reaction rate and CH₃OH production rate at time on stream

Table A.6.1 CO₂ reaction rate and CH₃OH production rate of CZA-PH7 catalyst

Time (h)	CO ₂ reaction rate (mol/g cat.h)×10 ⁻⁷	CH ₃ OH production rate (mol/g cat.h)×10 ⁻⁷
0	-	-
0.5	37.74	4.49
1	21.56	2.30
1.5	15.60	1.53
2	10.92	1.13
2.5	11.15	0.91
3	7.12	0.75
3.5	5.61	0.63
4	8.352	0.56
4.5	4.91	0.50
5	4.79	0.44
5.5	4.23	0.41

Table A.6.2 CO₂ reaction rate and CH₃OH production rate of CZA-PH8 catalyst

Time (h)	CO ₂ reaction rate (mol/g cat.h)×10 ⁻⁷	CH ₃ OH production rate (mol/g cat.h)×10 ⁻⁷
0	-	-
0.5	45.37	4.49
1	23.08	2.30
1.5	14.96	1.53
2	10.00	1.13
2.5	10.16	0.91
3	6.73	0.75
3.5	6.13	0.63
4	5.30	0.56
4.5	5.02	0.50
5	4.08	0.44
5.5	4.35	0.41



Table A.6.3 CO₂ reaction rate and CH₃OH production rate of CZA-PH9 catalyst

Time (h)	CO ₂ reaction rate (mol/g cat.h)×10 ⁻⁷	CH ₃ OH production rate (mol/g cat.h)×10 ⁻⁷
0	-	-
0.5	14.61	1.42
1	5.40	0.68
1.5	5.05	0.47
2	3.73	0.33
2.5	1.84	0.27
3	2.35	0.23
3.5	1.96	0.19
4	1.58	0.16
4.5	1.07	0.15
5	1.50	0.14
5.5	1.05	0.12



Table A.6.4 CO₂ reaction rate and CH₃OH production rate of CZA-PH8-Si catalyst

Time (h)	CO ₂ reaction rate (mol/g cat.h)×10 ⁻⁷	CH ₃ OH production rate (mol/g cat.h)×10 ⁻⁷
0	-	-
0.5	64.76	2.71
1	34.85	1.22
1.5	15.92	0.84
2	20.69	0.62
2.5	13.32	0.46
3	8.71	0.39
3.5	9.44	0.33
4	6.50	0.29
4.5	5.25	0.27
5	4.19	0.23
5.5	5.41	0.21

Table A.6.5 CO₂ reaction rate and CH₃OH production rate of CZA-PH8-Mn catalyst

Time (h)	CO ₂ reaction rate (mol/g cat.h)×10 ⁻⁷	CH ₃ OH production rate (mol/g cat.h)×10 ⁻⁷
0	-	-
0.5	84.73	7.95
1	37.63	3.99
1.5	28.53	2.65
2	23.27	2.04
2.5	18.64	1.64
3	15.04	1.37
3.5	13.60	1.18
4	8.72	1.05
4.5	9.16	0.91
5	10.39	0.84
5.5	7.65	0.75

Table A.6.6 CO₂ reaction rate and CH₃OH production rate of CZA-PH8-Zr catalyst

Time (h)	CO ₂ reaction rate (mol/g cat.h)×10 ⁻⁷	CH ₃ OH production rate (mol/g cat.h)×10 ⁻⁷
0	-	-
0.5	78.11	7.054
1	39.16	3.62
1.5	25.52	2.38
2	14.87	1.86
2.5	17.29	1.47
3	13.70	1.23
3.5	11.84	1.06
4	7.43	0.93
4.5	7.44	0.83
5	9.19	0.75
5.5	6.91	0.69

A.7 Activity of CZA catalyst

Table A.7.1 The activity of CZA-PH7.

Time (min)	CO ₂ conversion (%)	CH ₃ OH selectivity (%)	CO selectivity (%)	CH ₃ OH yield (%)
0	2.02	11.89	88.10	0.24
30	2.31	10.65	89.35	0.25
60	2.51	9.79	90.21	0.25
90	2.34	10.38	89.62	0.24
120	2.99	8.17	91.83	0.24
150	2.29	10.53	89.47	0.24
180	2.11	11.30	88.70	0.24
210	3.59	6.76	93.24	0.24
240	2.37	10.11	89.89	0.24

270	2.57	9.20	90.80	0.24
300	2.49	9.69	90.31	0.24

Table A.7.2 The activity of CZA-PH8.

Time (min)	CO ₂ conversion (%)	CH ₃ OH selectivity (%)	CO selectivity (%)	CH ₃ OH yield (%)
0	2.43	9.89	90.11	0.24
30	2.47	9.95	90.05	0.25
60	2.40	10.21	89.79	0.25
90	2.14	11.33	88.67	0.24
120	2.72	8.96	91.04	0.24
150	2.16	11.13	88.87	0.24
180	2.30	10.34	89.66	0.24
210	2.27	10.65	89.35	0.24
240	2.42	9.89	90.11	0.24
270	2.18	10.82	89.18	0.24
300	2.56	9.42	90.58	0.24

Table A.7.3 The activity of CZA-PH9.

Time (min)	CO ₂ conversion (%)	CH ₃ OH selectivity (%)	CO selectivity (%)	CH ₃ OH yield (%)
0	0.84	9.71	90.29	0.08
30	0.62	12.54	87.46	0.08
60	0.88	9.37	90.63	0.08
90	0.86	8.75	91.25	0.08
120	0.53	14.50	85.50	0.08
150	0.82	9.60	90.40	0.08
180	0.81	9.63	90.37	0.08
210	0.73	10.33	89.67	0.08
240	0.56	13.92	86.08	0.08

270	0.87	9.19	90.81	0.08
300	0.67	11.41	88.59	0.08

Table A.7.4 The activity of CZA-PH8-Si.

Time (min)	CO ₂ conversion (%)	CH ₃ OH selectivity (%)	CO selectivity (%)	CH ₃ OH yield (%)
0	3.58	4.18	95.82	0.15
30	3.86	3.50	96.50	0.14
60	2.64	5.26	94.74	0.14
90	4.58	3.01	96.99	0.14
120	3.68	3.44	96.56	0.13
150	2.89	4.48	95.52	0.13
180	3.66	3.53	96.47	0.13
210	2.88	4.45	95.55	0.13
240	2.62	5.07	94.93	0.13
270	2.32	5.52	94.48	0.13
300	3.30	3.73	96.27	0.12

Table A.7.5 The activity of CZA-PH8-Mn.

Time (min)	CO ₂ conversion (%)	CH ₃ OH selectivity (%)	CO selectivity (%)	CH ₃ OH yield (%)
0	4.74	9.38	90.62	0.44
30	4.21	10.61	89.39	0.45
60	4.78	9.30	90.70	0.45
90	5.20	8.76	91.24	0.46
120	5.21	8.82	91.18	0.46
150	5.04	9.12	90.88	0.46
180	5.32	8.68	91.32	0.46
210	3.90	11.75	88.25	0.46
240	4.61	9.91	90.09	0.46

270	5.81	8.11	91.89	0.47
300	4.70	9.86	90.14	0.46

Table A.7.6 The activity of CZA-PH8-Zr.

Time (min)	CO ₂ conversion (%)	CH ₃ OH selectivity (%)	CO selectivity (%)	CH ₃ OH yield (%)
0	4.22	9.03	90.62	0.38
30	4.23	9.25	89.39	0.39
60	4.14	9.33	90.70	0.39
90	3.21	12.48	91.24	0.40
120	4.67	8.52	91.18	0.40
150	4.44	8.90	90.88	0.40
180	4.48	8.98	91.32	0.40
210	3.21	12.54	88.25	0.40
240	3.62	11.15	90.08	0.40
270	4.97	8.16	91.89	0.41
300	4.11	9.99	90.14	0.41

APPENDIX.B CALCULATION OF CRYSTALLINE SIZE

B.1 The Scherrer's equation

$$D = \frac{K\lambda}{\beta \cos\theta}$$

D = Crystallite size (°A)

K = Crystallite – shape factor = 0.9

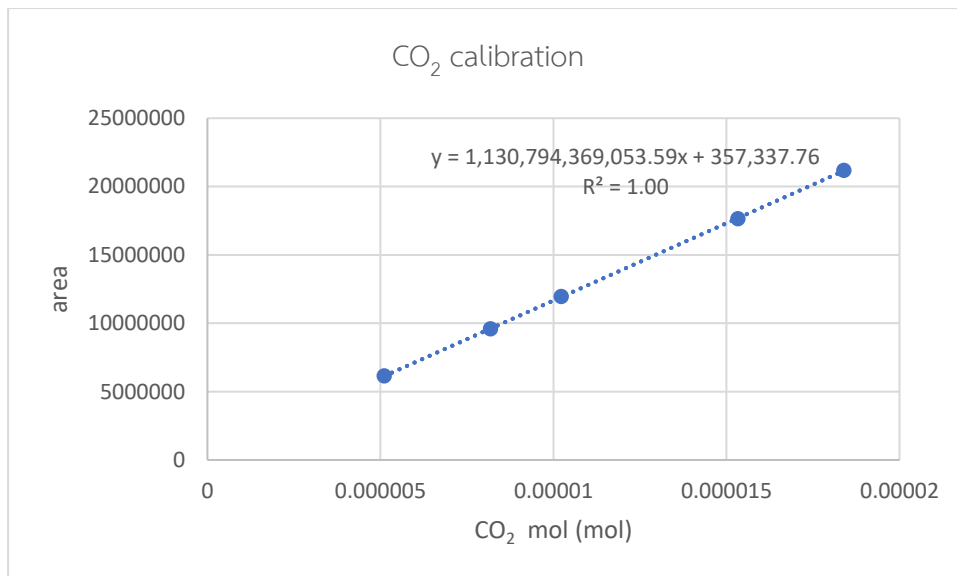
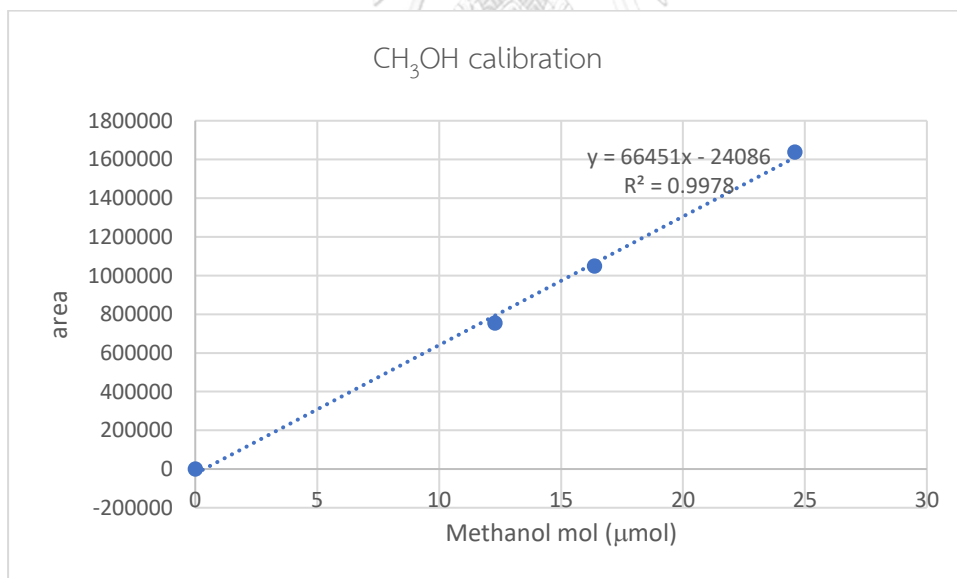
λ = X – ray wavelength, 1.5418 °A for CuK α

θ = Observes peak angel (degree)

β = X – ray diffraction broadening (radian)



APPENDIX.C CALBRATION

C.1 CO₂ calibrationFigure C.1.1 The calibration of CO₂ by using sample loops (mol)C.2 CH₃OH calibrationFigure C.1.2 The calibration of CH₃OH by using sample loops (µmol)

C.3 NH₃-TPD calibration

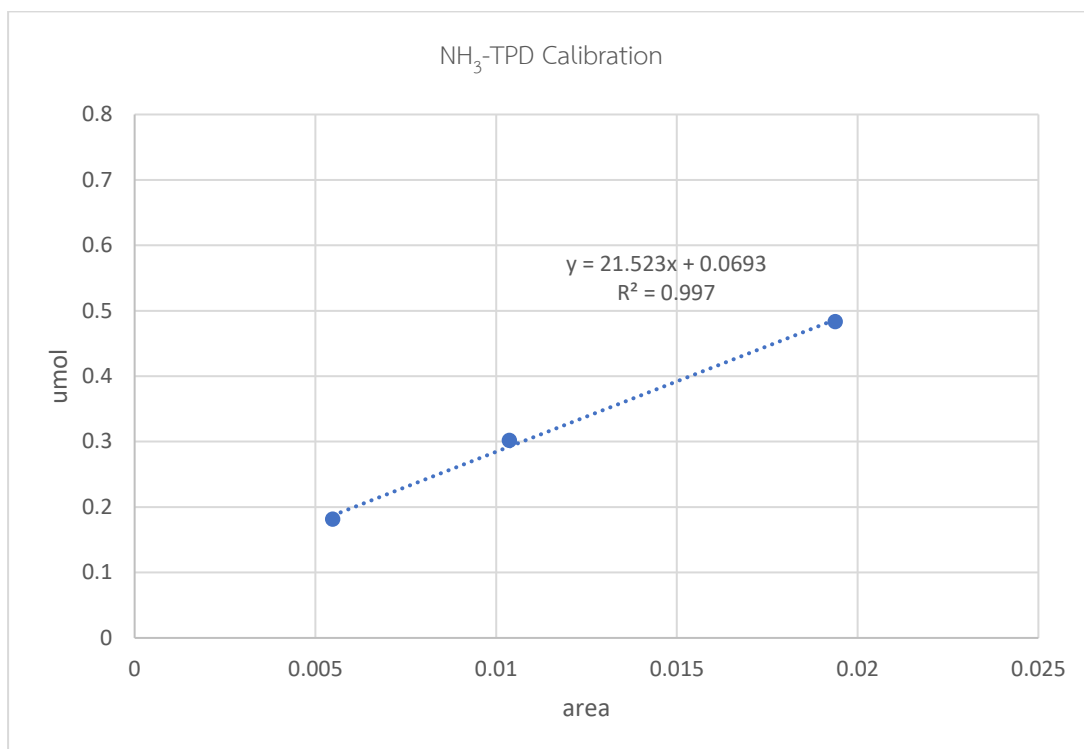


Figure C.1.3 The calibration of NH₃-TPD.

C.4 CO₂-TPD calibration

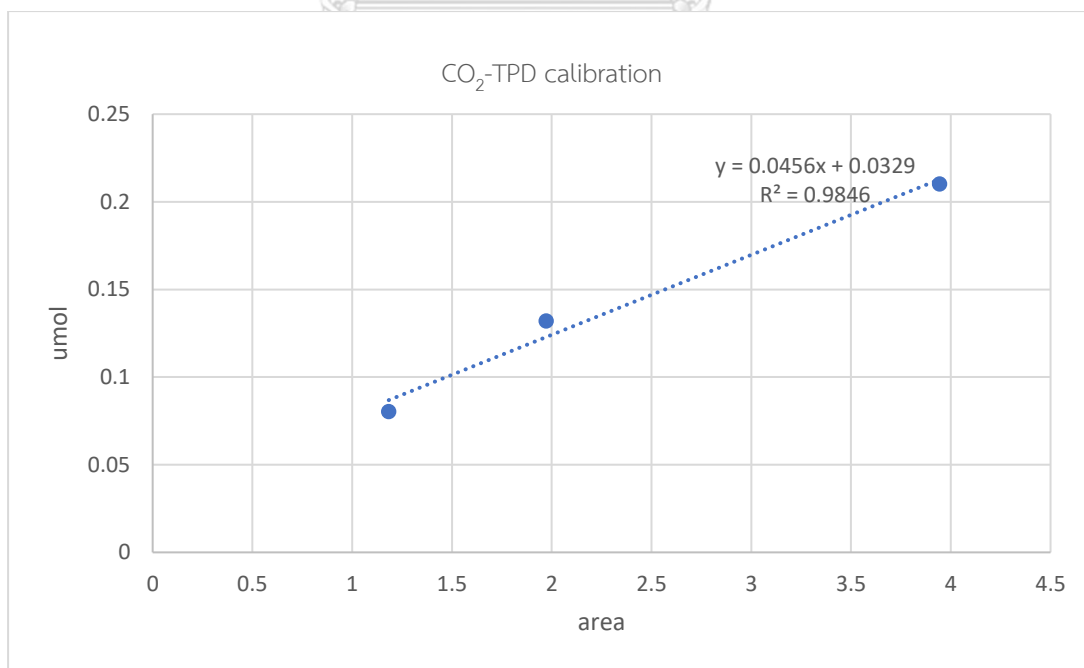
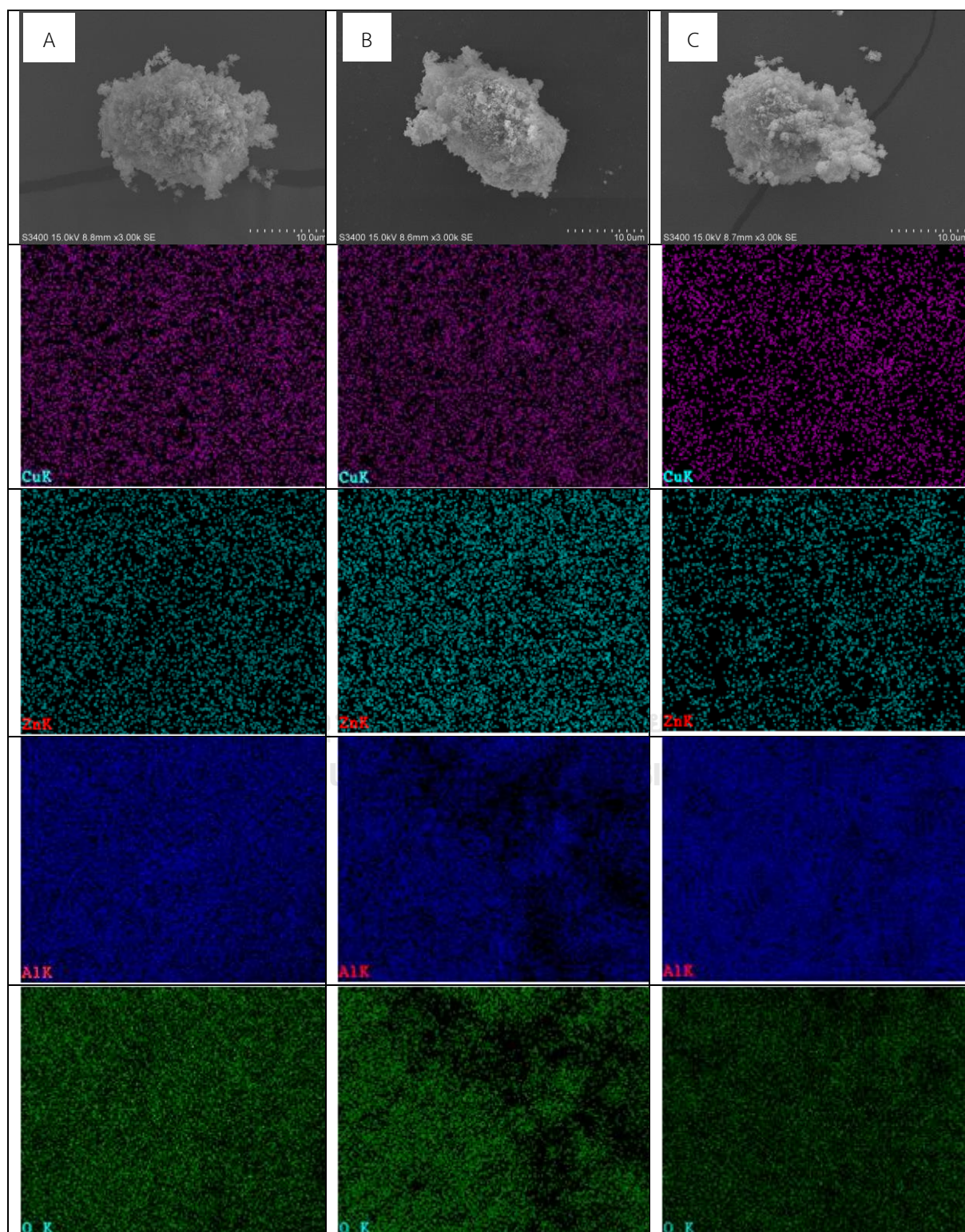


Figure C.1.4 The calibration of CO₂-TPD.

APPENDIX.D SCANNING ELECTRON MICROSCOPE (SEM) AND ENERGY-DISPERSIVE
X-RAY SPECTROSCOPY (EDX)

D.1 SEM-EDX of effect of metals promoters.



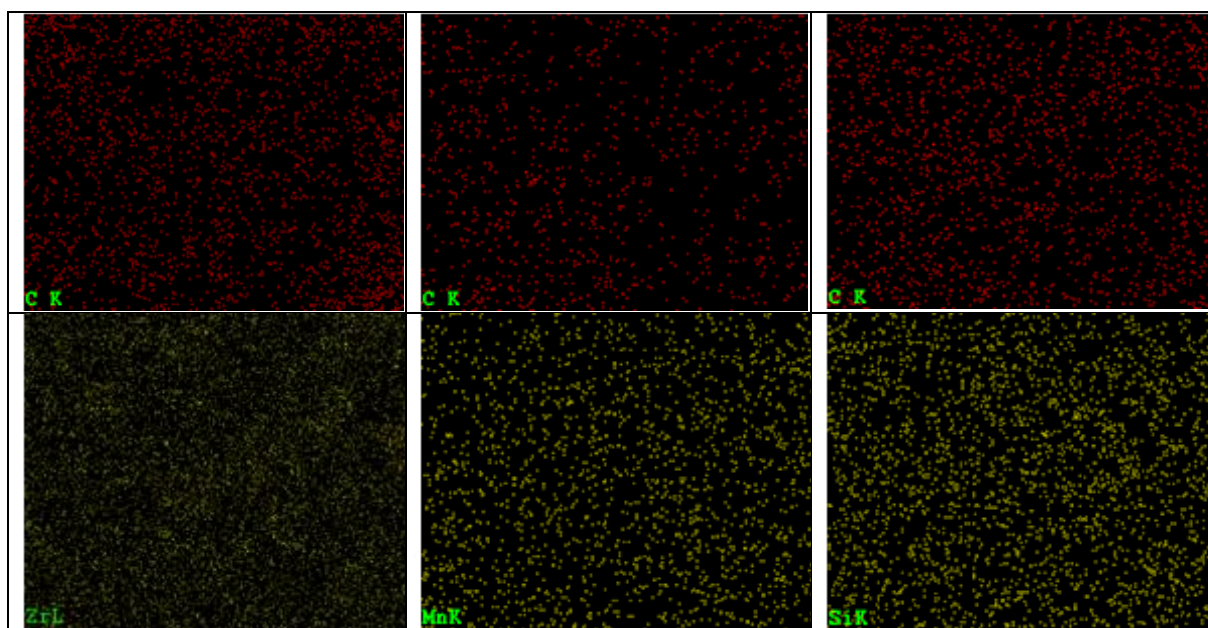


Figure D.1.1 SEM-EDX of all elements of A; CZA-PH8-Zr, B; CZA-PH8-Mn, C; CZA-PH8-Si.

Table D.1.1 EDX of CZA-PH8-Zr

Element	Wt%	At%
CK	04.67	12.11
OK	22.03	42.89
AlK	15.90	18.36
ZrL	07.77	02.66
CuK	24.50	12.01
ZnK	25.13	11.98
Matrix	Correction	ZAF

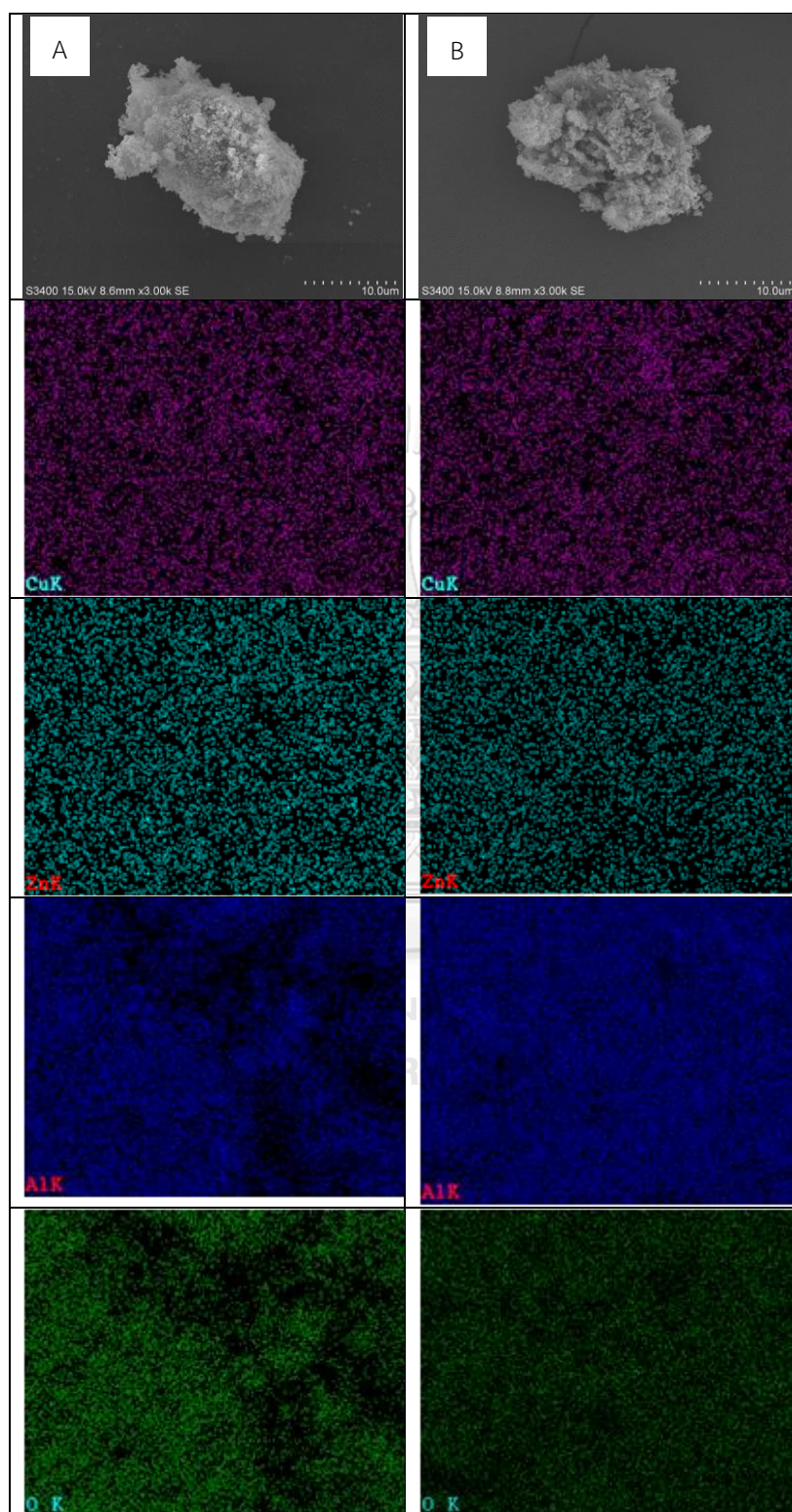
Table D.1.2 EDX of CZA-PH8-Mn

Element	Wt%	At%
CK	01.73	05.34
OK	15.41	35.63
AlK	14.32	19.63
MnK	00.97	00.65
CuK	30.60	17.81
ZnK	36.98	20.93
Matrix	Correction	ZAF

Table D.1.3 EDX of CZA-PH8-Si

Element	Wt%	At%
CK	04.30	10.14
OK	25.14	44.47
AlK	23.52	24.67
SiK	00.13	00.14
CuK	22.30	09.93
ZnK	24.60	10.65
Matrix	Correction	ZAF

D.2 SEM-EDX of effect of metals promoters in stability test.



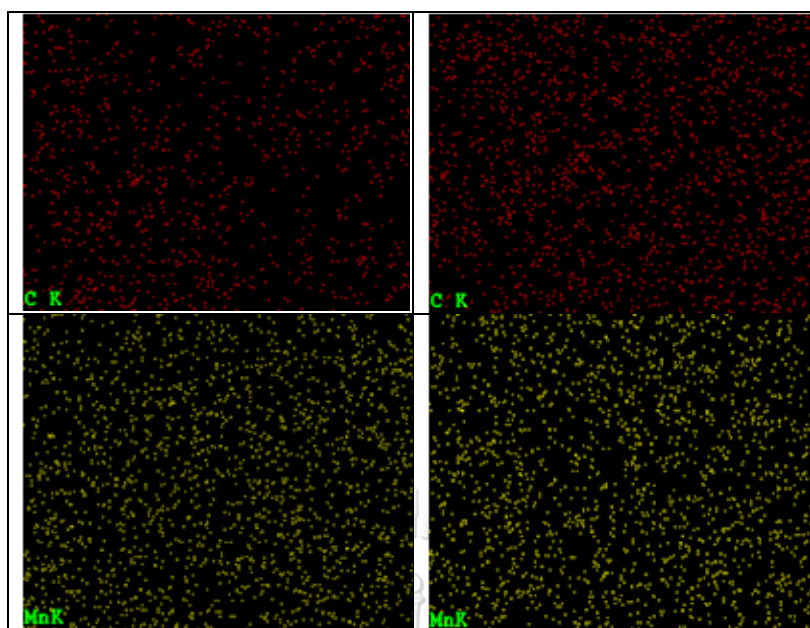
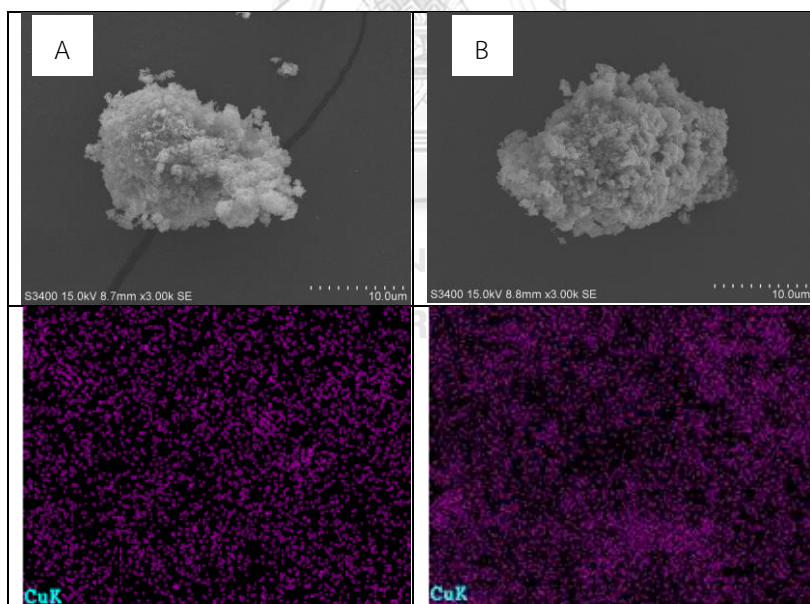


Figure D.2.1 SEM-EDX of all elements of stability A; CZA-PH8-Mn (fresh catalyst), B; sCZA-PH8-Mn (spent catalyst).



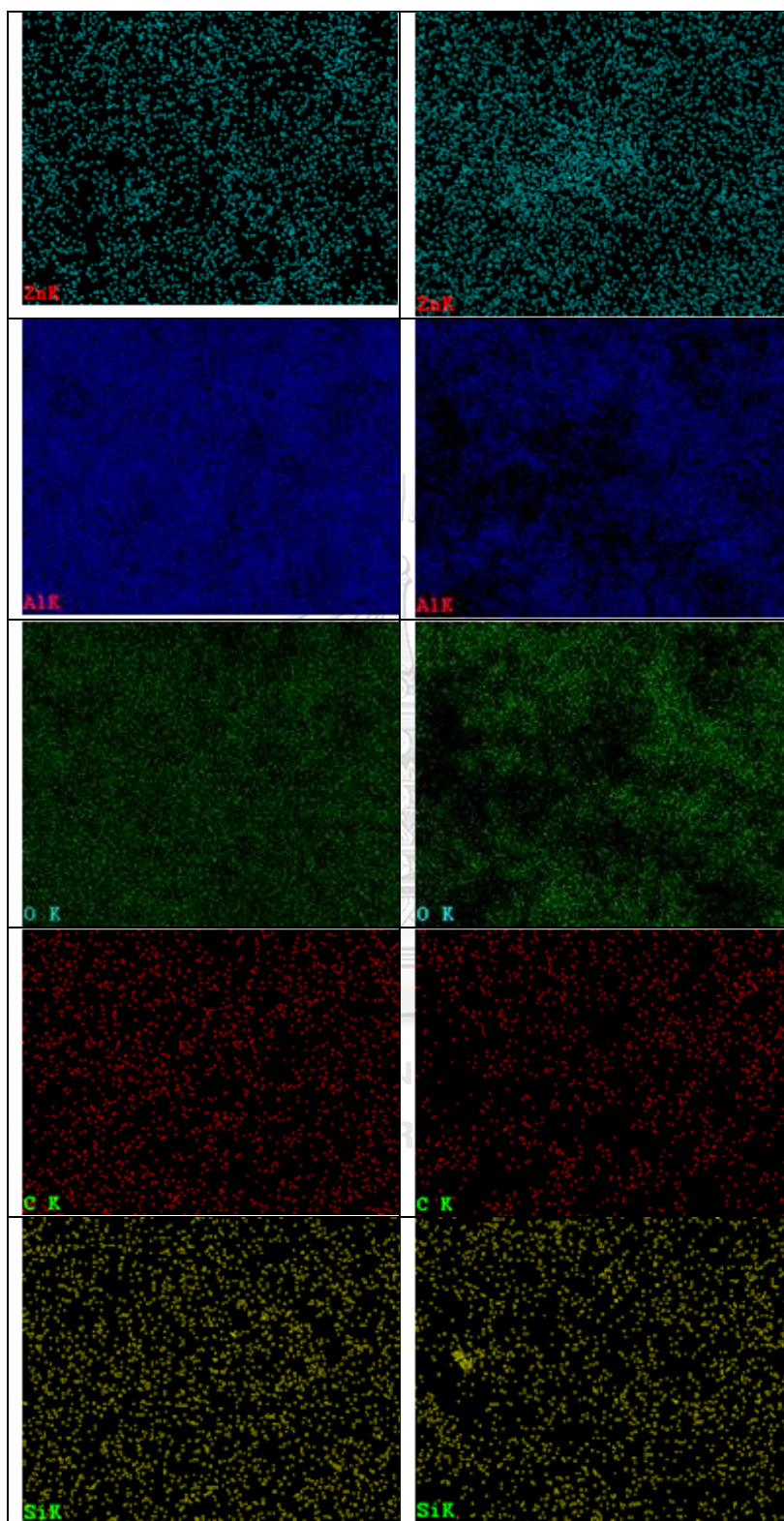


Figure D.2.2 SEM-EDX of all elements of stability A; CZA-PH8-Si (fresh catalyst), B; sCZA-PH8-Si (spent catalyst).

Table D.2.1 EDX of sCZA-PH8-Mn

Element	Wt%	At%
CK	01.97	05.65
OK	18.52	39.96
AlK	15.78	20.19
MnK	00.86	00.54
CuK	30.87	16.77
ZnK	31.99	16.89
Matrix	Correction	ZAF

Table D.2.1 EDX of sCZA-PH8-Si

Element	Wt%	At%
CK	04.94	14.19
OK	17.53	37.77
AlK	08.68	11.09
SiK	00.14	00.17
CuK	34.28	18.60
ZnK	34.43	18.16
Matrix	Correction	ZAF

APPENDIX.E X-RAY PHOTOELECTRON SPECTROSCOPY

E.1 Chemical species of CZA-PH7 catalyst.

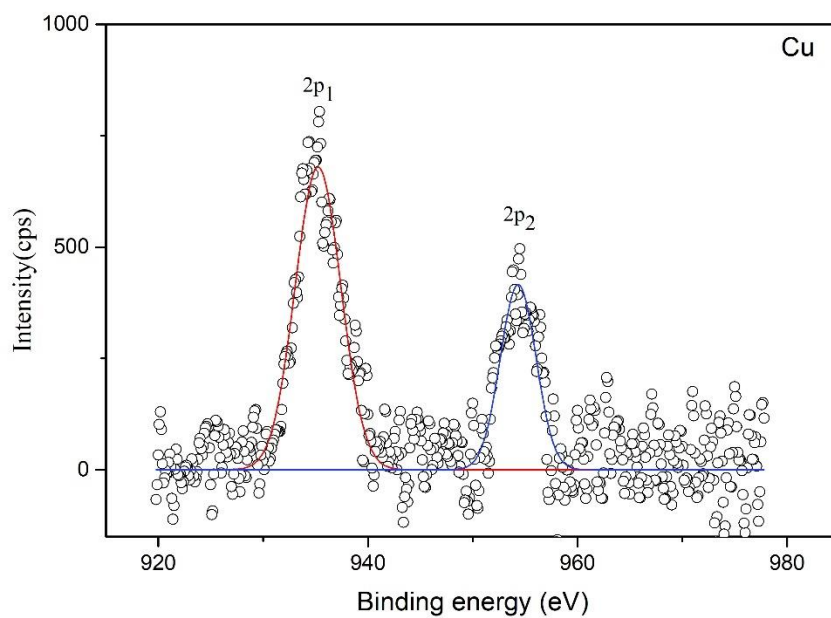


Figure E.1.1 XPS spectra of Cu species on CZA-PH7.

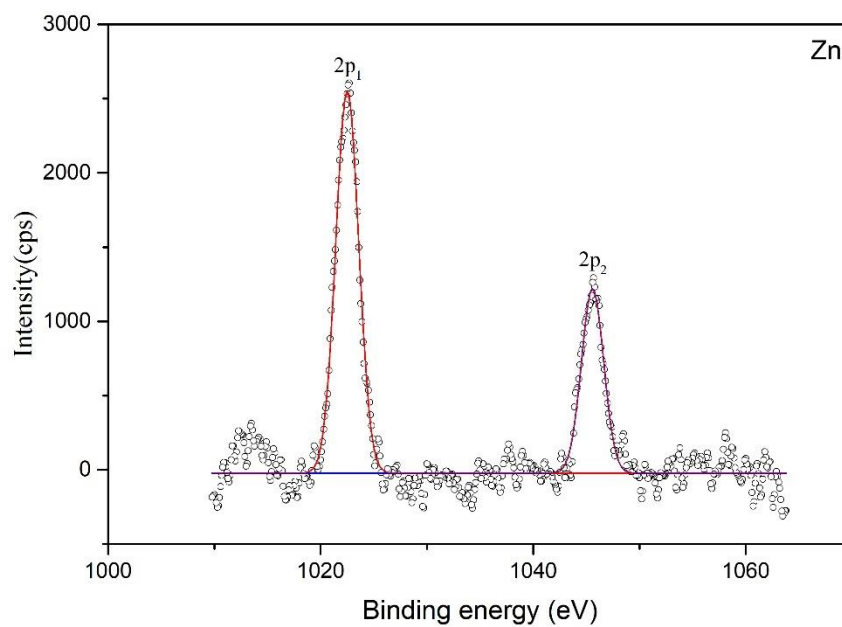


Figure E.1.2 XPS spectra of Zn species on CZA-PH7.

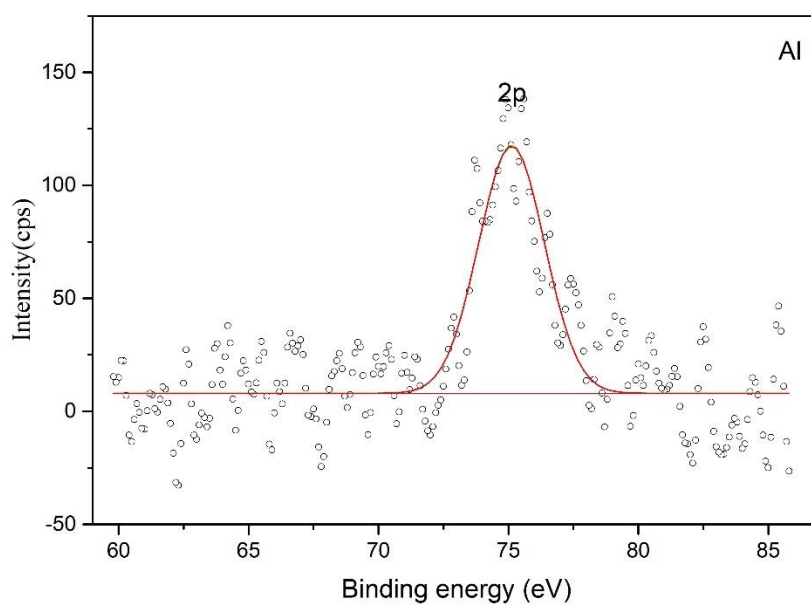


Figure E.1.3 XPS spectra of Al species on CZA-PH7.

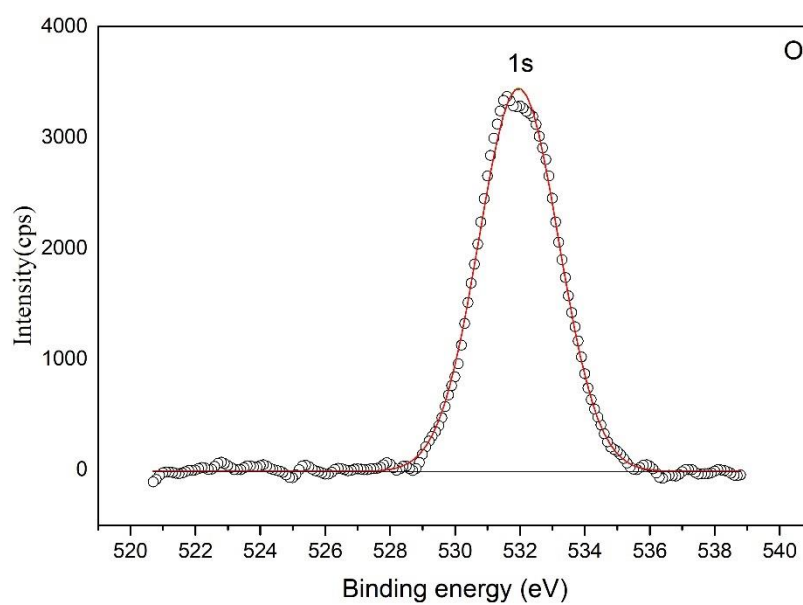


Figure E.1.4 XPS spectra of O species on CZA-PH7.

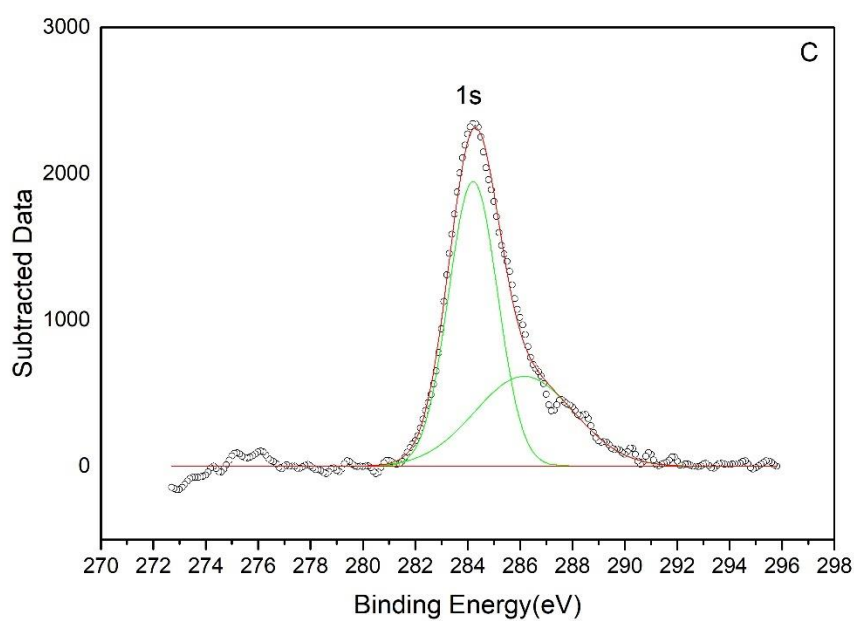


Figure E.1.5 XPS spectra of C species on CZA-PH7.

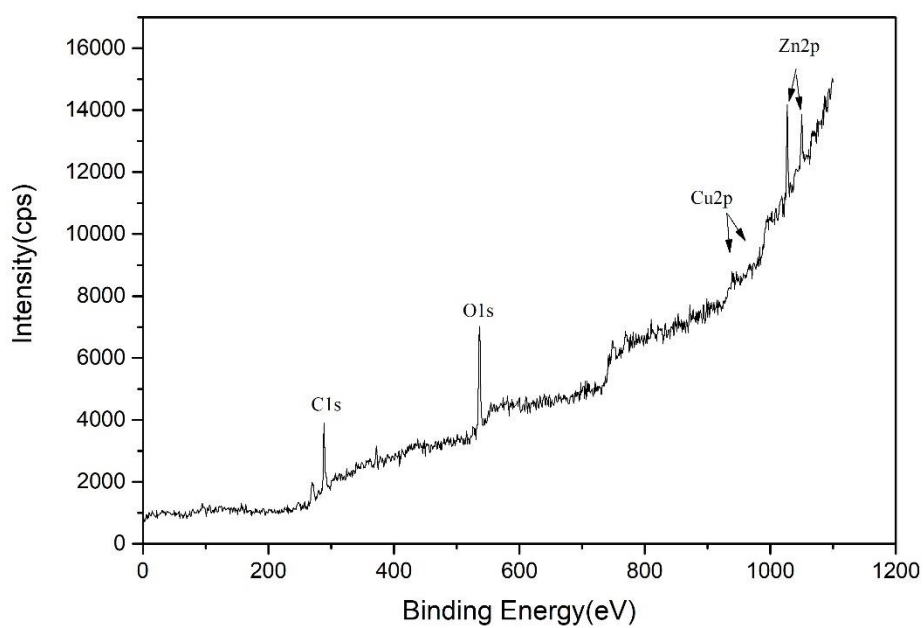


Figure E.1.6 XPS spectra of all species on CZA-PH7

E.2 Chemical species of CZA-PH8 catalyst.

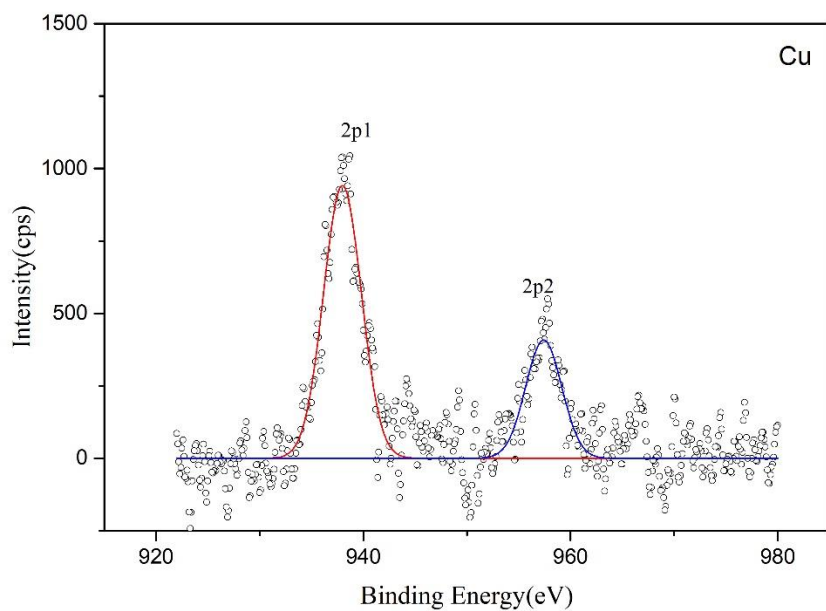


Figure E.2.1 XPS spectra of Cu species on CZA-PH8.

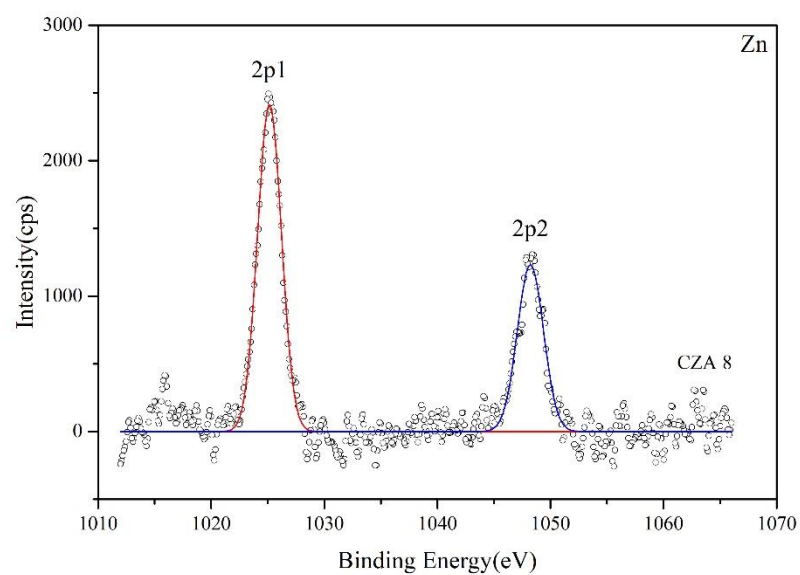


Figure E.2.2 XPS spectra of Zn species on CZA-PH8.

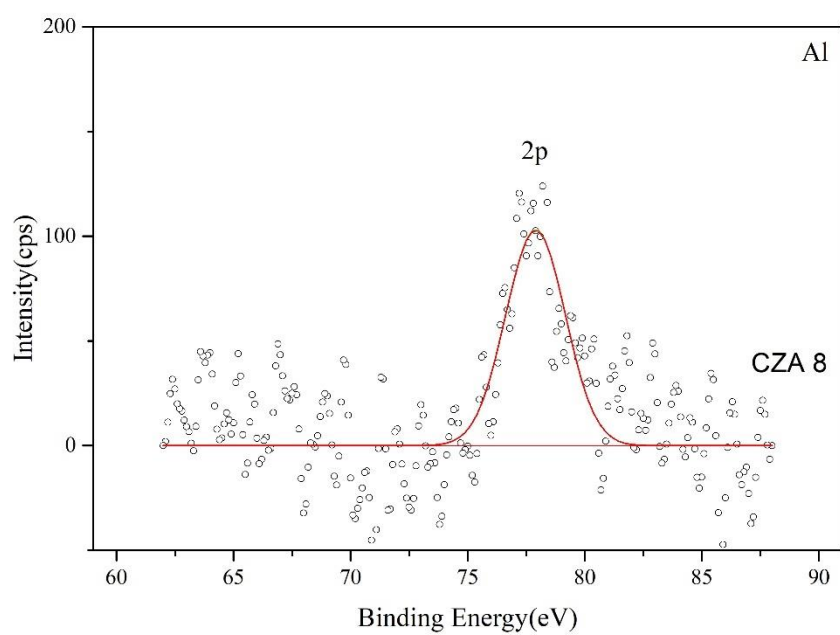


Figure E.2.3 XPS spectra of Al species on CZA-PH8.

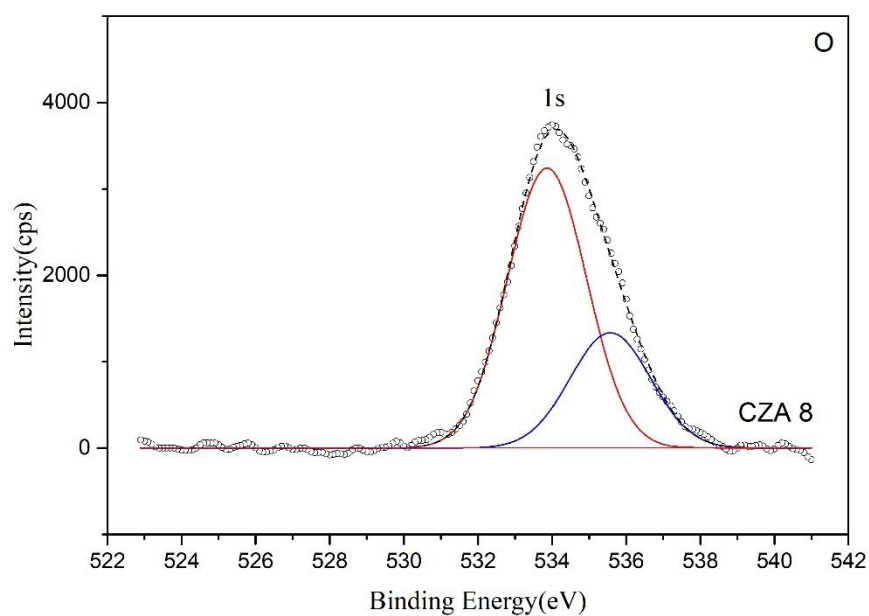


Figure E.2.4 XPS spectra of O species on CZA-PH8.

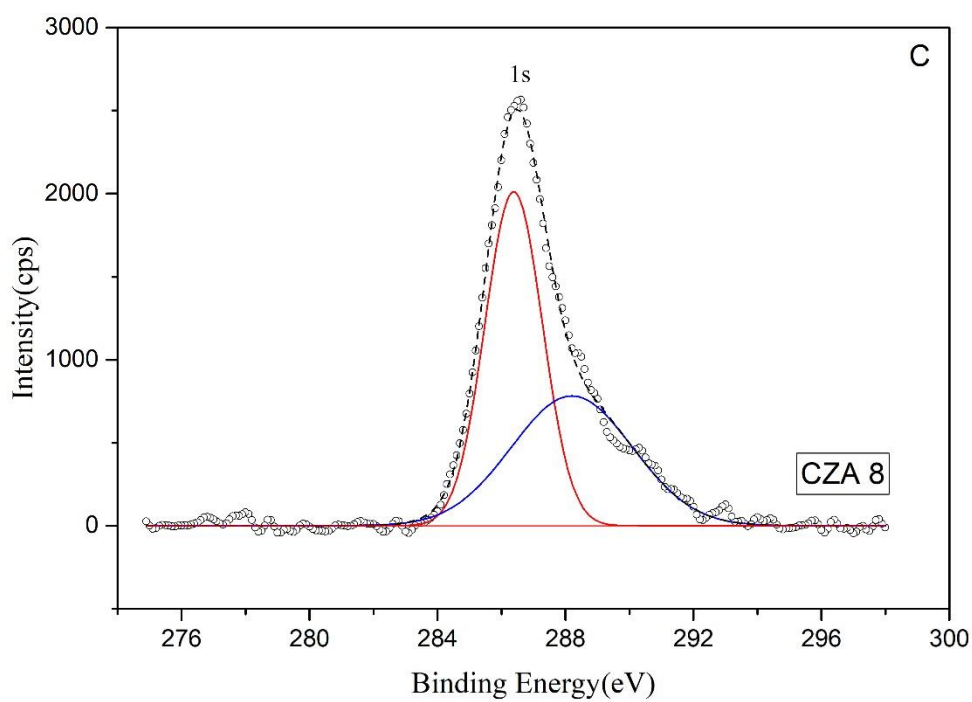


Figure E.2.5 XPS spectra of C species on CZA-PH8.

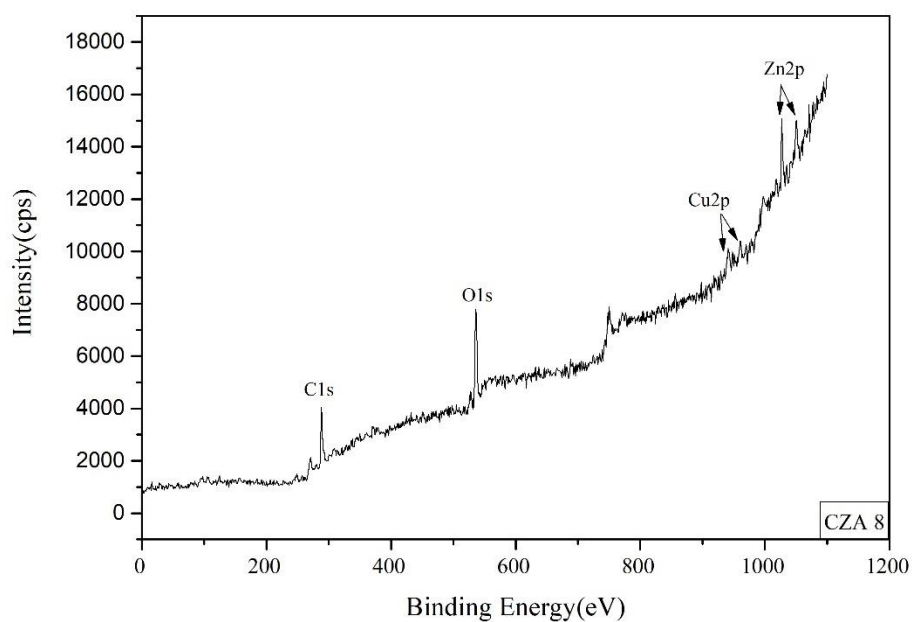


Figure E.2.6 XPS spectra of all species on CZA-PH8.

E.3 Chemical species of CZA-PH9 catalyst.

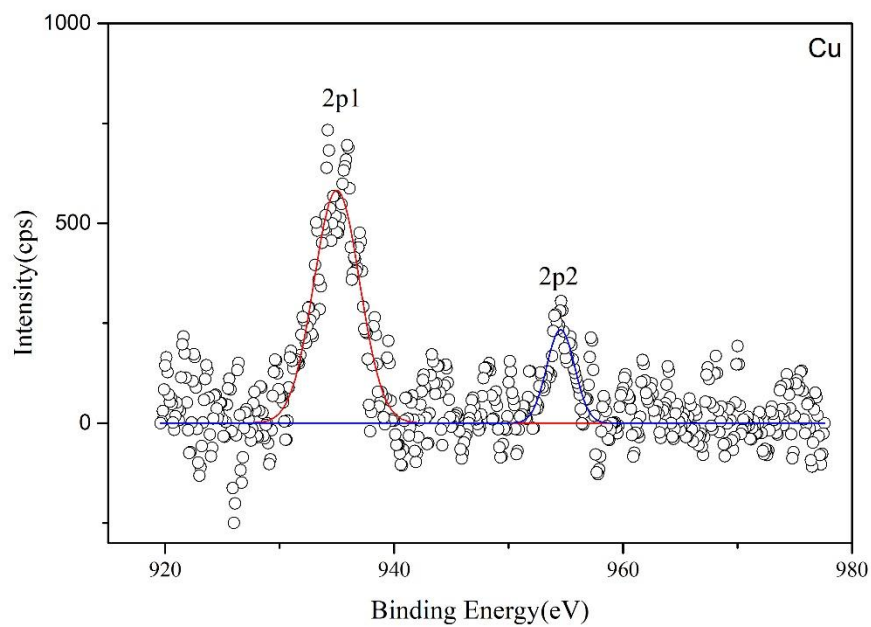


Figure E.3.1 XPS spectra of Cu species on CZA-PH8.

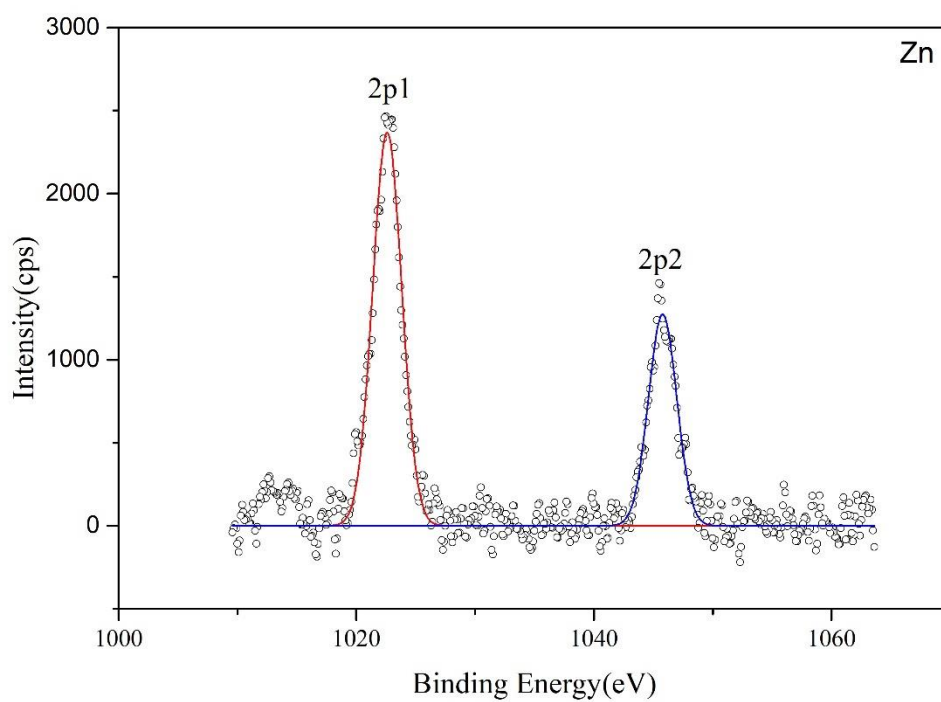


Figure E.3.2 XPS spectra of Zn species on CZA-PH8.

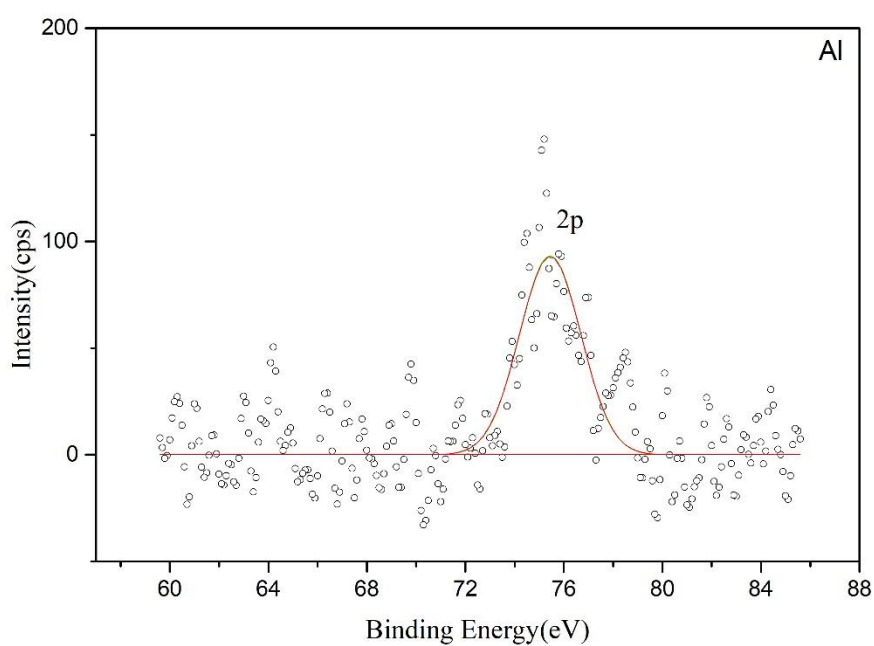


Figure E.3.3 XPS spectra of Al species on CZA-PH8.

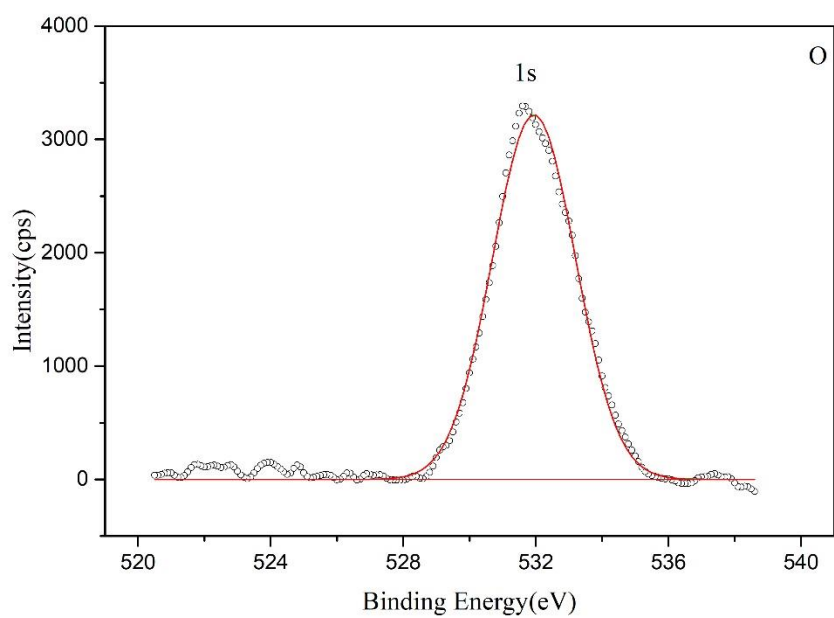


Figure E.3.4 XPS spectra of O species on CZA-PH8.

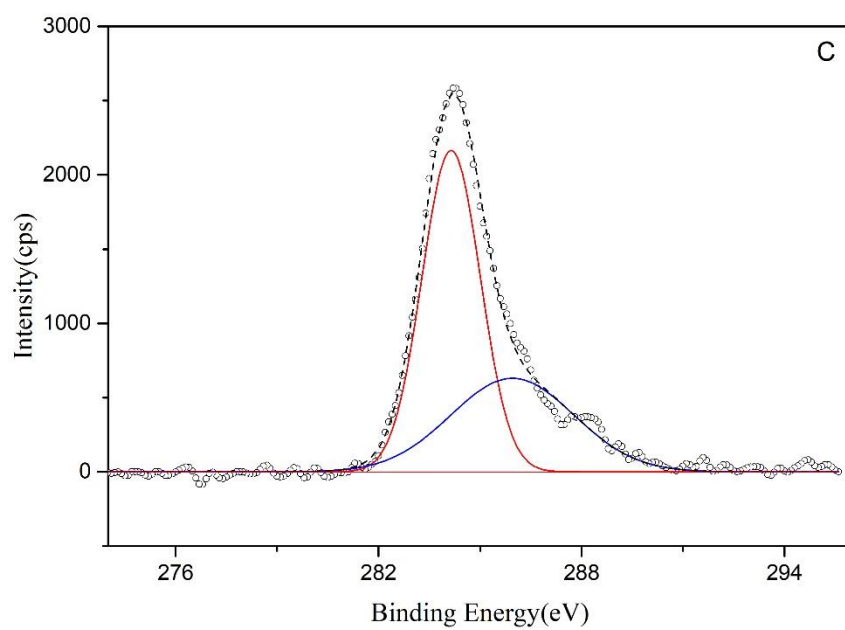


Figure E.3.5 XPS spectra of C species on CZA-PH8.

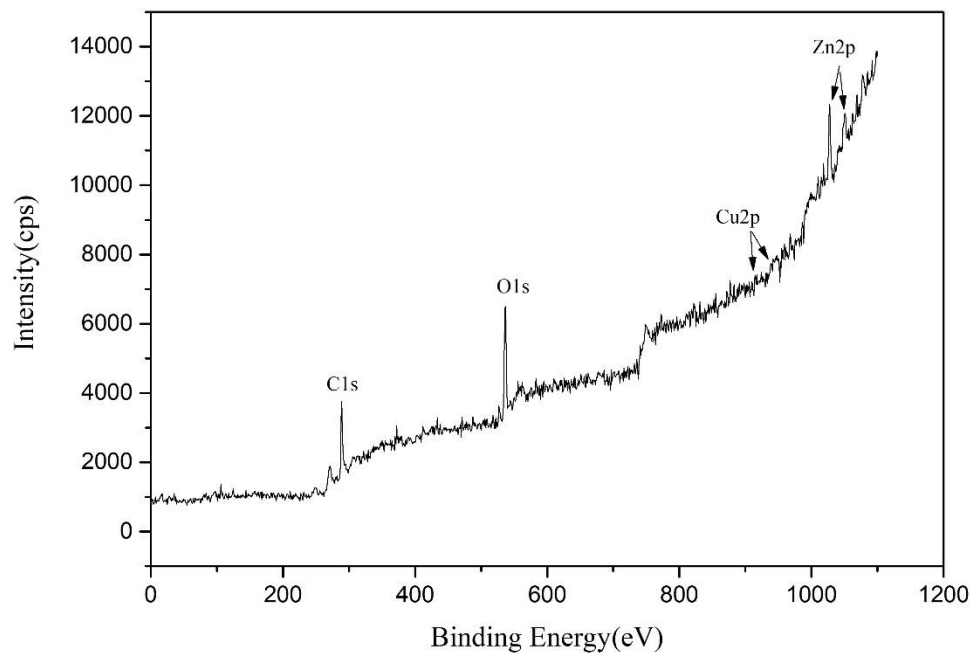


Figure E.3.6 XPS spectra of all species on CZA-PH8.

E.4 Chemical species of CZA-PH8-Zr catalyst.

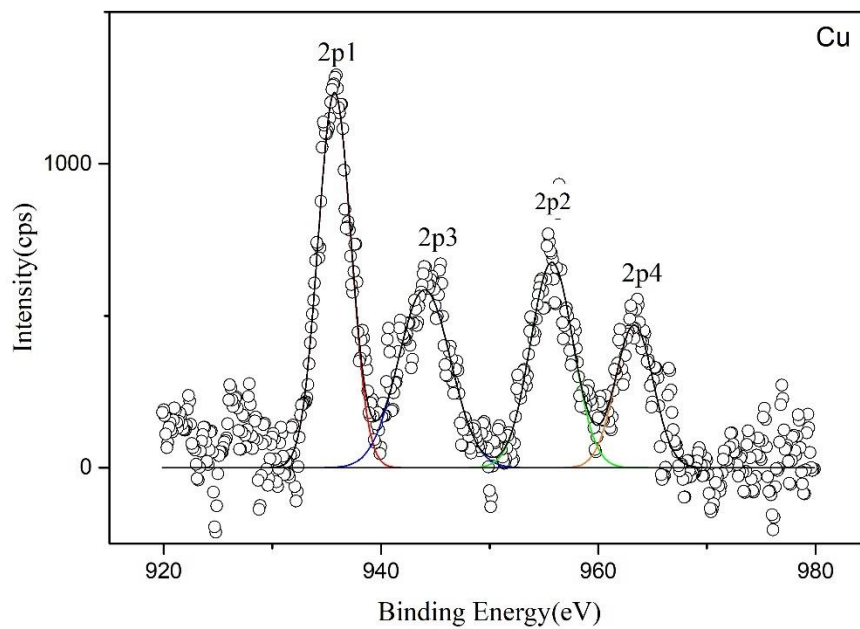


Figure E.4.1 XPS spectra of Cu species on CZA-PH8-Zr.

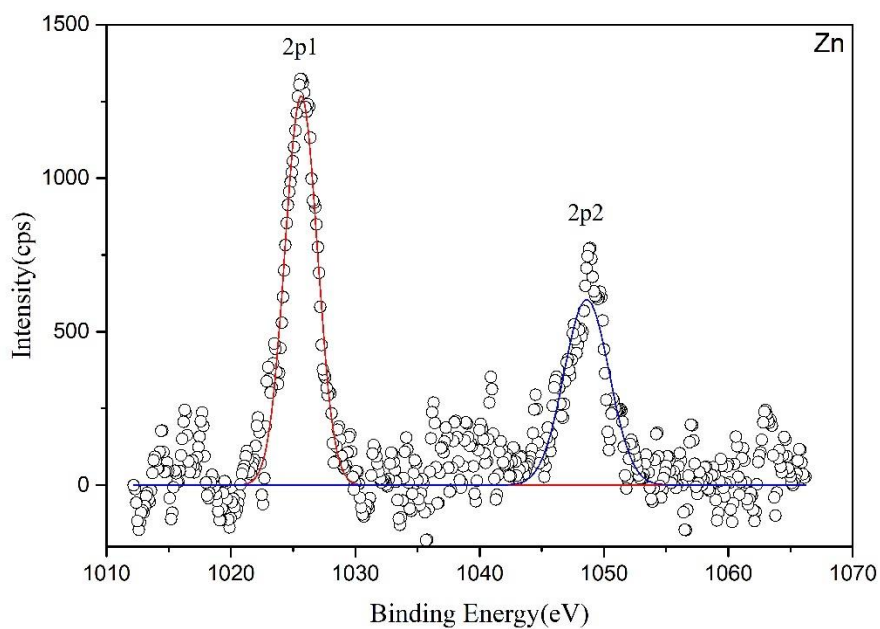


Figure E.4.2 XPS spectra of Zn species on CZA-PH8-Zr.

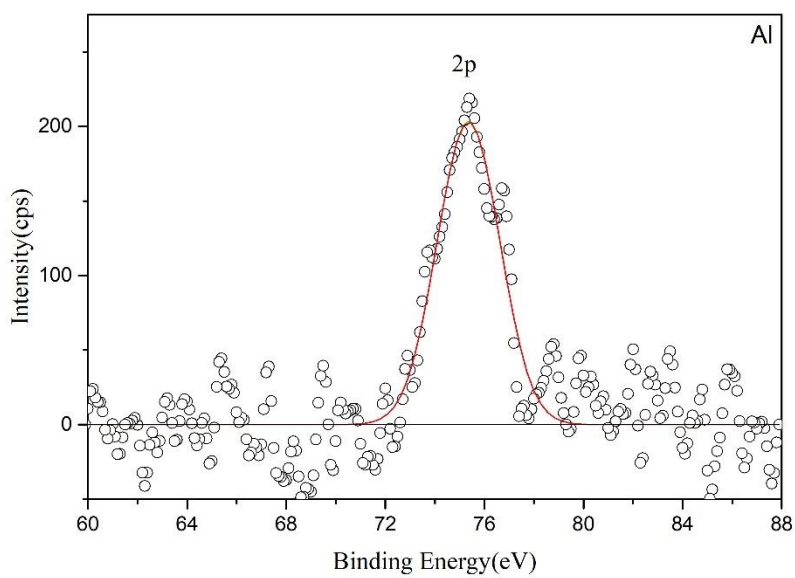


Figure E.4.3 XPS spectra of Al species on CZA-PH8-Zr.

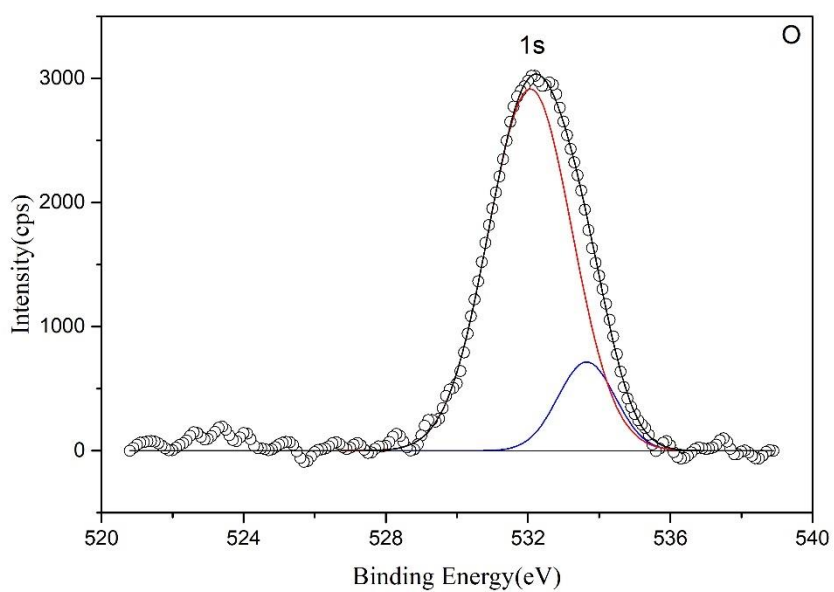


Figure E.4.4 XPS spectra of O species on CZA-PH8-Zr.

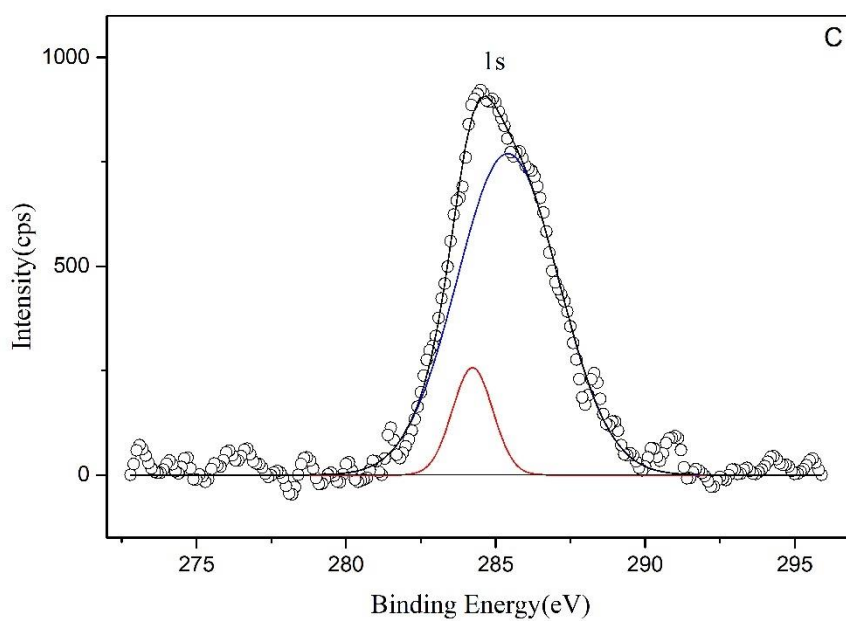


Figure E.4.5 XPS spectra of C species on CZA-PH8-Zr.

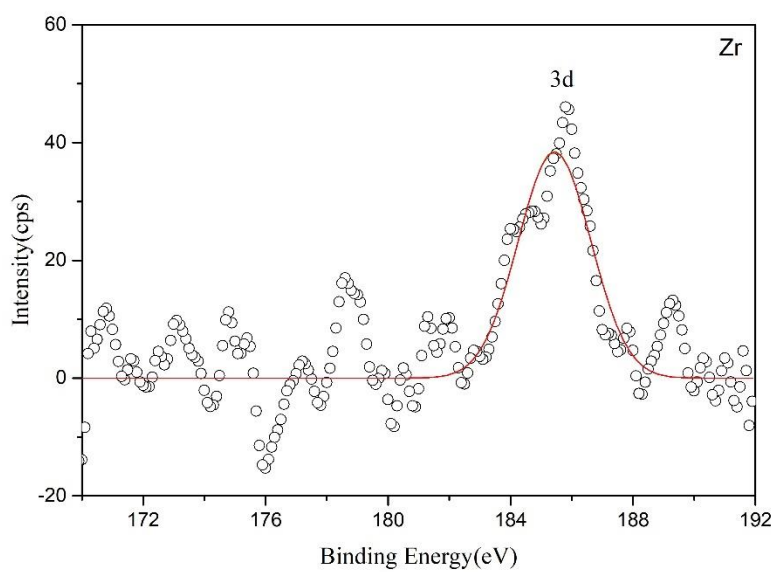


Figure E.4.6 XPS spectra of Zr species on CZA-PH8-Zr.

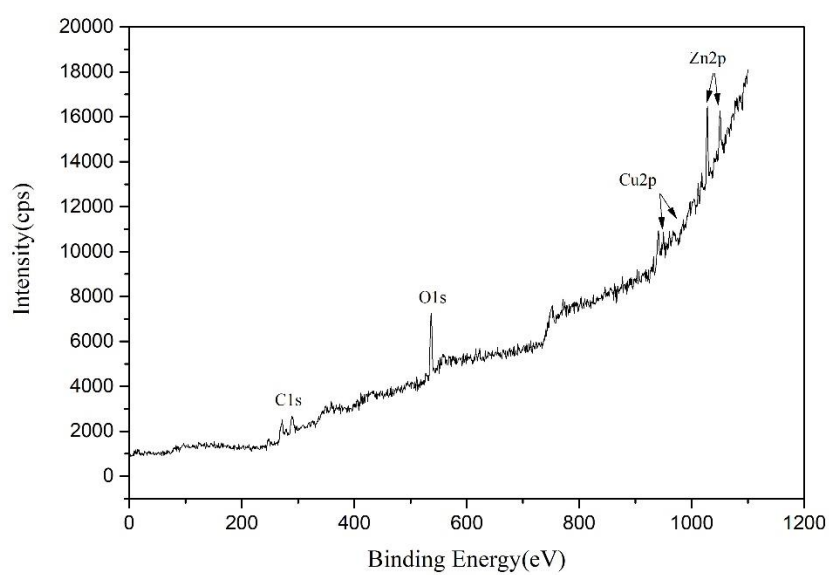


Figure E.4.7 XPS spectra of all species on CZA-PH8-Zr.

E.5 Chemical species of CZA-PH8-Mn catalyst.

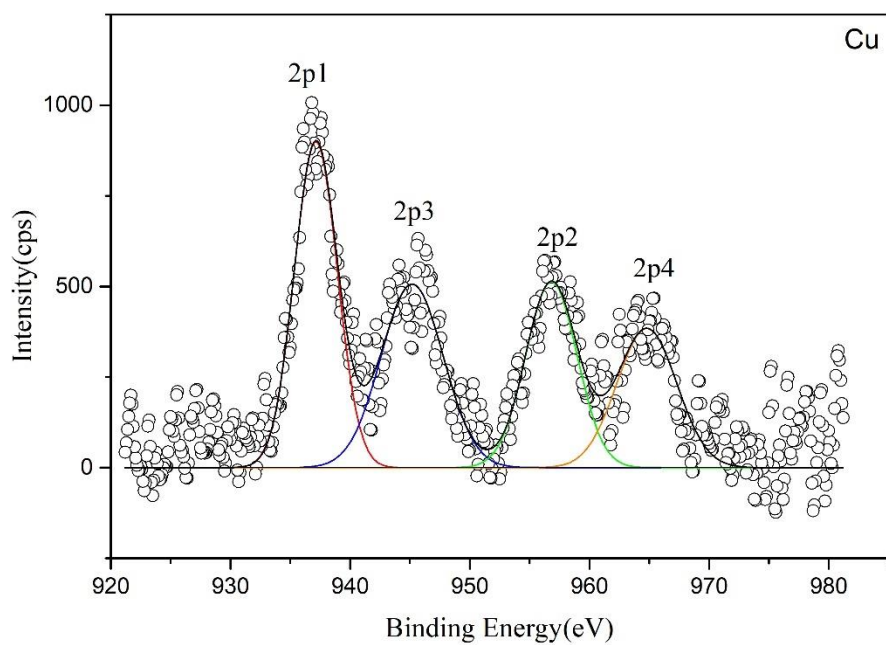


Figure E.5.1 XPS spectra of Cu species on CZA-PH8-Mn.

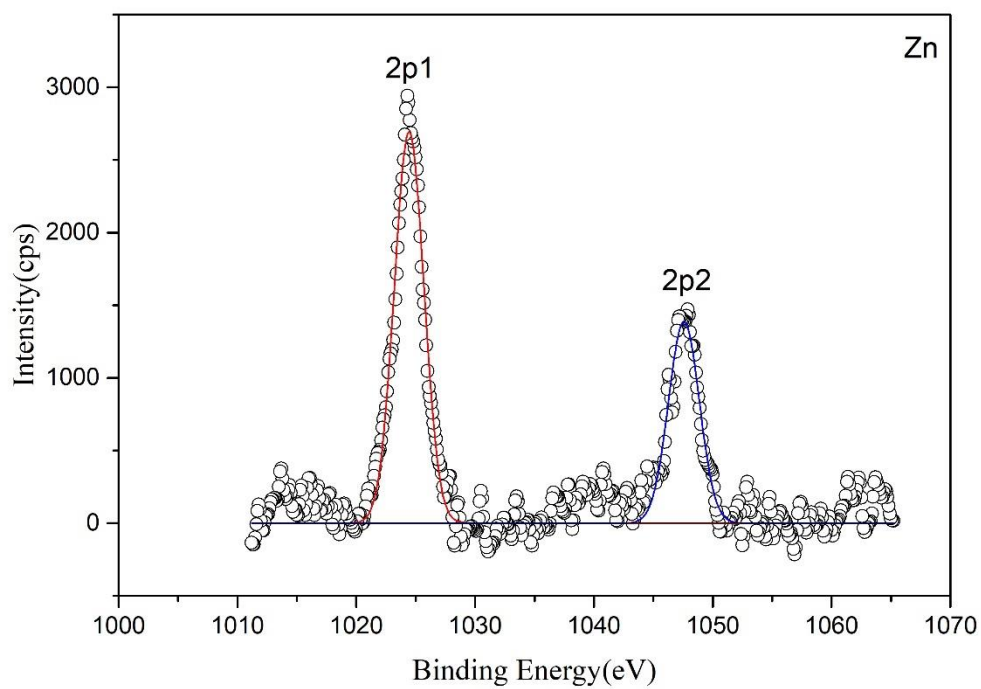


Figure E.5.2 XPS spectra of Zn species on CZA-PH8-Mn.

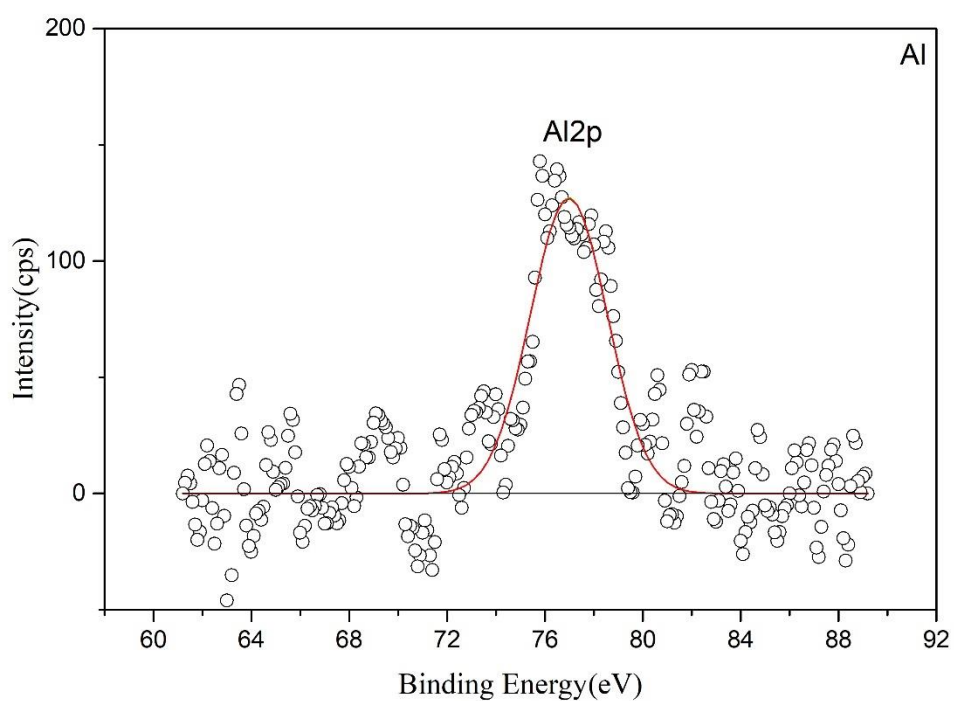


Figure E.5.3 XPS spectra of Al species on CZA-PH8-Mn.

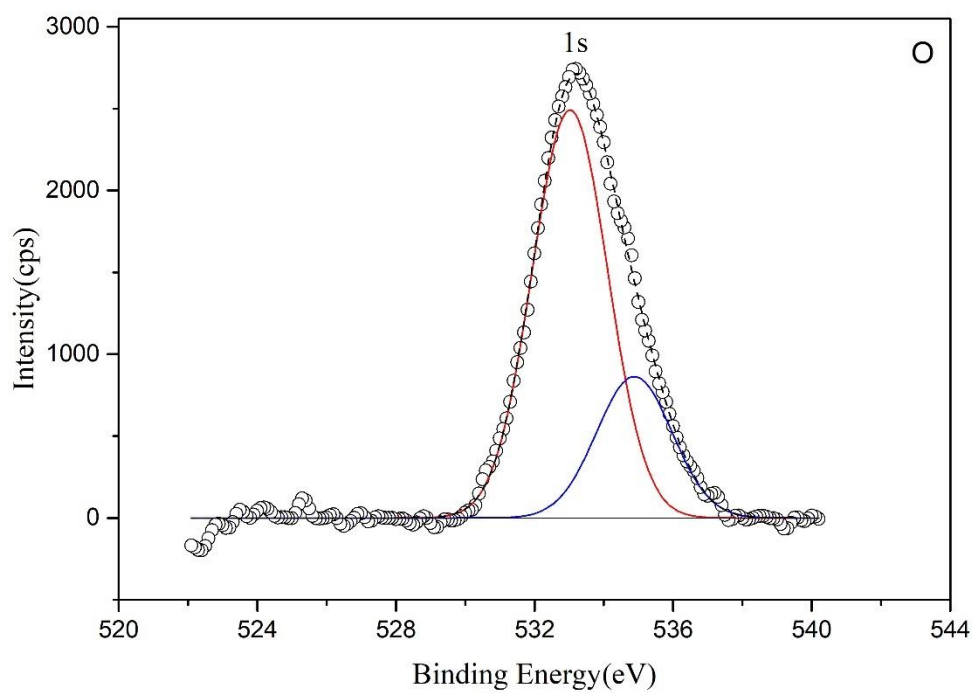


Figure E.5.4 XPS spectra of O species on CZA-PH8-Mn.

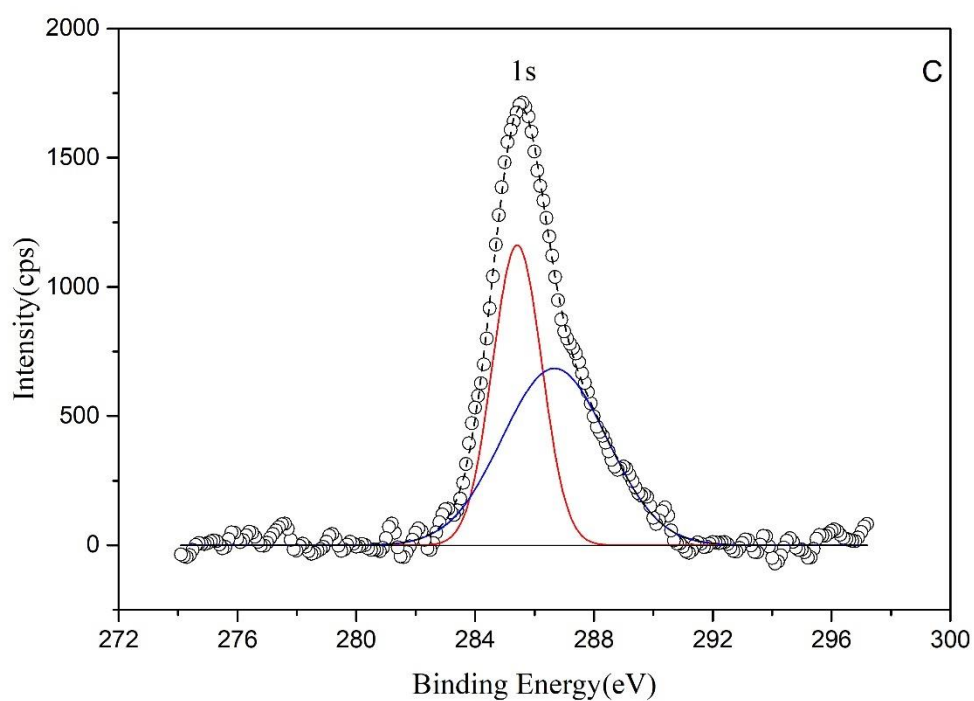


Figure E.5.5 XPS spectra of C species on CZA-PH8-Mn.

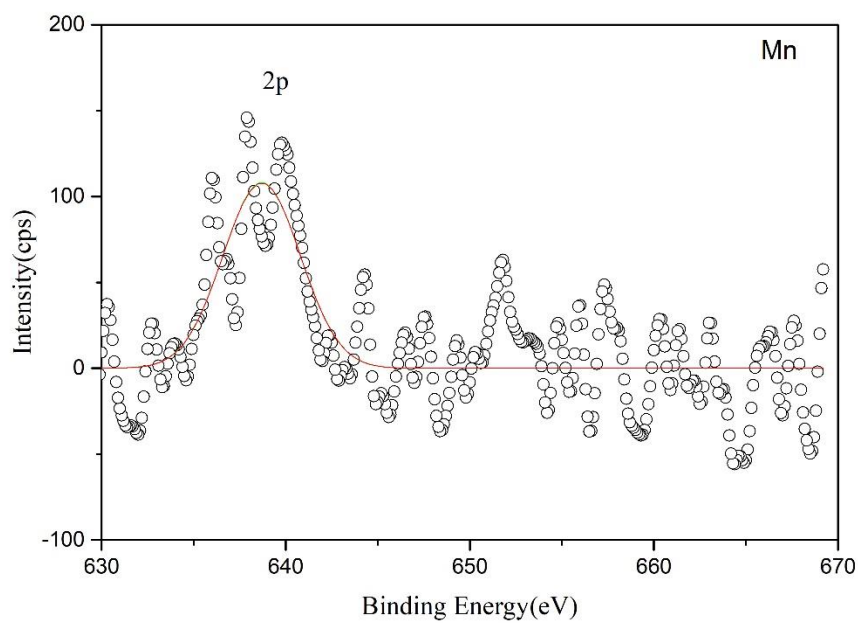


Figure E.5.6 XPS spectra of Mn species on CZA-PH8-Mn.

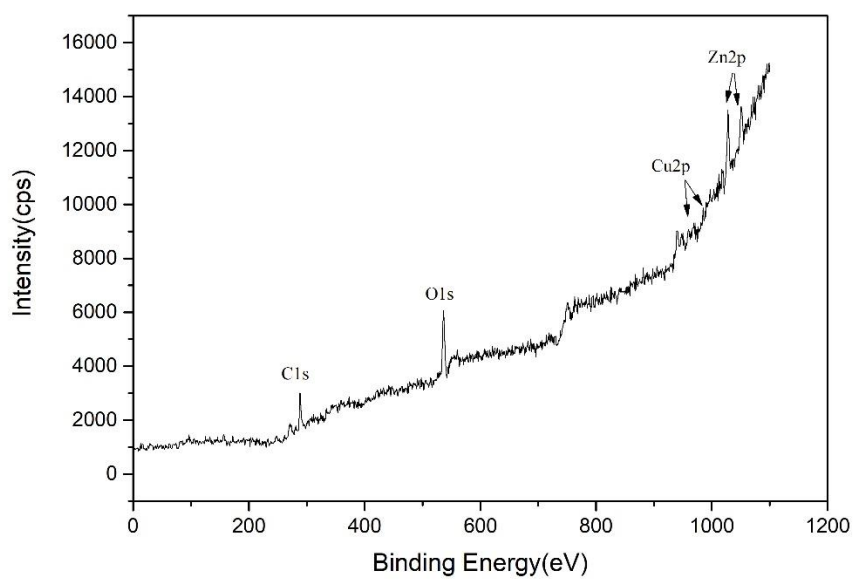


Figure E.5.7 XPS spectra of all species on CZA-PH8-Mn.

E.6 Chemical species of CZA-PH8-Si catalyst.

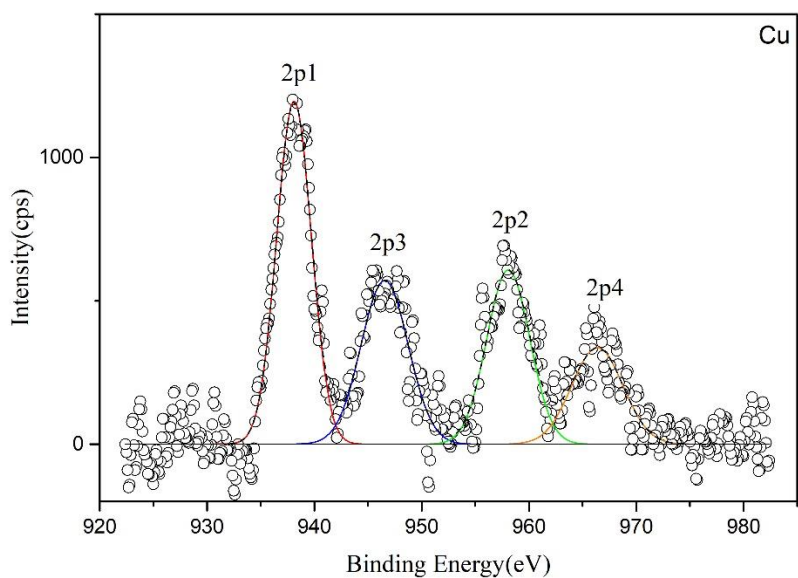


Figure E.6.1 XPS spectra of Cu species on CZA-PH8-Si.

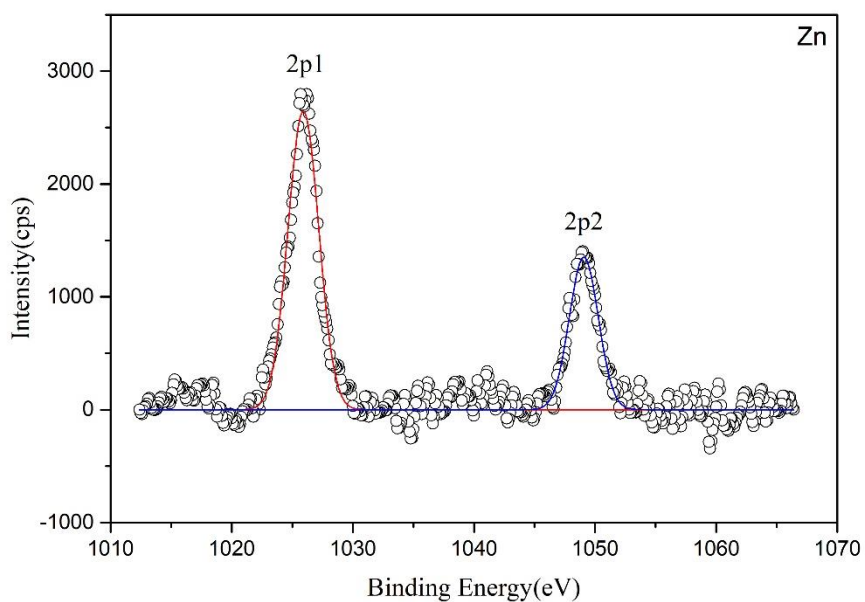


Figure E.6.2 XPS spectra of Zn species on CZA-PH8-Si.

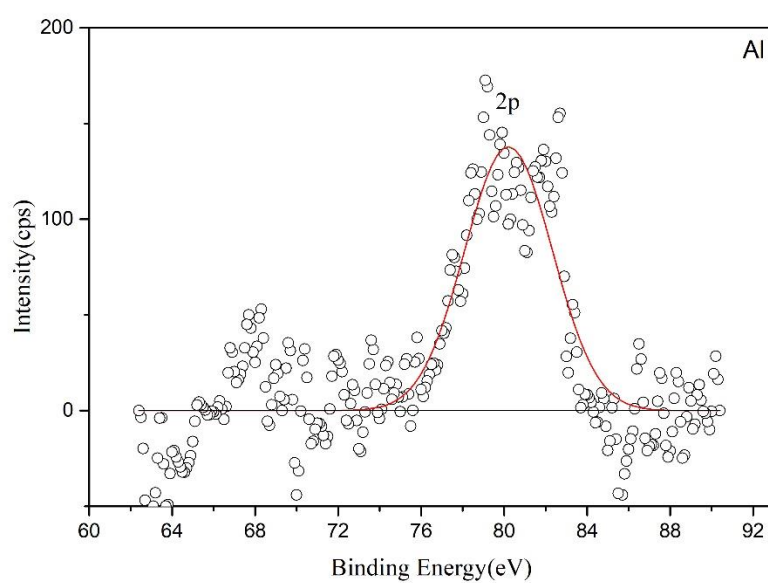


Figure E.6.3 XPS spectra of Al species on CZA-PH8-Si.

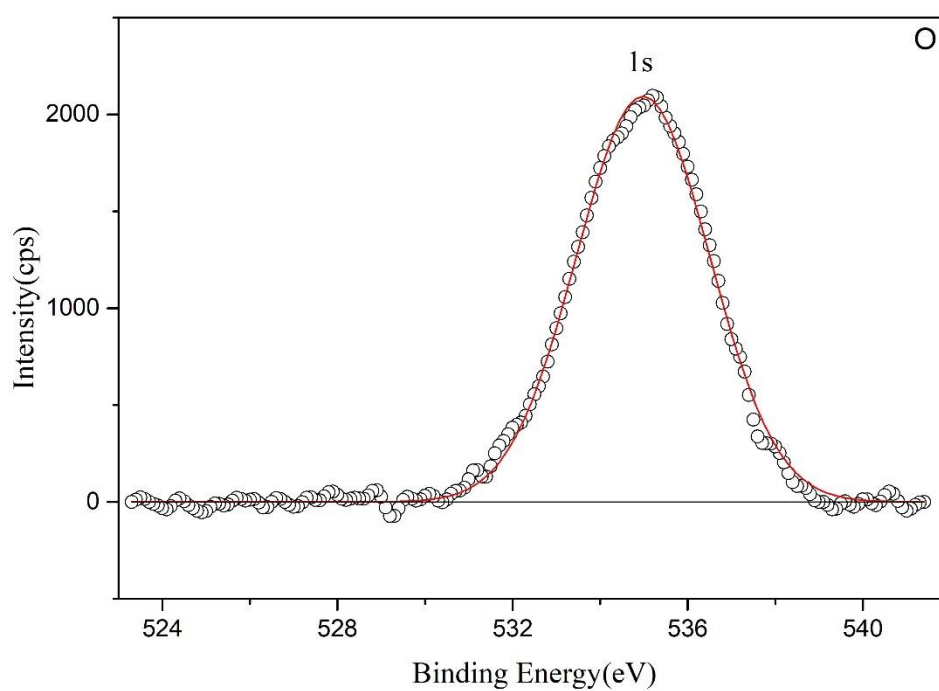


Figure E.6.4 XPS spectra of O species on CZA-PH8-Si.

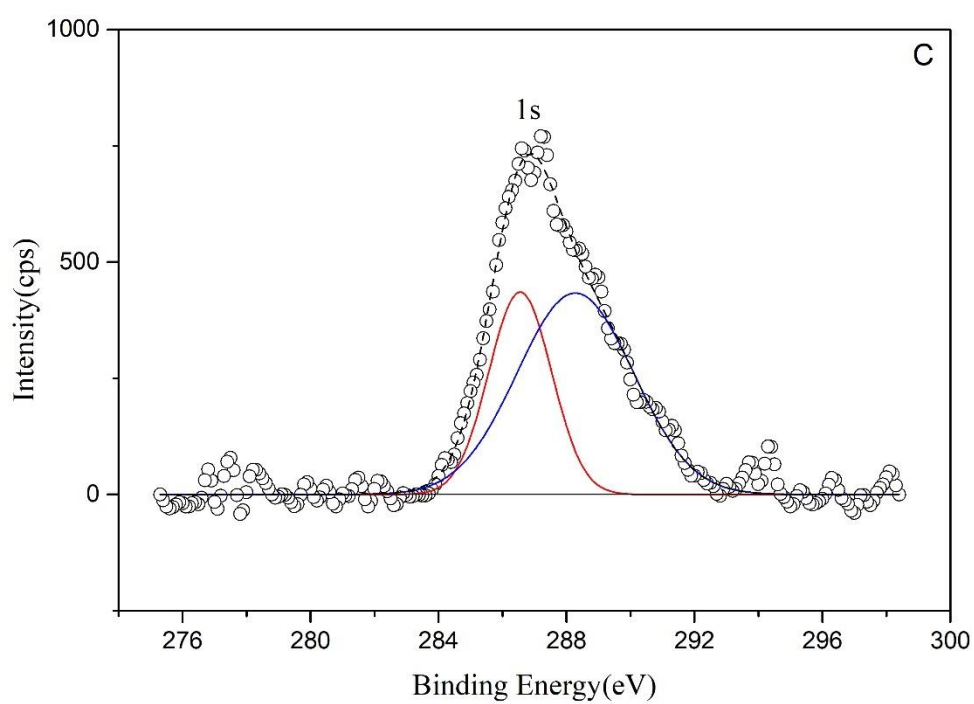


Figure E.6.5 XPS spectra of C species on CZA-PH8-Si.

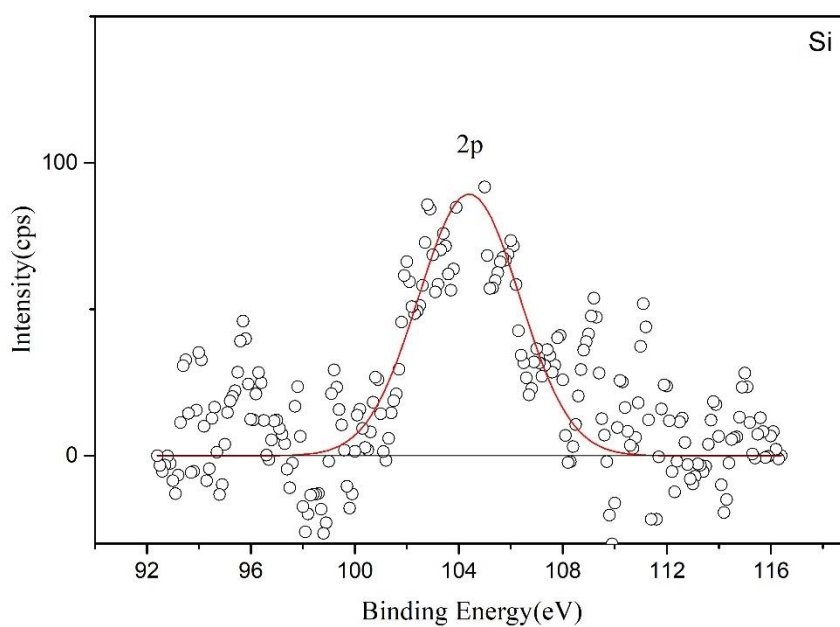


Figure E.6.6 XPS spectra of Si species on CZA-PH8-Si.

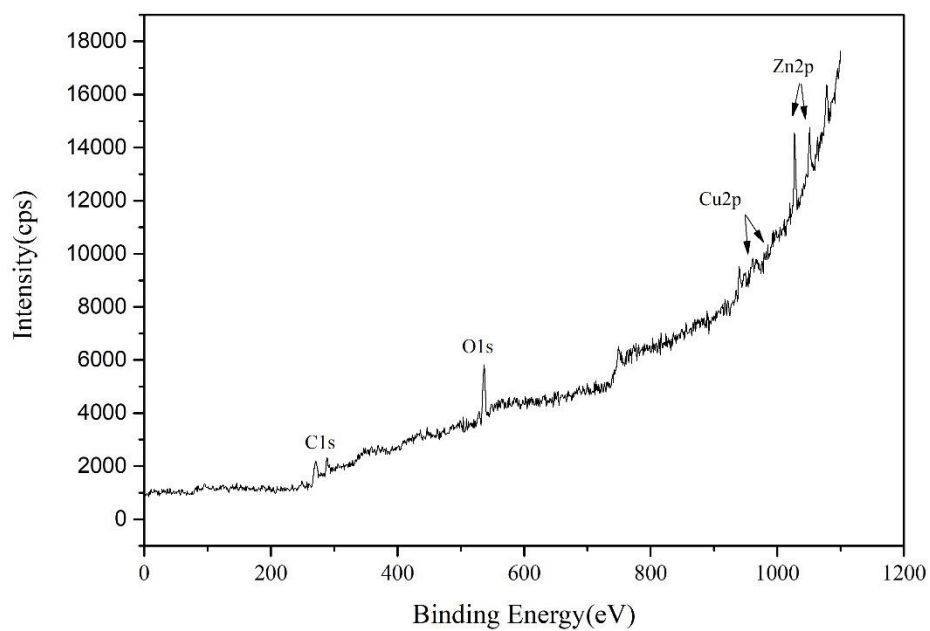


Figure E.6.7 XPS spectra of all species on CZA-PH8-Si.

E.7 Chemical species of sCZA-PH8 catalyst.

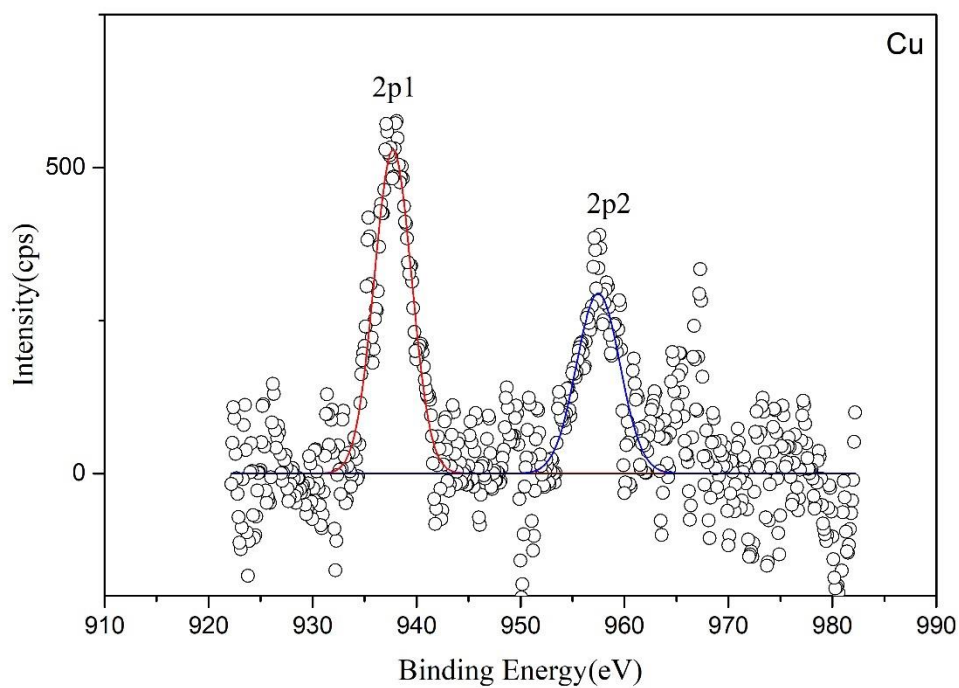


Figure E.7.1 XPS spectra of Cu species on sCZA-PH8.

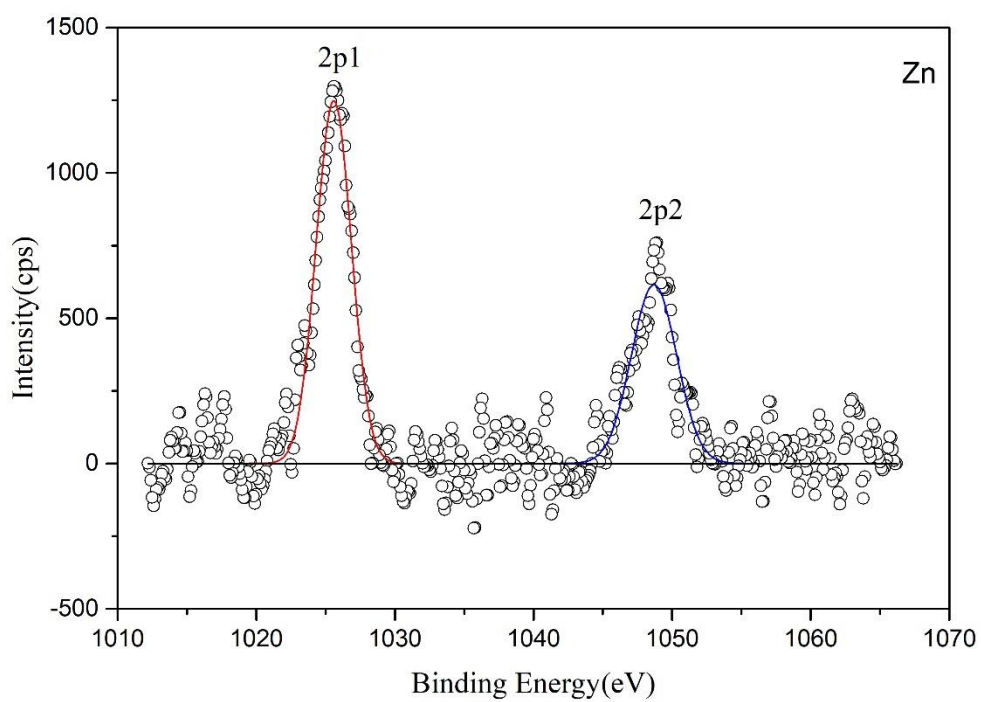


Figure E.7.2 XPS spectra of Zn species on sCZA-PH8.

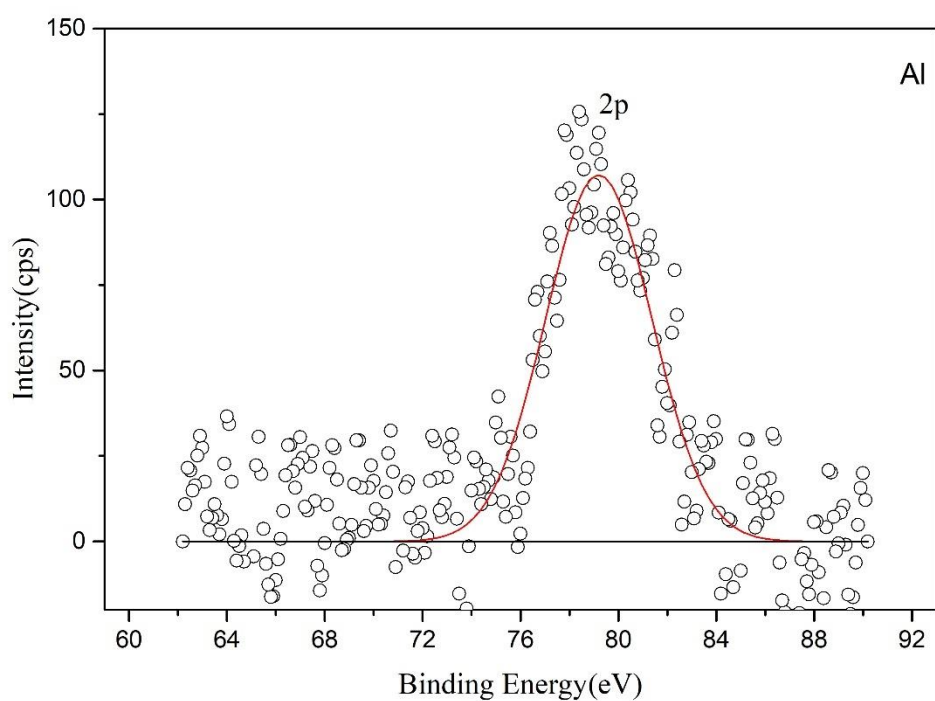


Figure E.7.3 XPS spectra of Al species on sCZA-PH8.

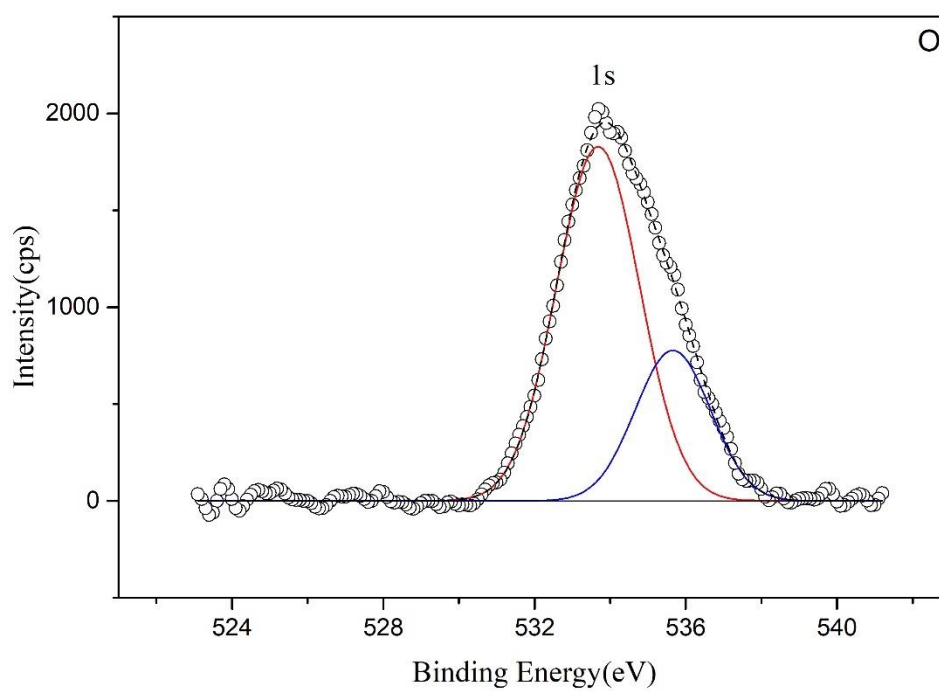


Figure E.7.4 XPS spectra of O species on sCZA-PH8.

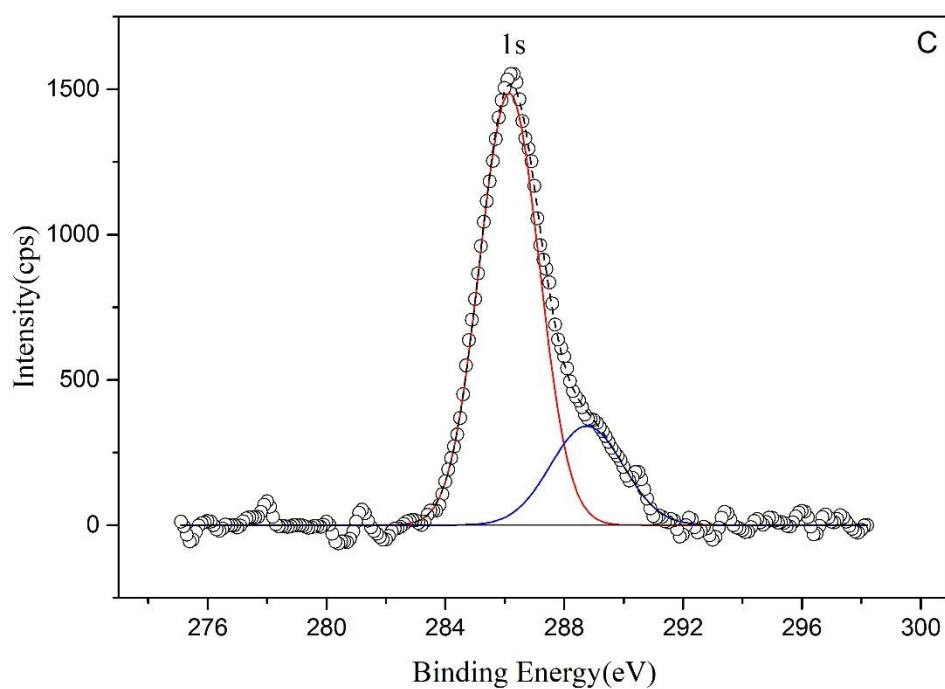


Figure E.7.5 XPS spectra of C species on sCZA-PH8.

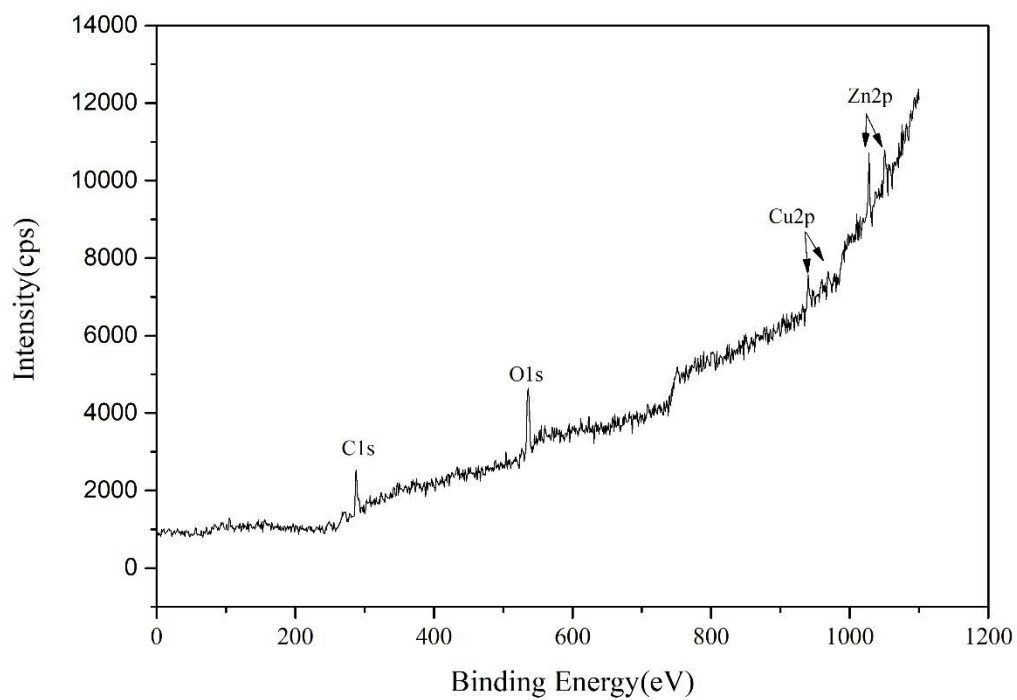


Figure E.7.6 XPS spectra of all species on sCZA-PH8.

E.8 Chemical species of sCZA-PH8-Mn catalyst.

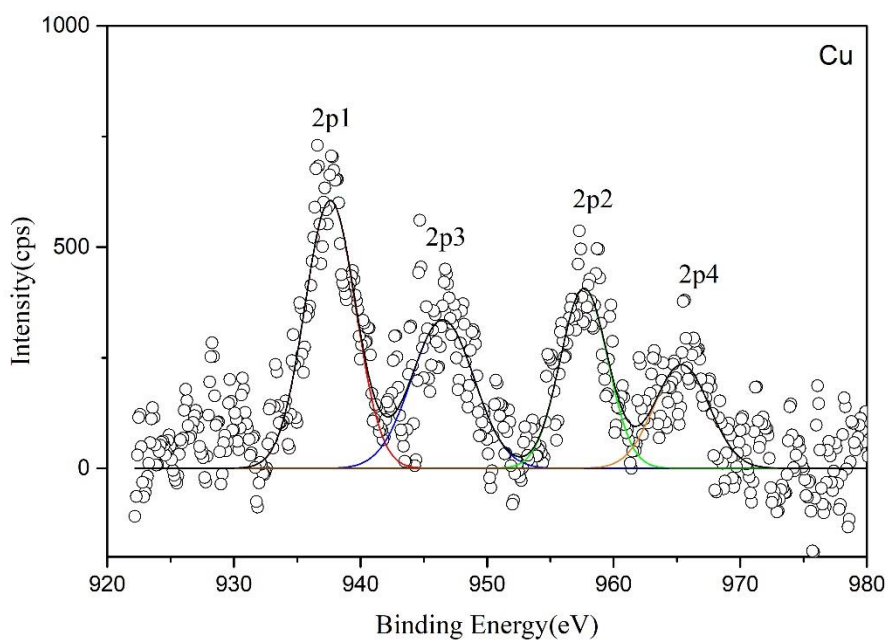


Figure E.8.1 XPS spectra of Cu species on sCZA-PH8-Mn.

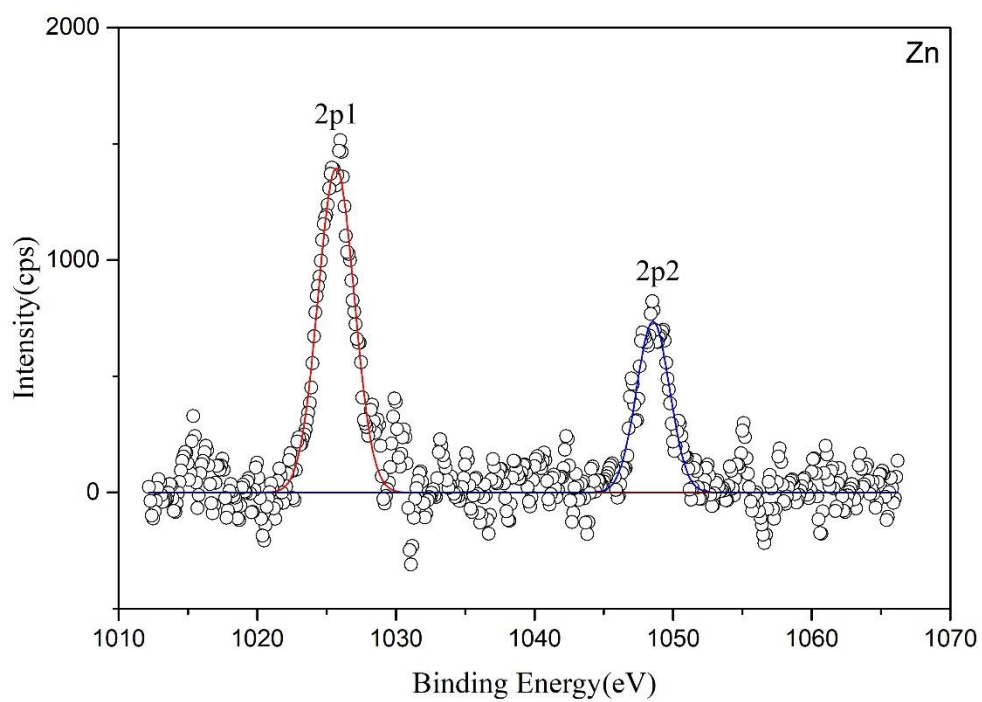


Figure E.8.2 XPS spectra of Zn species on sCZA-PH8-Mn.

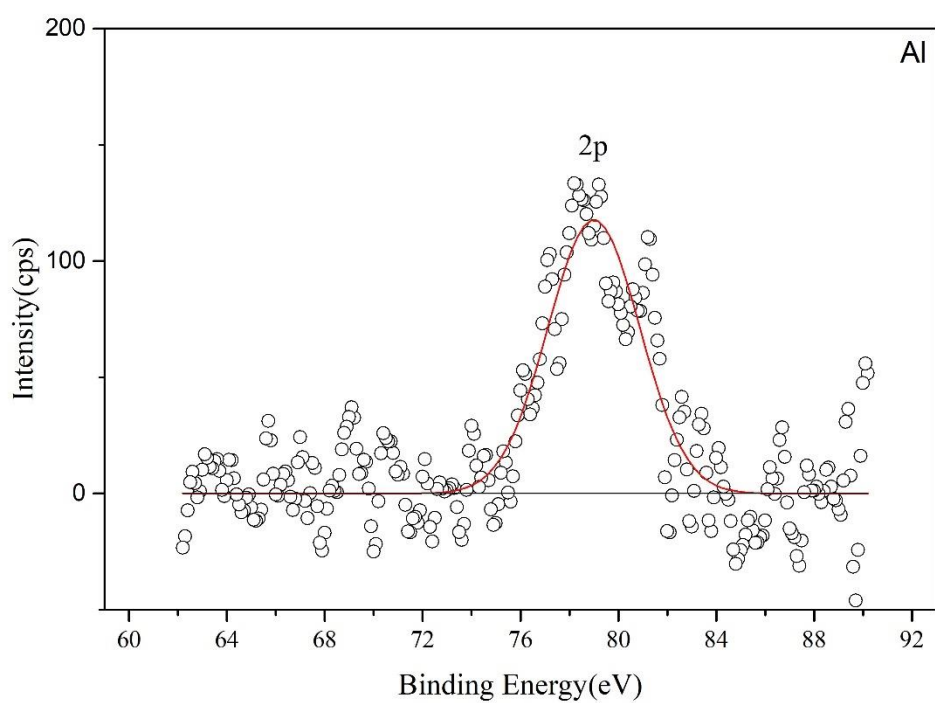


Figure E.8.3 XPS spectra of Al species on sCZA-PH8-Mn.

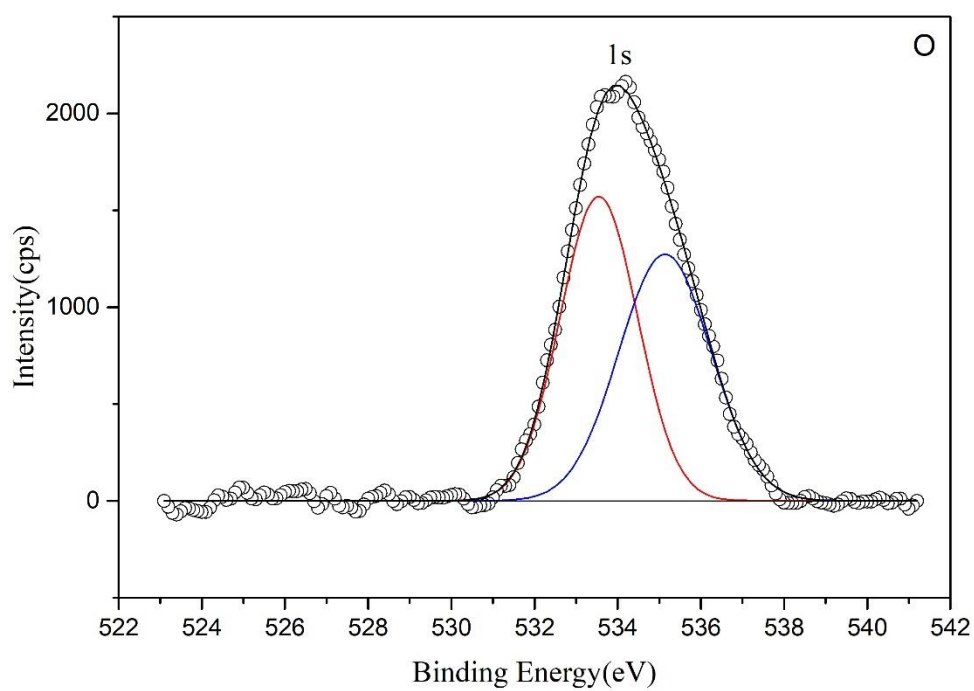


Figure E.8.4 XPS spectra of O species on sCZA-PH8-Mn.

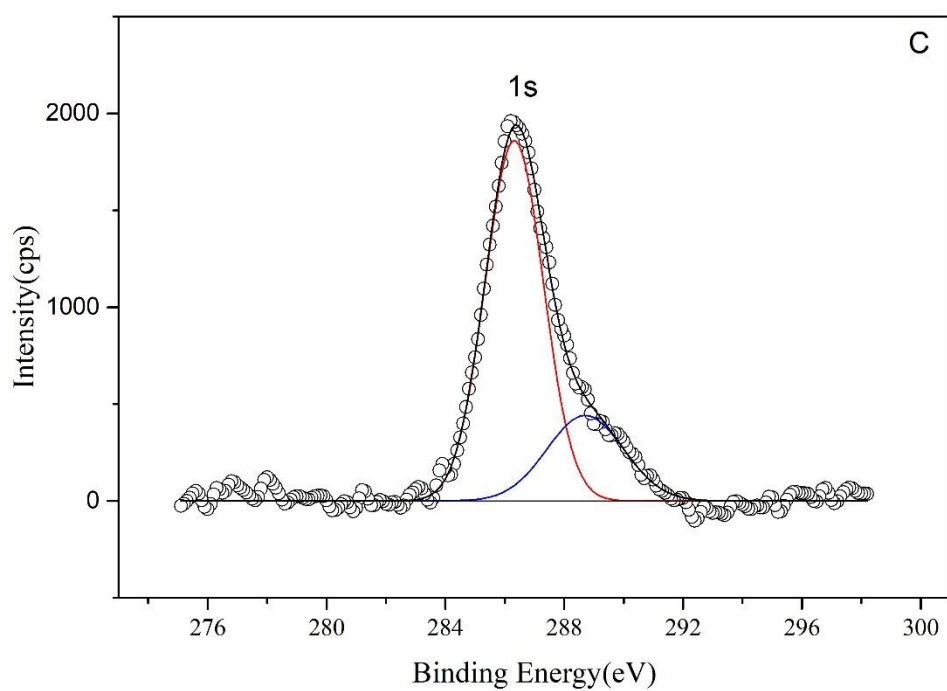


Figure E.8.5 XPS spectra of C species on sCZA-PH8-Mn.

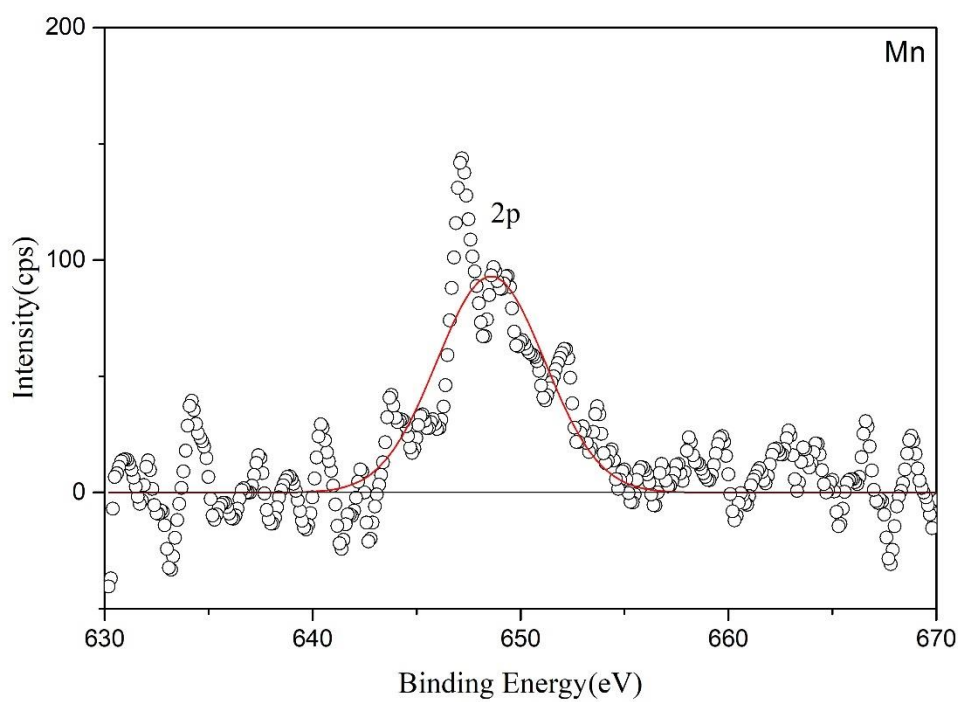


Figure E.8.6 XPS spectra of Mn species on sCZA-PH8-Mn.

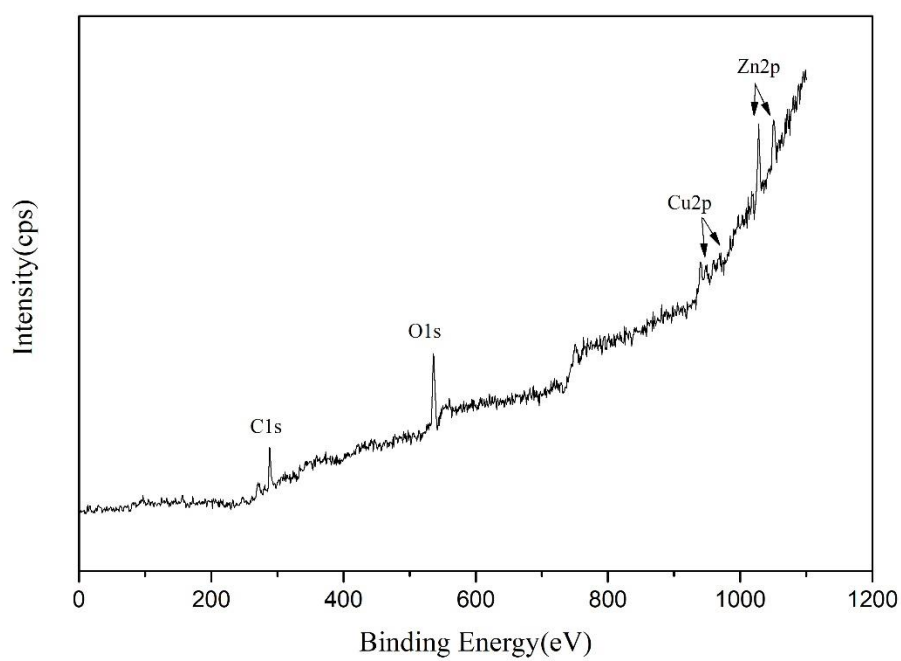


Figure E.8.7 XPS spectra of all species on sCZA-PH8-Mn.

E.9 Position of binding energy(eV) and element of all species.

Table E.9.1 Position binding energy (eV) of XPS spectra of all species.

Sample	Position of binding energy(eV)							
	Cu 2p _{3/2}	Cu2p _{1/2}	Zn2p _{3/2}	Zn2p _{1/2}	Al2p	O1s	C1s	Ag3d
CZA-PH7	935.3	954.5	1022.6	1045.7	74.9	531.6	284.2	368.2
CZA-PH8	935.3	954.5	1022.6	1045.7	74.9	531.6	284.2	368.2
CZA-PH9	935.3	954.5	1022.6	1045.7	74.9	531.6	284.2	368.2
sCZA-PH8	937.2	957.1	1025.6	1048.8	77.8	533.7	286.2	368.2

Table E.9.2 Mass (%) of XPS spectra of all species.

Sample	Mass (%)					
	Cu	Zn	Al	O	C	Ag
CZA-PH7	8.57	20.69	4.83	31.80	32.09	2.02
CZA-PH8	11.24	18.74	4.34	33.12	31.46	1.11
CZA-PH9	6.55	21.65	4.25	31.68	33.76	2.12
sCZA-PH8	10.08	17.38	10.20	30.27	30.39	1.71

Table E.9.3 Position binding energy (eV) of XPS spectra of all species in effect of metal loading.

Sample	Position of binding energy(eV)					
	Cu 2p _{3/2}	Cu 2p _{1/2}	satellite Cu2p ₃	satellite Cu2p ₄	Zn 2p _{3/2}	Zn 2p _{1/2}
CZA-PH8-Zr	935.7	956.4	944	963.6	1023.1	1046
CZA-PH8-Mn	936.8	956.3	945.6	964	1022.6	1045.7
CZA-PH8-Si	938.2	957.7	945.6	966.2	1025.8	1049
sCZA-PH8-Mn	937.8	957.3	946.8	965.6	1026	1048

Sample	Position of binding energy(eV)			
	Al2p	O1s	C1s	Ag3d
CZA-PH8-Zr	75.4	532.2	284.5	368.2
CZA-PH8-Mn	74.9	531.6	284.2	368.2
CZA-PH8-Si	79.1	535.2	287.2	368.2
sCZA-PH8-Mn	78.3	534.1	286.3	368.2

Table E.9.4 Mass (%) of XPS spectra of all species in effect of metal loading.

Sample	Mass (%)						
	Cu	Zn	Al	O	C	Ag	X
CZA-PH8-Zr	18.81	26.08	9.29	27.94	15.04	1.32	1.51
CZA-PH8-Mn	15.09	22.59	8.82	25.35	22.12	1.33	4.52
CZA-PH8-Si	19.35	23.23	12.91	23.55	15.59	0.77	4.61
sCZA-PH8-Mn	14.43	14.19	9.29	25.77	31.32	1.33	3.67

APPENDIX.F H₂-CHEMISORPTION AND DISPERSIONF.1 Calculation dispersion in H₂-chemisorption.

Variables

Assumption: $\text{CuO} + \text{H}_2 \rightarrow \text{Cu}^0 + \text{H}_2\text{O}$

H₂ adsorption Integral area from first peak = A1

H₂ adsorption Integral area from Second peak = A2

H₂ adsorption Integral area from Third peak = A3

H₂ adsorption Integral area from X peak (X=1,2,3,4, ...) = A_x

H₂ adsorption Integral area from standard peak = A0

(Area equality 3 times)

Volume of H₂ injection = 20 μL

Calculation

Volume of H₂ adsorption = $\frac{[(A0-A1)+(A0-A2)+(A0-Ax)] \times 20}{A0}$ μL

Mol of H₂ adsorption = $\frac{[(A0-A1)+(A0-A2)+(A0-Ax)] \times 20}{A0 \times 22.4}$ μmol

Catalyst weight = 0.5 g_{cat}

Total H₂-Chemisorption = $\frac{[(A0-A1)+(A0-A2)+(A0-Ax)] \times 20}{A0 \times 22.4 \times 0.5}$ $\mu\text{mol}/\text{g}_{\text{cat}}$

(Cu:H₂ = 1:1)

Dispersion

Dispersion = (mole of Cu⁰/g)/(mole of total/g)

Catalyst weight = 0.5 g

Cu loading = 40 %wt.

Mw of Cu = 63.55 g/mol

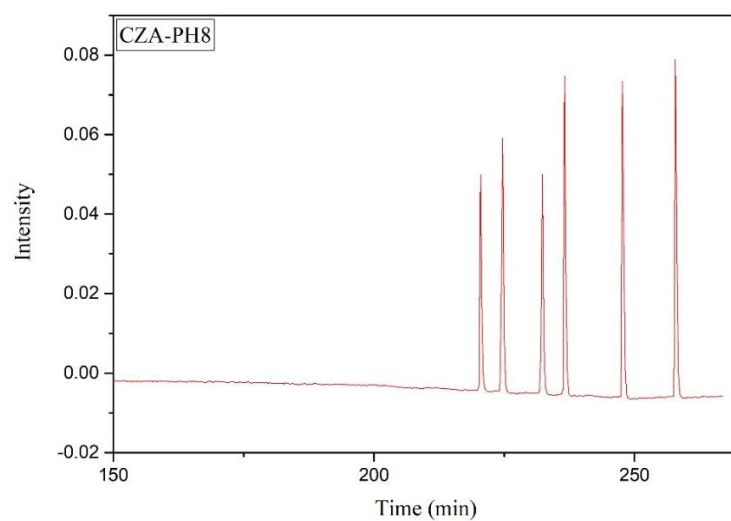
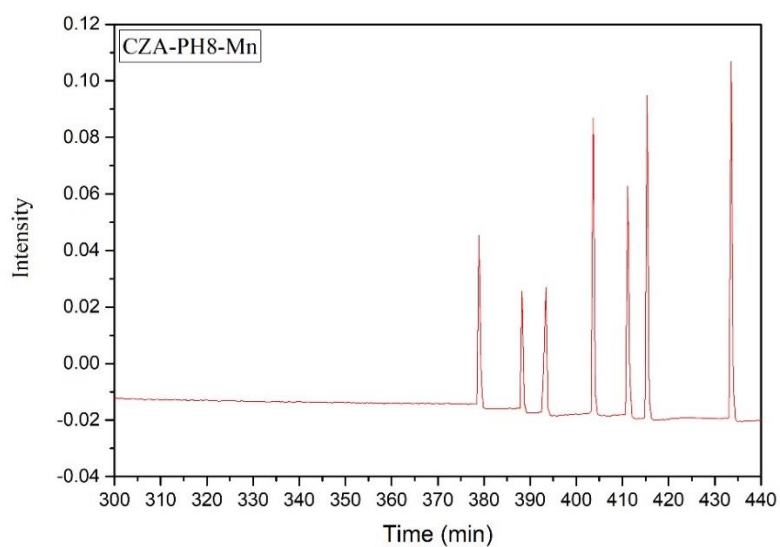
Mol of Cu⁰ = $\frac{[(A0-A1)+(A0-A2)+(A0-Ax)] \times 20}{A0 \times 22.4 \times 0.5}$ $\mu\text{mol}/\text{g}_{\text{cat}}$

Mol total Cu of CZA catalyst = $\left(\frac{40}{100}\right) \times 63.55$ $\text{g}_{\text{cat}}/\text{mol}$

Dispersion (fraction) = $\left[\frac{[(A0-A1)+(A0-A2)+(A0-Ax)] \times 20}{A0 \times 22.4 \times 0.5} \right] \times 10^{-6} / \left[\left(\frac{40}{100}\right) \times 63.55 \right]$

Table F.1.1 Cu⁰ dispersion from H₂-Chemisorption (20 μL)

Sample	H ₂ adsorption (μmol/g _{cat})	Cu ⁰ dispersion (×10 ⁶)	Cu ⁰ dispersion (%)
CZA-PH8	7.11	0.27	27
CZA-PH8-Mn	16.28	0.64	64

Figure F.1.1 H₂-Chemisorption of CZA-PH8Figure F.1.2 H₂-Chemisorption of CZA-PH8-Mn

REFERENCES

1. Tijm, P.J.A., F.J. Waller, and D.M. Brown, *Methanol technology developments for the new millennium*. Applied Catalysis A: General, 2001. **221**(1): p. 275-282.
2. Li, J.L. and T. Inui, *Characterization of precursors of methanol synthesis catalysts, copper/zinc/aluminum oxides, precipitated at different pHs and temperatures*. Applied Catalysis A: General, 1996. **137**(1): p. 105-117.
3. Pasupulety, N., et al., *Studies on Au/Cu-Zn-Al catalyst for methanol synthesis from CO₂*. Applied Catalysis A: General, 2015. **504**: p. 308-318.
4. Gao, P., et al., *Influence of modifier (Mn, La, Ce, Zr and Y) on the performance of Cu/Zn/Al catalysts via hydrotalcite-like precursors for CO₂ hydrogenation to methanol*. Applied Catalysis A: General, 2013. **468**: p. 442-452.
5. Zhang, L., Y. Zhang, and S. Chen, *Effect of promoter SiO₂, TiO₂ or SiO₂-TiO₂ on the performance of CuO-ZnO-Al₂O₃ catalyst for methanol synthesis from CO₂ hydrogenation*. Applied Catalysis A: General, 2012. **415-416**: p. 118-123.
6. Wittich, K., et al., *Catalytic Dry Reforming of Methane: Insights from Model Systems*. ChemCatChem, 2020. **n/a**(n/a).
7. Argyle, D.M. and H.C. Bartholomew, *Heterogeneous Catalyst Deactivation and Regeneration: A Review*. Catalysts, 2015. **5**(1).
8. Ali, K.A., A.Z. Abdullah, and A.R. Mohamed, *Recent development in catalytic technologies for methanol synthesis from renewable sources: A critical review*. Renewable and Sustainable Energy Reviews, 2015. **44**: p. 508-518.
9. Wu, J., et al., *The stability of Cu/ZnO-based catalysts in methanol synthesis from a CO₂-rich feed and from a CO-rich feed*. Applied Catalysis A: General, 2001. **218**: p. 235-240.
10. Słoczyński, J., et al., *Effect of Mg and Mn oxide additions on structural and adsorptive properties of Cu/ZnO/ZrO₂ catalysts for the methanol synthesis from CO₂*. Applied Catalysis A: General, 2003. **249**(1): p. 129-138.
11. Atake, I., et al., *Catalytic behavior of ternary Cu/ZnO/Al₂O₃ systems prepared by homogeneous precipitation in water-gas shift reaction*. Journal of Molecular

- Catalysis A: Chemical, 2007. **275**(1): p. 130-138.
12. An, X., et al., *A Cu/Zn/Al/Zr Fibrous Catalyst that is an Improved CO₂ Hydrogenation to Methanol Catalyst*. Catalysis Letters - CATALYSIS LETT, 2007. **118**: p. 264-269.
 13. Zhang, Y., et al., *Study of CO₂ Hydrogenation to Methanol over Cu-V/Al₂O₃ Catalyst*. Journal of Natural Gas Chemistry, 2007. **16**(1): p. 12-15.
 14. Raudaskoski, R., M.V. Niemelä, and R.L. Keiski, *The effect of ageing time on co-precipitated Cu/ZnO/ZrO₂ catalysts used in methanol synthesis from CO₂ and H₂*. Topics in Catalysis, 2007. **45**(1): p. 57-60.
 15. Gao, P., et al., *Influence of Zr on the performance of Cu/Zn/Al/Zr catalysts via hydrotalcite-like precursors for CO₂ hydrogenation to methanol*. Journal of Catalysis, 2013. **298**: p. 51-60.
 16. Arena, F., et al., *Effects of oxide carriers on surface functionality and process performance of the Cu-ZnO system in the synthesis of methanol via CO₂ hydrogenation*. Journal of Catalysis, 2013. **300**: p. 141-151.
 17. Arena, F., et al., *How oxide carriers control the catalytic functionality of the Cu-ZnO system in the hydrogenation of CO₂ to methanol*. Catalysis Today, 2013. **210**: p. 39-46.
 18. Gao, P., et al., *Influence of fluorine on the performance of fluorine-modified Cu/Zn/Al catalysts for CO₂ hydrogenation to methanol*. Journal of CO₂ Utilization, 2013. **2**: p. 16-23.
 19. Li, C., X. Yuan, and K. Fujimoto, *Development of highly stable catalyst for methanol synthesis from carbon dioxide*. Applied Catalysis A: General, 2014. **469**: p. 306-311.
 20. Zhan, H., et al., *Methanol synthesis from CO₂ hydrogenation over La-M-Cu-Zn-O (M = Y, Ce, Mg, Zr) catalysts derived from perovskite-type precursors*. Journal of Power Sources, 2014. **251**: p. 113-121.
 21. Ding, W., et al., *Promoting effect of a Cu-Zn binary precursor on a ternary Cu-Zn-Al catalyst for methanol synthesis from synthesis gas*. RSC Advances, 2014. **4**: p. 30677.

22. Lei, H., et al., *Hydrogenation of CO₂ to CH₃OH over Cu/ZnO catalysts with different ZnO morphology*. Fuel, 2015. **154**: p. 161-166.
23. Lei, H., Z. Hou, and J. Xie, *Hydrogenation of CO₂ to CH₃OH over CuO/ZnO/Al₂O₃ catalysts prepared via a solvent-free routine*. Fuel, 2016. **164**: p. 191-198.
24. Fan, Y.J. and S.F. Wu, *A graphene-supported copper-based catalyst for the hydrogenation of carbon dioxide to form methanol*. Journal of CO₂ Utilization, 2016. **16**: p. 150-156.
25. Gao, P., et al., *Fluorinated Cu/Zn/Al/Zr hydrotalcites derived nanocatalysts for CO₂ hydrogenation to methanol*. Journal of CO₂ Utilization, 2016. **16**: p. 32-41.
26. Xiao, S., et al., *Highly efficient Cu-based catalysts via hydrotalcite-like precursors for CO₂ hydrogenation to methanol*. Catalysis Today, 2017. **281**: p. 327-336.
27. Zhang, C., et al., *Preparation and CO₂ hydrogenation catalytic properties of alumina microsphere supported Cu-based catalyst by deposition-precipitation method*. Journal of CO₂ Utilization, 2017. **17**: p. 263-272.
28. Sadeghinia, M., A. Nemati Kharat Ghaziani, and M. Rezaei, *Component ratio dependent Cu/Zn/Al structure sensitive catalyst in CO₂/CO hydrogenation to methanol*. Molecular Catalysis, 2018. **456**: p. 38-48.
29. Mureddu, M., F. Ferrara, and A. Pettinau, *Highly efficient CuO/ZnO/ZrO₂@SBA-15 nanocatalysts for methanol synthesis from the catalytic hydrogenation of CO₂*. Applied Catalysis B: Environmental, 2019. **258**: p. 117941.
30. Ren, S., et al., *Enhanced catalytic performance of Zr modified CuO/ZnO/Al₂O₃ catalyst for methanol and DME synthesis via CO₂ hydrogenation*. Journal of CO₂ Utilization, 2020. **36**: p. 82-95.
31. Samei, E., M. Taghizadeh, and M. Bahmani, *Enhancement of stability and activity of Cu/ZnO/Al₂O₃ catalysts by colloidal silica and metal oxides additives for methanol synthesis from a CO₂-rich feed*. Fuel Processing Technology, 2012. **96**: p. 128-133.
32. Wang, D., et al., *Characterization and performance of Cu/ZnO/Al₂O₃ catalysts prepared via decomposition of M(Cu, Zn)-ammonia complexes under sub-*

- atmospheric pressure for methanol synthesis from H₂ and CO₂*. *Journal of Natural Gas Chemistry*, 2011. **20**(6): p. 629-634.
33. Zhang, L.-x., Y.-c. Zhang, and S.-y. Chen, *Effect of promoter TiO₂ on the performance of CuO-ZnO-Al₂O₃ catalyst for CO₂ catalytic hydrogenation to methanol*. *Journal of Fuel Chemistry and Technology*, 2011. **39**(12): p. 912-917.
34. Tisseraud, C., et al., *The C• ZnO synergy in methanol synthesis from CO₂, Part 2: Origin of the methanol and CO selectivities explained by experimental studies and a sphere contact quantification model in randomly packed binary mixtures on C• ZnO coprecipitate catalysts*. *Journal of Catalysis*, 2015. **330**: p. 533-544.
35. Roy, K., C.P. Vinod, and C.S. Gopinath, *Design and Performance Aspects of a Custom-Built Ambient Pressure Photoelectron Spectrometer toward Bridging the Pressure Gap: Oxidation of Cu, Ag, and Au Surfaces at 1 mbar O₂ Pressure*. *The Journal of Physical Chemistry C*, 2013. **117**(9): p. 4717-4726.
36. Forni, A., et al., *The chemisorption of hydrogen on Cu(111): A dynamical study*. *International Journal of Quantum Chemistry*, 1994. **52**(4): p. 1067-1080.
37. Kattel, S., et al., *Active sites for CO₂ hydrogenation to methanol on Cu/ZnO catalysts*. *Science*, 2017. **355**(6331): p. 1296-1299.



จุฬาลงกรณ์มหาวิทยาลัย
CHULALONGKORN UNIVERSITY

VITA

NAME Kamonlak Pongpanumaporn

DATE OF BIRTH 11 January 1996

PLACE OF BIRTH Nonthaburi

INSTITUTIONS ATTENDED Chemical Engineering, Faculty of Engineering and Industrial Technology, Silpakorn

HOME ADDRESS No. 92/300, Bangraknoi, Muang, Nonthaburi 11000.

